Zircon U-Pb, Hf and O isotope constraints on the growth versus recycling of continental crust in the Grenville orogen, Ohio, USA

Andreas Petersson

Master thesis in Geology at Lund University - Lithosphere and Paleobiosphere Sciences, no. 265 (45 hskp/ECTS)

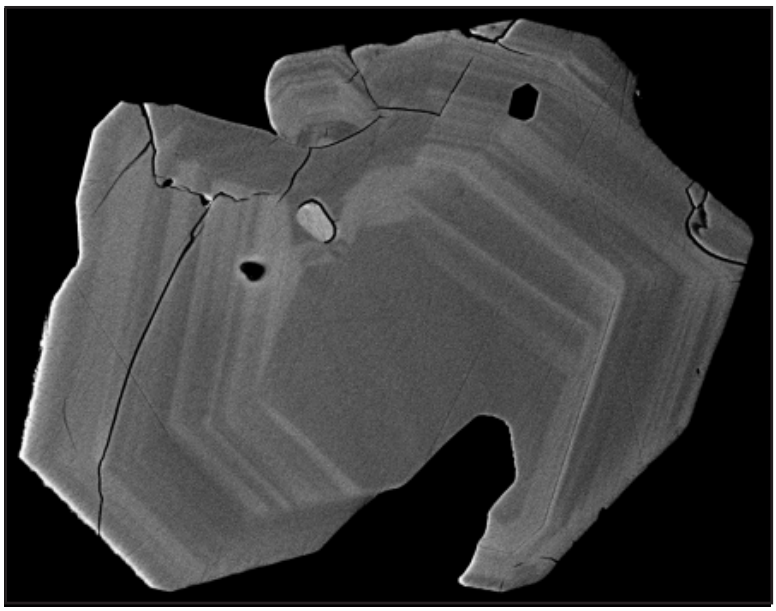

Department of Earth- and Ecosystem Sciences
Division of Geology
Lund University
2010

Zircon U-Pb, Hf and O isotope constraints on the growth versus recycling of continental crust in the Grenville orogen, Ohio, USA.

Master Thesis

Mikael Andreas Petersson

Department of Earth and Ecosystem Sciences
Lund University

2010

To Olof, of course

Table of Content

Cover Picture: Back Scattered Electrone image of a zircon from Logan

Zircon U-Pb, Hf and O isotope constraints on the growth versus recycling of continental crust in the Grenville orogen, Ohio, USA.

MIKAEL ANDREAS PETERSSON

Petersson, M.A., 2010: Zircon U-Pb, Hf and O isotope constraints on growth versus recycling of continental crust in the Grenville orogen, Ohio, USA.

Abstract

The Grenville orogen forms a major, continental scale, Mesoproterozoic orogenic belt along the present day eastern North American continent, from Labrador in the north to Mexico in the south. It is, however, mainly exposed in the northeastern parts of North America. Most of the orogen forms a basement to thick piles of Phanerozoic sedimentary rocks, and the geological evolution of the extensive covered parts of the orogen is poorly known. In this thesis, samples of the Precambrian basement from six drill-cores in Ohio (USA) were examined. Zircon was separated for U-Pb, Hf- and O-isotope analyses and the first robust and reproducible isotope-data for this part of the unexposed Grenville orogen is presented here. Ages were obtained using SIMS (Secondary Ionization Mass Spectrometry) analysis. Zircon U–Pb dates are interpreted as magmatic and metamorphic zircon crystallization ages that span from 1643 ±54 Ma to 1025 ±8 Ma, with additional crystallization ages around 1450 Ma and 1230 Ma. In situ zircon LA-MC-ICP-MS (Laser Ablation Multi Collector Inductively Coupled Plasma Mass Spectrometry) Lu-Hf analyses were obtained from all six samples. Zircon $\varepsilon_{Hf\ (t:\ 1650\text{-}1025\ Ma)}$ values that range from 1.9 ±1.2 to 9.0 ±0.6 are explained by reworking of a single crustal reservoir that was derived from the mantle at 1640 ±40 Ma and that evolved with a $^{176}Lu/^{177}Hf$ value of 0.014. One sample, *Lake*, deviates from this trend and its spread in $\varepsilon_{Hf\ t=1230\ Ma}$ indicates a 0-33 wt% contribution of a depleted mantle component to the $t_{DM\ =\ 1650\ Ma}$ reservoir. Zircon (SIMS) $\delta^{18}O$ weighted mean values range from 5.36 ±0.65‰ to 10.88 ±0.21‰, which corresponds to juvenile mantle and recycled crustal oxygen signatures respectively. There is a broad negative correlation between zircon Th/U and $\delta^{18}O$ and age respectively. The general increase in $\delta^{18}O$ with time and progressive metamorphic recrystallization is best explained by the increasing effect of heavy $\delta^{18}O$ metamorphic fluids during continent-continent collision. Together, the new data presented here suggests that the crustal evolution of this part of the North American continent is significantly older, and that the influence of metamorphic fluids on the O-isotope system in zircon is stronger than previously reported.

Keywords: zircon, U-Pb, geochronology, Hf-isotopes, O-isotopes, Grenville, crustal growth, North-American craton

Mikael Andreas Petersson, Department of Earth and Ecosystem Sciences, Lund University, Sölvegatan 12, SE-223 62 Lund, Sweden. E-mail: andreas.zircon@gmail.com

U-Pb, Hf och O-isotopanalyser av Prekambrisk zirkon från Ohio, USA: modellering av nytillväxt kontra omarbetning av kontinental jordskorpa i den Grenvilliska orogenen.

MIKAEL ANDREAS PETERSSON

Petersson, M.A., 2010: U-Pb, Hf och O-isotopanalyser av Prekambrisk zirkon från Ohio, USA: modellering av nytillväxt kontra omarbetning av kontinental jordskorpa i den Grenvilliska orogenen.

Sammanfattning

Den Grenvilliska orogenen utgör spåren efter mäktiga mesoproterozoiska bergskedjebildningar längs den nordöstra Nordamerikanska kontinenten, från Labrador i norr till Mexiko i söder. Den Grenvilliska berggrunden är huvudsakligen exponerad i de nordöstra sköldområdena i Nordamerika medan största delen av orogenen bildar underlag till tjocka lager av Fanerozoiska sedimentära bergarter. Detta gör att kunskap om den geologiska evolutionen i de centrala och södra delarna av den Grenvilliska orogenen är mycket begränsad. I denna avhandling har sex prov från borrkärnor av den prekambriska kristallina berggrunden i Ohio (USA) undersökts och U-Pb, Hf- och O-isotop analyser av zirkon från dessa prover har gjorts. Dessa analyser utgör de första robusta reproducerbara isotopgeologiska data från denna del av den begravda Grenvilliska orogenen. Åldrar erhölls via SIMS (Secondary Ionization Mass Spectrometry) analyser. Zirkon U–Pb dateringarna är tolkade som magmatiska och metamorfa kristallisationsåldrar av zirkon och spänner från 1643 ±54 Ma till 1025 ±8 Ma, med ytterligare kristallisationsåldrar omkring 1450 Ma och 1230 Ma. In situ LA-MC-ICP-MS (Laser Ablation Multi Collector Inductively Coupled Plasma Mass Spectrometry) Lu-Hf analyser av zirkon erhölls från alla sex prov. Zirkon $\varepsilon_{Hf\ (t:\ 1650\text{-}1025\ Ma)}$ som spänner från 1,9 ±1,2 till 9,0 ±0,6 förklaras genom omarbetning av en enstaka reservoar som härstammar från manteln för 1640 ±40 miljoner år sedan och som utvecklades med ett $^{176}Lu/^{177}Hf$ värde på 0,014. Det nordöstligaste provet, *Lake*, avviker från denna trend och dess spridning i $\varepsilon_{Hf\ t=1230\ Ma}$ indikerar ett 0-33% (vikts %) biddrag från en utarmad mantel komponent till $t_{DM\ =\ 1650\ Ma}$ reservoaren. Viktade (SIMS) $\delta^{18}O$ medelvärden från zirkon spänner från 5,36 ±0,65‰ till 10,88 ±0,21‰, vilket motsvarar O-signaturer från juvenil mantel respektive omarbetad kontinental jordskorpa. Den generella ökningen av $\delta^{18}O$ med tiden och en progressiv metamorf omkristallisation förklaras med ett ökat inslag av metamorfa fluider med tung $\delta^{18}O$-signatur under Grenvillisk kontinent-kontinent kollision. Data som tagits fram i denna avhandling indikerar att jordskorpans utveckling i denna del av den nordamerikanska kontinenten är betydligt äldre, och att metamorfa fluider har haft en kraftigare inverkan på O-isotopystemet i zirkon, än vad som framkommit i tidigare studier.

Nyckelord: zirkon, U-Pb, geochronology, Hf-isotoper, O-isotopeer, Grenville, kontinenttillväxt, Nord Amerikanska kratonen

Mikael Andreas Petersson, Institutionen för geo- och ekosystemvetenskaper, Lunds universitet, Sölvegatan 12, SE-223 62 Lund, Sverige. E-mejl: andreas.zircon@gmail.com

1 Introduction

Only a small portion of all Earth's Precambrian crust is exposed, and this makes geological interpretation and modelling of the Precambrian evolution difficult. One example is the evolution of the Grenville Province/orogen in North America where data mainly comes from the exposed northern parts in Canada. The Grenvillian rocks underneath the Phanerozoic sedimentary rock cover in the USA are, however, poorly known. In Ohio and neighbouring states of the Midwest USA a 800-5000 m thick Phanerozoic sedimentary rock sequence cover the Grenvillian basement rocks. In addition to problems associated with investigation of crust through deep drill core, research on the reworked deeply buried part of this part of the Grenville orogen has been severely hampered by the lack of robust investigative methods, i.e. lack of appropriate analytical techniques.

Earlier isotopic studies of drill core samples in the North American Grenville Province have been highly problematic due to the apparent complex resetting of isotopic systems. For example, previous attempts to date subsurface rocks of the Grenville Province in the state of Ohio have produced cooling ages of different isotopic mineral systems and mixed ages of isotopically complex mineral systems resulting in unclear age patterns, difficult to tie to any geological events. Robust ages of both igneous and metamorphic crystallization of the Grenvillian basement rocks are virtually unknown as is the genetic origin and evolution of this part of the North American continent. Zircon is a mineral that shows extreme ability to withstand breakdown due to external forces such as increased temperatures and pressures during metamorphism, chemical and physical weathering without diffusing any elements or isotopes. This means that zircon preserves its isotopic information in environments where most other minerals do not (Faure and Mensing, 2005). It can therefore be used as a powerful tool to obtain information on the crustal evolution, even of altered rocks exposed to repeated phases of reworking. For example, the U-Pb, Lu -Hf and O isotopic systems in zircon has proven robust (Harley & Kelly, 2007) and when analysed by present day highly refined high-sensitive, high-spatial resolution analytical techniques, earlier problems concerning late cooling and partial or complete isotopic resetting can be reduced or eliminated. With textural control obtained by micro-imaging techniques such as back-scattered electron (BSE) and cathodoluminesence (CL) imaging, it is possible to date both crystallization and metamorphic events in a single grain. It is also possible to use O- and Hf-isotopic analysis to determine the origin, host rock composition and geological history of rocks. This study is based on petrographic rock characterisation, *in situ* zircon U-Pb dating and combined O and Hf isotope analysis of zircon from drill core samples of the subsurface Grenvillian basement of Ohio, USA. U-Pb dating and O-isotope analyses were carried out on a SIMS (Secondary Ion Mass Sepctrometer) and Hf -isotope analysis on a LA-ICP-MS (Laser Ablation Inductively Coupled Plasma Mass Spectrometer). The advantage with SIMS and LA-ICP-MS compared to conventional Thermal Ionization Mass Spectrometry (TIMS) dating techniques is the possibility of in situ analysis of concordant positions within a single grain. Furthermore, it enables analysis without chemical preparation, and the precision loss is less than an order of magnitude than that of conventional mineral dissolution analytical techniques (Košler & Sylvester, 2003).

Another important aspect of the in situ analytical approach is that it does not suffer from the mixing effects that plague whole rock analyses, or even single grain solution work. The in situ data benefits from texturally well-constrained age domains, while the single grain solution work might have included zircon of several generations.

Collected data shed new light on the characteristics, origin and metamorphic history of the subsurface basement in Ohio. Continental crust is enriched in $\delta^{18}O$ relative to the Earth's mantle. Therefore, O- isotope data enables the recognition of juvenile mantle derived magmas or the presence of reworked continental crust. Furthermore, zircon normally preserves its crystallization $\delta^{18}O$ value, and heavy O signals (i.e. $\delta^{18}O$ >5.7‰ for the mantle) indicate influence of reworked crustal components at the time of crystallization.

Hf isotope ratios are the function of Lu/Hf and time. During partial melting, Lu/Hf fractionation takes place due to the greater incompatibility of Hf over Lu. This has led to a mantle reservoir with high (depleted) $^{176}Lu/^{177}Hf$ and low (enriched) $^{176}Lu/^{177}Hf$ in the continental crust. With time, these reservoirs develop suprachondiritc and subchondritic $^{176}Hf/^{177}Hf$ respectively. It is therefore possible to distinguish between juvenile sources (suprachondritic $^{176}Hf/^{177}Hf$) and the influence of evolved crustal components(subchondritic $^{176}Hf/^{177}Hf$). Furthermore, combined zircon U-Pb dating and Hf-isotope analysis enables the determination of when a protolith separated from the depleted mantle reservoir. Combined zircon U-Pb, O- and Hf-isotope analyses is therefore a powerful tool for the investigation of the evolution of the continental crust (c.f. Kemp *et al.*, 2006).

In this thesis, this combined method is used to investigate six deep drill cores from the deeply buried Precambrian crust of Ohio. Drill-core samples were provided by the Ohio Geological Survey. Robust zircon U-Pb crystallization and metamorphic ages are presented. I also discuss the involvement of juvenile versus reworked mid- to Palaeoproterozoic continental crust, and suggest models of crustal growth evolution. This thesis includes a combination of isotopic analytical data sets obtained by highly advanced analytical techniques. However, the understanding of the geology can never be better than the understanding of the investigative methods. This thesis, therefore, also in-

cludes in depth descriptions of the mineral-isotope systems and analytical techniques applied.

2 The Grenville Province: Geological setting

The term Grenville is normally used both for the Grenville orogenic province in North America and for a time period connected to a global event of coeval orogenesis. In this thesis, the term Grenville is only used when the province is intended and the nomenclature of Rivers (2008) is used concerning geological setting and orogenesis.

The Grenville Province comprises a number of orogenic thrust stacks on the present-day east coast of North America. It formed in the Mesoproterozoic Era, during the assembly of the supercontinent Rodinia. A proto-North-American plate collided with another continent at the Laurentian margin, possibly Amazonia (Rivers, 1997). The orogenic evolution of the Grenville Province started with accretion of outboard arcs onto the Laurentian margin, the closure of a back arc basin, and proceeded as a continent-continent, Himalayan style collision. The Grenville Province extends from the Labradorian coast in the north, down to Mexico in the south, and perhaps all the way down to Australia and Antarctica (Fig. 1). It is, however, mainly exposed in the northern parts of North America from the Labradorian coast down to the great lakes. South thereof, it is covered by thick Phanerozoic deposits only to resurface in Texas, the Llano Uplift (Mosher, 1998).

2.1 Orogenic phases

The term orogenic phase is used for orogenic components separated in time and/or by geographic location, not large enough to constitute a separate orogeny.

2.1.1 Pre-Grenvillian

Grenvillian crust is divided into thrust stacks placed over the southern periphery of the Superior Province ranging in age from Archean to late Mesoproterozoic (Rivers, 1997). Gower and Krogh (2002) divide the geological evolution of the eastern pre-Grenvillian craton and the Grenville Province into three different stages. The first stage, >1710-1600 Ma (pre-Labradorian to Labradorian time period), includes the formation of an outboard arc, subduction and accretion to a pre Labradorian proto-North-American plate. The second stage consists of the formation of a continental margin arc during the Pinwarian time period (1520-1460 Ma), followed by magmatism related to subduction during the Elsonian (1460-1230 Ma). The third stage includes the Elzevirian (1250-1190 Ma; Rivers, 1997) and the Grenville orogenesis, which is discussed in this thesis.

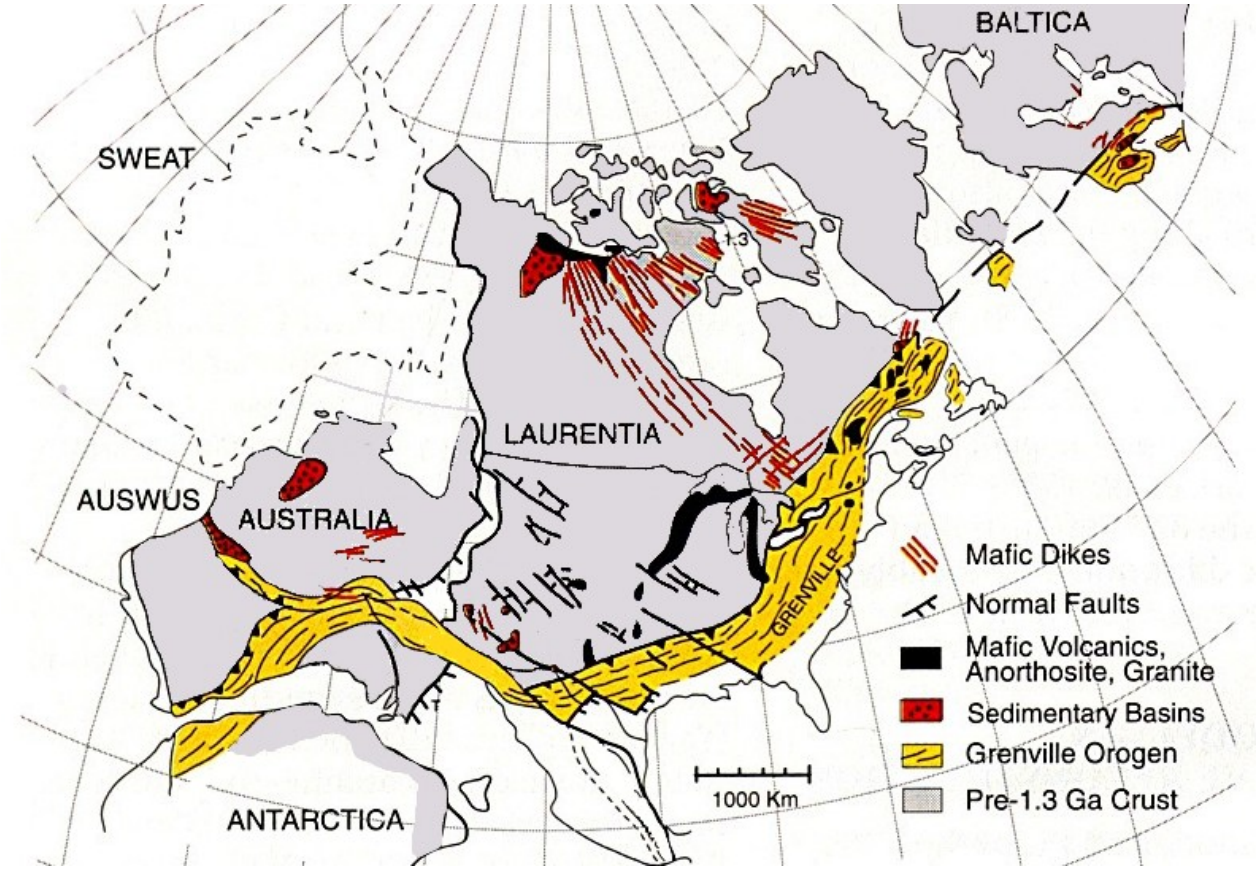

Fig. 1. Global distribution of Grenvillian orogenic rocks. (Redrawn after Karlström et al.2001)

2.1.2 Accretionary orogenesis: the Elzevirian and Shawinigan orogenic phases

The Elzevirian orogeny relates to closure of the Elzevir back arc basins and the accretion of these outboard terranes onto Laurentia (Windley, 1986; McLelland et al., 1988; Gower et al., 1990; McEachern & van Breemen, 1993; Corriveau et al., 1994; Rivers, 1997). At ~ 1230 Ma, back arc magmatism related to subduction ends (Corrigan & Hanmer, 1995). Most of the Elzevirian terrain reached amphibolite facies but the metamorphic grade ranges from greenschist to granulite facies (van Breemen & Corriveau, 1995). Outside of the Central Metasedimentary Belt the Elzevirian orogeny is not clearly known, but Rivers (1997) mentions a few indications of seemingly coeval tectonism.

Rivers (2008) also excludes the Shawinigan orogenic phase (~1190-1140 Ma) from the Grenvillian orogeny. He suggests that it should be treated as a separate orogeny since it is not part of the subsequent continent-continent collision, and since it is spatially restricted to accreted terrains in the south-western Grenville Province.

2.1.3 Continent-continent-collision orogenies: the Ottawan and Rigolet phases

Numerous geological and geophysical studies have been made on the Grenville orogen. Today, a widely accepted model includes a continent-continent collision between a proto-North-American continent and another plate, possibly Amazonia, which collided into a crustal scale thick, south-east dipping, imbricate thrust stack at the Laurentian margin (Rivers, 1997). Rivers (2008) suggests that the Grenvillian orogeny include two orogenic phases, the Ottawan (~1090-1020 Ma) and Rigolet (~1005-980 Ma), respectively. The Grenville Province has two principal tectonic boundaries. The Grenville Front which constitutes the north-western periphery of the province, and the Allochthon Boundary Thrust (Fig. 2). Between the two boundaries is the Parautochthonous Belt. This belt is lithologically similar to the foreland and has the Grenville Front as its floor thrust. The metamorphic evolution of the Parautochthonous Belt is connected to the Rigolet orogenic phase. The Allochthon Boundary Thrust defines its south-eastern boundary and has acted as the floor thrust of the overlying allochthonous belts. The latter have been metamorphosed during the Ottawan orogenic phase. Parts of the Parautochthonous Belt also show isotopic, mineralogical and textural signs of Ottawan metamorphose which later has been overprinted by the Rigolet metamorphose (Rivers, 2008 and ref. therein).

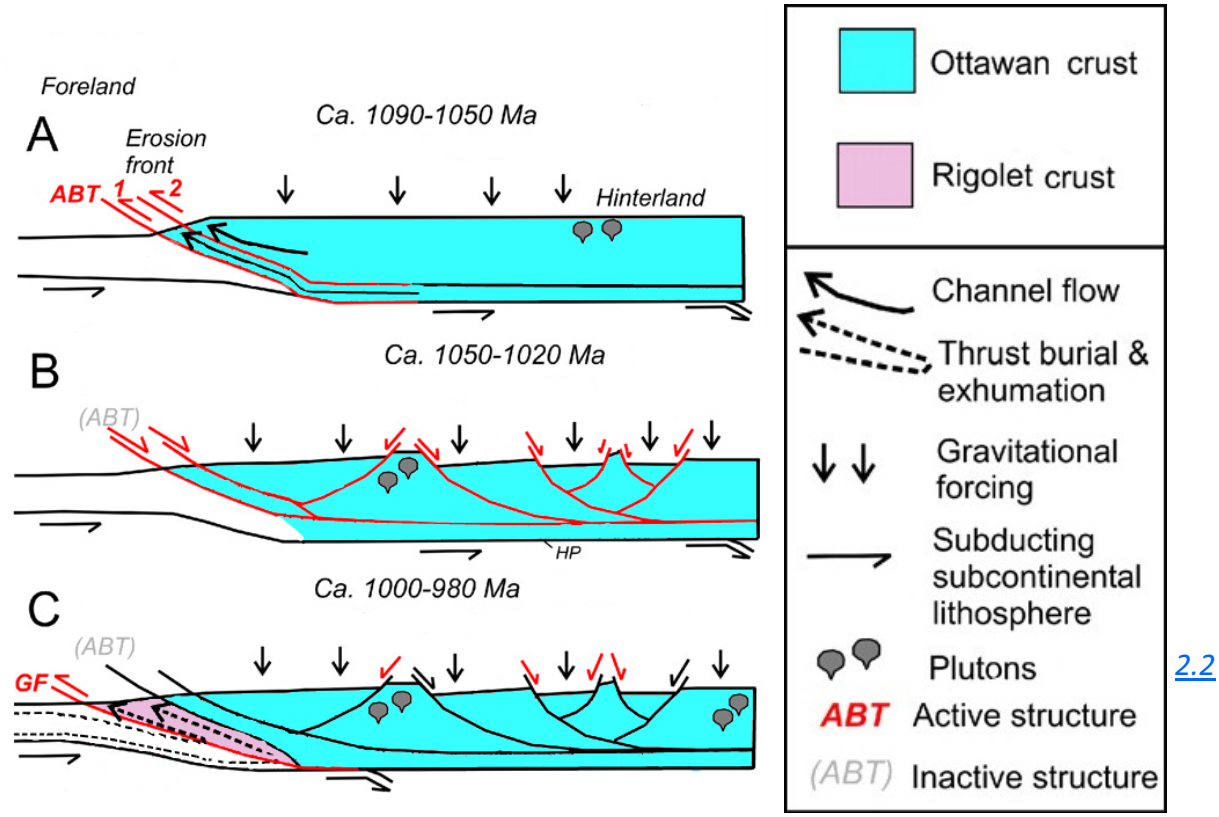

2.2

Fig.2. Principal sketch of the late tectonic Grenvillian development (corrected and simplified after Rivers, 2008). Active structures are highlighted in red. A) Metamorphism and exhumation through channel flow above the Allochthon Boundary Thrust (ABT). B) Gravitational orogenic collapse of the hinterland. Note the reverse shear sense along ABT. C) Formation of the Grenville Front (GF) and associated high-grade metamorphism during thrusting of crust under the ABT. The Parautochthonous Belt is the crustal segment in pink between GF and ABT.

Subsurface Precambrian of the Midwest US (Local geology)

In Ohio, Grenvillian rocks are found in the eastern part of the state covered by 800-5000 m thick Phanerozoic strata (Fig. 3). The western parts of the subsurface Precambrian of Ohio, west of the Grenville Province consist of the between 1500-1320 Ma old unmetamorphosed igneous rocks of the Eastern Granite Rhyolite Province and sedimentary and igneous rocks of the less than 1030 Ma old East Continent Rift Basin (Santos et al., 2002) (Fig. 3).

Since the Precambrian basement is not exposed, all available information comes from deep drill cores from old oil and gas wells, and from potential field data.

2.2.1 West of the Grenville Front: Eastern Granite Rhyolite Province and East Continent Rift Basin

The Precambrian basement west of the Grenville Front in Ohio is primarily composed of < 1500 Ma granites and rhyolites of the Eastern Granite Rhyolite Province, which was later rifted to form a horst and graben complex at around 1300 Ma (Ohio History Central, 2006; Fig. 3). In western Ohio, this rifting resulted in grabens that are filled with ≥6000 meters of sedimentary rocks, mainly lithic arenites, and constitutes the Eastern Continent Rift Basin (Baranoski et al., 2007). Two NE-striking conspicuous rift zones composed of mainly mafic igneous rocks cut trough western Ohio, the Fort Wayne Rift (not dated) and the Midcontinent Rift ~1100 Ma (Davis & Paces, 1990). The role of these rift events are unclear, but are interpreted by Drahovzal et al., (1992) to have preceded the Grenville orogenies (Baranoski et al., 2009).

2.2.2 East of the Grenville Front-The Grenville Province

The Grenville Front in Ohio forms a conspicuous tectonic boundary that separates variably metamorphosed rocks of the Grenville Province in the east from unmetamorphosed rocks of the Eastern Granite Rhyolite Province and the East Continent Rift Basin in the west. Rocks within the Ohio Grenville Province are predominantly penetratively recrystallized meta-igneous and meta-supracrustal rocks deformed and metamorphosed during the Ottawan and Rigolet orogenic

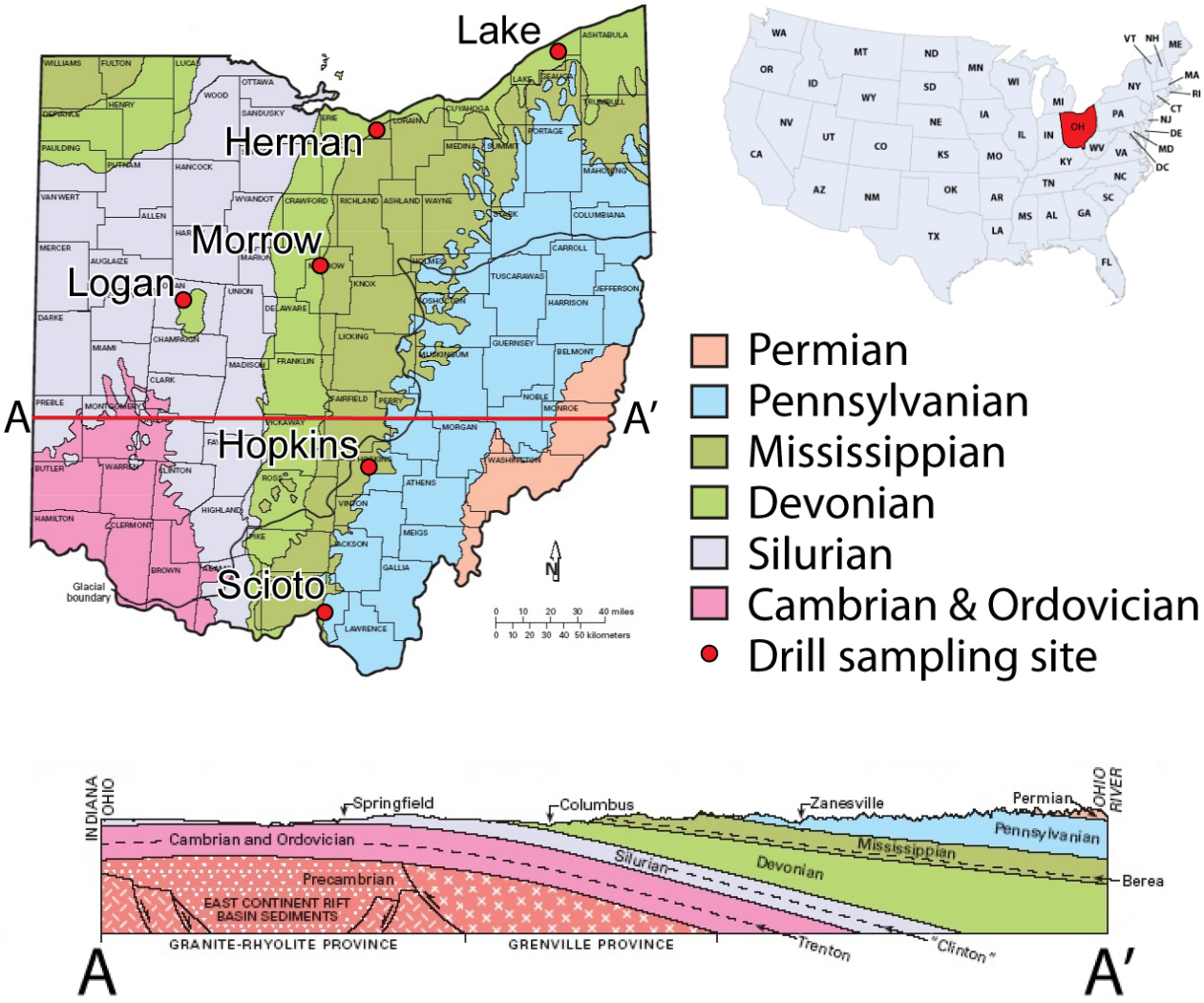

Fig.3. Geological map of Ohio showing the distribution of Phanerozoic sedimentary cover and the glacial boundary. Drill sampling sites are shown with red dots. Profile A-A' shows the distribution of subsurface rocks with an exaggerated vertical scale.

phases (Rivers, 2008). The main rock types of the basement, recovered from drill-cores, are felsic orthogneisses, in places veined and commonly compositionally banded (intermediate compositions also occur), amphibolite, K-feldspar rich medium-grained metagranite, and seemingly unmetamorphosed and undeformed medium-grained, red post-kinematic granites. Some marble, both pure and impure is found in scattered drill-cores and in the most north-eastern part of Ohio, quartz-feldspar-biotite gneiss was located in one core (Ohio Division of Geological Survey, 2010). Potential field data for the Grenville province in Ohio suggest that it is composed of stacks of auto- to allochthonous nappes, which dips towards the east (Baranoski et al., 2007, Rivers 2008) (Fig. 2).

2.2.3 Orogenic Lid

The uppermost segments in the Grenville Province are called the Orogenic Lid and appear in two parts of the region: in the north-central part of Grenville, northwest of the Allochthon Boundary Thrust and in accreted terranes in the south-western part of the province. The reciprocal feature of the different parts of the Orogenic lid is the lack of Ottawan metamorphism and $^{40}Ar/^{39}Ar$ cooling ages that are older than 1100 Ma. The northern segments consist primarily of high-grade Labradorian gneisses and Paleo-to Mesoproterozoic intrusions while the segments in southern Grenville are parts of the accreted terranes with metamorphic signatures of the Elzevirian and Shawinigan (Rivers 2008 and ref. therein).

2.3 Previous work

Several attempts have been made to date the Precambrian basement in Ohio. Reliable reproducible data have, however, been difficult to obtain and the results from previous isotopic work clearly indicates complex disturbance of the mineral isotopic systems used, likely caused by post-crystallization alteration (metamorphism, hydrothermal alteration). Attempts to date igneous or metamorphic crystallization of the Ohio Precambrian basement were mainly baed on isotopic chronometers that are non-robust during post-crystallization alteration. Rb-Sr and a few Sm-Nd dating attempts have been made on deep well drill cores around Ohio. Whole-rock Rb-Sr dates range from ~900 to 1300 Ma (Lucius & von Frese 1988). In 1983, Mensing & Faure and Faure & Barbis, used Rb-Sr to date metasupracrustal rocks from *Scioto* County (Fig. 3) on K-feldspar and whole rock respectively. Presented dates were 599 ±69 Ma and 1162 ±11 Ma for the K-feldspar (Mensing & Faure 1983), and 699 ±16 Ma and 1173 ±41 Ma for the whole rock samples (Faure & Barbis, 1983). In 1972, Hofman et al. tried to date a granitic gneiss with Rb-Sr on K-feldspar and Biotite and obtained 1242 ±46 Ma for the K-feldspar and 898 ±40 Ma for the biotite (Hofman et al. 1972). These samples were taken from the same core and from more or less the same depth. Lidiak et al. (1966) date a Rhyolite whole-rock with Rb/Sr model age in *Logan* County, core 645, to 1325 Ma. As Lucius & von Frese (1988) suggests, these Rb/Sr dates probably were reset by later thermal or geochemical events.

3 Analytical methods: principal outlines and applied procedures

Because of the complex alteration history of the Ohio Precambrian basement, including resetting of isotopic systems, not as robust as the U-Pb system on zircon, previous geochronological and geochemical work yields ambiguous data that are difficult to interpret in a geological meaningful context. These problems were recognised by earlier workers, e.g. Lucius & von Frese (1988). Today, analytical techniques are available that offers both spatial resolution and high-sensitivity analysis. *In situ* zircon U-Pb dating and *in situ* O- and Hf-isotope analysis, with e.g. ion probes and laser ablation help to avoid previous predicaments. These techniques also enable new applications and possibilities to, foremost, isotopic -geochronology and -geochemistry. The general principles of the zircon isotope systems and the applied techniques to analyse these isotopes are given below, together with more detailed descriptions of the analytical procedures used in this study.

3.1 Zircon

Zircon has the chemical composition of $ZrSiO_4$ and is a tetragonal orthosilicate with SiO_4 tetrahedra sharing edges with intervening ZrO_8 dodecahedra. It is most common in igneous rocks of intermediate to quartz saturated composition. In a pure state, zircon would not be interesting. It is the impurities and substitutions that occur in zircon that makes it so useful. Commonly zircon contains trace amounts of P, Y, Hf, U, Th and lanthanides. The presence of the radioactive mother isotopes (as ions) U^{4+} and Th^{4+} substituting for Zr^{4+}, together with the fact that crystalline zircon cannot incorporate Pb, and that the Pb present in zircon is radiogenic end products, makes it the best geological time keeper known to man. Furthermore, Hf^{4+} substitutes for Zr^{4+}, and since $^{176}Hf/^{177}Hf$ depends on time and Lu/Hf, the $^{176}Hf/^{177}Hf$ of zircon with its low Lu/Hf enables the investigation of crustal residence times, and mantle/crust composition of magmas. The O-isotopes in zircon allow us to investigate crustal recycling and the involvement of sediments and crustal components to magmas. All these methods are used in this paper. In addition, but not applied in this work, He formed through the decay U and Th, enables the determination of exhumation and erosion rates, Ti^{4+} substituting for Si^{4+} can be used as a thermometer to unravel the T of zircon crystallization (Harley & Kelly 2007) and REE can be used to fingerprint different magma sources and to hypothesis magmatic evolutions (Harley & Kelly 2007; Rubatto & Hermann 2007).

Zircon is stable up to 1690 °C (1963 K) at ambient pressure, whereupon it decomposes into oxides and zircon is also one of the most incompressible min-

erals known to man (Finch & Hanchar 2003). An important feature of zircon is the fact that most of its cations have low diffusivity. This allows zircon to preserve its chemical signatures of crystallization (Cherniak & Watson 2003). Together with the fact that zircon is hard and refractory makes it uniquely robust. So robust that it can withstand its host rock being thoroughly metamorphosed, molten and/or mechanically weathered and still preserves its isotopic information (Scherer et al. 2007).

The closure temperature (T_c), can be described as the temperature below which the diffusion of a certain element and its radiogenic daughters is negligible (Dodson 1973). The T_c of an isotope in a mineral is, however, not a fixed value, but is controlled by a number of factors such as e.g. the size and morphological character of the grains (Cherniak et al. 1997). For the U-Th-Pb isotopic system in natural zircon, the Tc is >900 °C, which is higher than the temperature of many granitic magmas and most metamorphic environments (i.e. crustal conditions, Lee et al. 1997). This means that diffusion of these isotopes and their daughters is negligible up to these temperatures. Because of this, zircon is a robust geochronometer with the ability to remain isotopically closed during high-grade metamorphism and partial melting of the host rock (Lee et al., 1997). The Rare Earth Elements (REE) show similar behaviour in zircon, where diffusion occur at temperatures in excess of 1000 °C (Dodson 1973; Cherniak et al. 1997).

Despite the robustness of zircon – secondary zircon may form through (i) new growth from Zr release from other minerals than zircon during metamorphic reactions (Fraser et al. 1997), (ii) dissolution of zircon in an aggressive fluid/melt and subsequent crystallization (Rubatto et al. 2008); (iii) in situ recrystallization through coupled *dissolution-reprecipitation* catalyst by a fluid-melt interaction (Rubatto et al. 2008); (iiii) *solid-state* recrystallization within the crystal lattice (Hoskin and Black, 2000; Giesler et al. 2007).

These different processes may generate morphologically and texturally different types of zircon. It may, however, often appear severely difficult to differ between different types of zones (e.g. recrystallized zircon, newly grown domains or zircon altered by fluids) and interpretations of secondary zircon are not always in consensus. This makes it important to have good textural control of both morphology and internal textural characteristics of the analyzed grains through e.g. BSE and/or CL. Combined with *in situ* analysis of the different types of zircon, the data can be used to discover isotopic and chemical signatures of genetically different parts of a crystal population. Trace element distribution between zircon and adjacent metamorphic minerals can also grant insight to whether a certain grain or domain is recrystallized, newly grown or a survivor from a protolith rock (Harley et al., 2007) This angle of approach is novel and promising but must be considered with care when gratifying that experimental data still is lacking (van Westrenen et al. 1999). Without full control of the before mentioned controlling factors, it is impossible to interpret the geological validity and significance of the collected data.

3.1.2 Textural characterization

A range of different factors will affect the composition and appearance of a zircon. External morphology is related to kinetic factors such as diffusion and adsorption, where tiny and flat grains with a high surface to volume ratio are more strongly affected (Hoskins & Schaltegger 2003). Internal textures, visible in BSE and CL, are useful because of the heterogeneous distribution of predominantly trace elements in the crystal (Hoskins & Schaltegger 2003). For example, areas with large quantities of high Z (atomic number) elements will appear lighter in BSE. In the case of zircon this means that domains with high U and Th content will be brighter compared to those with a lower content.

Crystallization and recrystallization of zircon can occur at practically all stages of a normal PTt-path (Harley et al. 2007). Different processes leading to different types of crystallization generate a variety of textures.

The most archetypal feature of an igneous unmetamorphosed zircon is an oscillatory growth zoning, seen in BSE and CL, and sometimes even in optical microscope and hand-lens. This zoning in BSE might represent variations in Zr and Si composition, but concentration variation of Hf, P, Y, U, Th and the REEs, which can vary up to an order of magnitude, is the main reason (Corfu et al. 2003). The characteristics of zircon growth zones can vary in a single grain from broad bands to fine oscillatory zoning. Zircon crystallized from a metamorphic reaction is not known to develop oscillatory zoning but may instead be sector zoned (Watson & Liang 1995). A wide range of textures can be labelled metamorphic due to the large number of conditions under which zircon can grow (Hoskins & Schaltegger 2003) e.g. mosaic texture, convolute zoning, "cross-bedding type" texture, heterogeneous patchy patterns (Corfu et al. 2003).
Lattice strain in trace element rich oscillatory zoned zircon makes it comparatively unstable at moderate to low temperatures (Sommerauer 1974; Hoskin & Black 2000). Hoskins & Black 2000 and Geisler et al. 2007 explain a process called *solid state* recrystallization triggered by lattice strain. This recrystallization often produces a BSE bright, U-rich "ghost zoning", a relict oscillatory zoning from the previously unaltered zircon. In *solid-state* recrystallization a relict chemical signature of the protolith zircon could retain, producing mixed ages to different extent depending on how complete the recrystallization is (Hoskins & Black, 2000). Recrystallization can also transpire through in situ *dissolution-reprecipitation*, for example explained by Rubatto et al. (2008) with an example from the Lanzo Massif. This is a process where interaction of a

fluid or melt causes dissolution and more or less simultaneous re-precipitation of zircon.

3.2 Mineral Processing

All samples were processed on the Wilfley shaking table in order to obtain heavy mineral separates from which zircon grains were handpicked. Heavy mineral separates obtained by heavy liquid separation from the samples from the *Scioto*, *Herman*, *Lake* and *Hopkins* wells were already available from earlier work by Jenny Andersson (Uppsala). These were, however, not clean and were therefore reprocessed on the Wilfley table before handpicking. The procedure was adapted from Söderlund & Johansson (2002). A small fraction of the tail of the heavy minerals was collected from the table, decanted and dried. Magnetic minerals were removed using a magnetic pencil. Ethanol was added to the samples and zircon grains were handpicked from Petri dishes using forceps and pipette under a binocular microscope. For samples with sufficiently large zircon populations, the best quality grains were chosen, in different size and shape, capturing both euhedral, subhedral and anhedral grains respectively. Between three and 105 grains were selected from the different samples and mounted on tape before casting into epoxy. The zircon standard 91500 (Wiedenbeck et al. 2004) was added to the mount. After hardening, the epoxy mount was polished to expose a cross section through each grain.

3.3 BSE imaging

The epoxy mount was carbon coated and examined using BSE. A standard Hitachi S-4300N electron microscope at the Department of Earth and Ecosystem Sciences, Lunds University, was used for the imaging. With this equipment, a high-energy primary electron beam can be used to produce secondary electrons, backscattered electrons, x-rays, CL, specimen current and transmitted electrons upon interaction with the mineral. Secondary electrons and back-scattered electrons were used to build up images of the zircon grains. In BSE analysis, a beam of electrons is reflected from the sample by elastic scattering (Egerton 2005). In elastic scattering the electrons keep their kinetic energy and only change their direction. The cross section of elastic scattering is proportional to Z^2, were Z is the atomic number. This leads to heavy elements appearing brighter than light elements. For zircon, the variation in U-concentration can be indicated by the brightness of the image.

To prevent accumulation of static electric charges on the sample, the mount was covered with a thin veneer of carbon. The analytical work is non destructive to the grains. The BSE images were used for guidance of the location of the isotopic spot analysis. The aim of this work was to avoid cracks and inclusions in analysed domains and to obtain analytical data from texturally different parts of the analysed zircon.

3.4 Principles of the U, Th-Pb method of dating zircon

Zircon, $ZrSiO_4$, is never totally pure and incorporates U and Th in its structure. The relatively small U^{4+} (0.89 Å, all ionic radii are from Shannon, 1976) and Th^{4+} (0.94 Å) ions substitute for the Zr^{4+} ion (0.72 Å). Pb^{2+}, on the other hand, is not easily incorporated in zircon due to its much larger size (1.19 Å) and different ionic charge. Instead, Pb in zircon is produced from the radioactive isotopes ^{238}U, ^{235}U and ^{232}Th that with time all decay through a chain of alpha and beta emissions into stable Pb isotopes. ^{238}U decays into ^{206}Pb, ^{235}U into ^{207}Pb and ^{232}Th into ^{208}Pb. All three radioactive parent isotopes have a predetermined half-life (i.e. time required to decay the radioactive parent into half of the initial amount) fixed by the IUGS Subcommission on Geochronology (Table. 1).

Table. 1. Half-lives of selected U and Th isotopes

Parent isotope	*Daughter isotope*	*Half-Life (years)*	*Decay constant (y^{-1})*	*Reference*
^{232}Th	^{208}Pb	$14.010X10^{9}$	$4.9475X10^{-11}$	1
^{235}U	^{207}Pb	$0.7038X10^{9}$	$9.8485X10^{-10}$	2
^{238}U	^{206}Pb	$4.468X10^{9}$	$1.55125X10^{-10}$	2

1. LeRoux et al. (1963)
2. Jaffey et al. (1971)

Since Pb is not readily incorporated into zircon and the decay rate of the radioactive U and Th-parents are known, U-Th-Pb isotope analyses of zircon can be used to calculate the time needed to establish the recorded proportions between the different parent-daughter isotopes. This data can be used to calculate the age of the analysed zircon assuming that the analysed zircon domains has remained closed since crystallization. The amount of initial common Pb (cPb, non radiogenic Pb incorporated into the crystal lattice) in a crystalline newly formed zircon is normally negligible. Nevertheless, cPb can be incorporated in zircon or occur in inclusions or introduced and hosted in cracks or radiation damaged areas. The cPb does not only contain ^{204}Pb but also ^{206}Pb, ^{207}Pb and ^{208}Pb in various proportions. The relative proportion of the different Pb-isotopic species varies with time (Stacey & Kramers 1975). As only ^{204}Pb can be used to monitor the presence of cPb, its isotopic composition has to be assumed, and here we assume that any cPb present in the grain was incorporated during sample preparation (i.e. cPb_t = 0 Ma). Modern cPb composition, i.e. U/Pb= 9.74, $^{206}Pb/^{204}Pb$= 18.703 and $^{207}Pb/^{204}Pb$= 15.629 (Stacey & Kramers 1975), was subtracted from the measured amounts of ^{206}Pb, ^{207}Pb, ^{208}Pb using the intensity of the ^{204}Pb-signal. The cPb-corrected data was used in the age calculations. For most samples, the cPb contribution is negligible, but in a few cases, cPb forms a significant contribution. These data are used with caution or not at all due to the uncertainties in the assumptions about the cPb-composition.

Taken together, the radiometric U-Pb data and the esti-

mates of cPb in the analysed zircon volume can be used to calculate an age of the analysed crystal using the following equations (1-2):

$$^{238}U/^{206}Pb = 1/(e^{\lambda_{238}t} - 1) \quad \text{[eq. 1]}$$

$$^{207}Pb/^{206}Pb = 1/137.88((e^{\lambda_{235}t}-1)/(e^{\lambda_{238}t} - 1)) \quad \text{[eq. 2]}$$

Note that this equation cannot be solved for t through algebraic methods but through iteration.

t=Time since closure of mineral
λ= Decay constant of mother isotope

Since these values are fixed they can be plotted against each other to create a logarithmic curve. The most commonly used method is to plot the ($^{206}Pb/^{238}U$)/($^{207}Pb/^{235}U$) ratios at any given time, the so-called Wetherill concordia diagram. The concordia curve defines the evolution of radioactive decay through time and gives the $^{238}U/^{206}Pb$- and $^{207}Pb/^{206}Pb$ ratios at any given point. The universal $^{238}U/^{235}U$-ratio of 137.88 is used in calculations (Faure &Mensing 2005). $^{238}U/^{206}Pb$- and $^{207}Pb/^{206}Pb$ ratios are measured by a mass spectrometer. In an optimal situation both ratios plot in the same point on the concordia curve. In this scenario, the data is *concordant*. If this is not the case, the two ratios will yield different ages. In this scenario the data is *discordant.* The distance from the concordia curve is expressed as the geometric distance between the ages, and is expressed in percent. Here, the analytical error is incorporated into the calculation and only data that is discordant beyond the analytical uncertainty is reported as discordant (Table. 2). Perfect concordance will be achieved in a system that has been closed relative to U, Th, Pb and all intermediate daughters, and were all initial values and calculations were correct (Faure & Mensing 2005).

Discordance might have several causes, for example, a recent or episodic Pb-loss, or incorporation of cPb (Fig. 4 A-C) Recent Pb-loss is commonly assumed to be due to Pb-loss in a more or less metamict

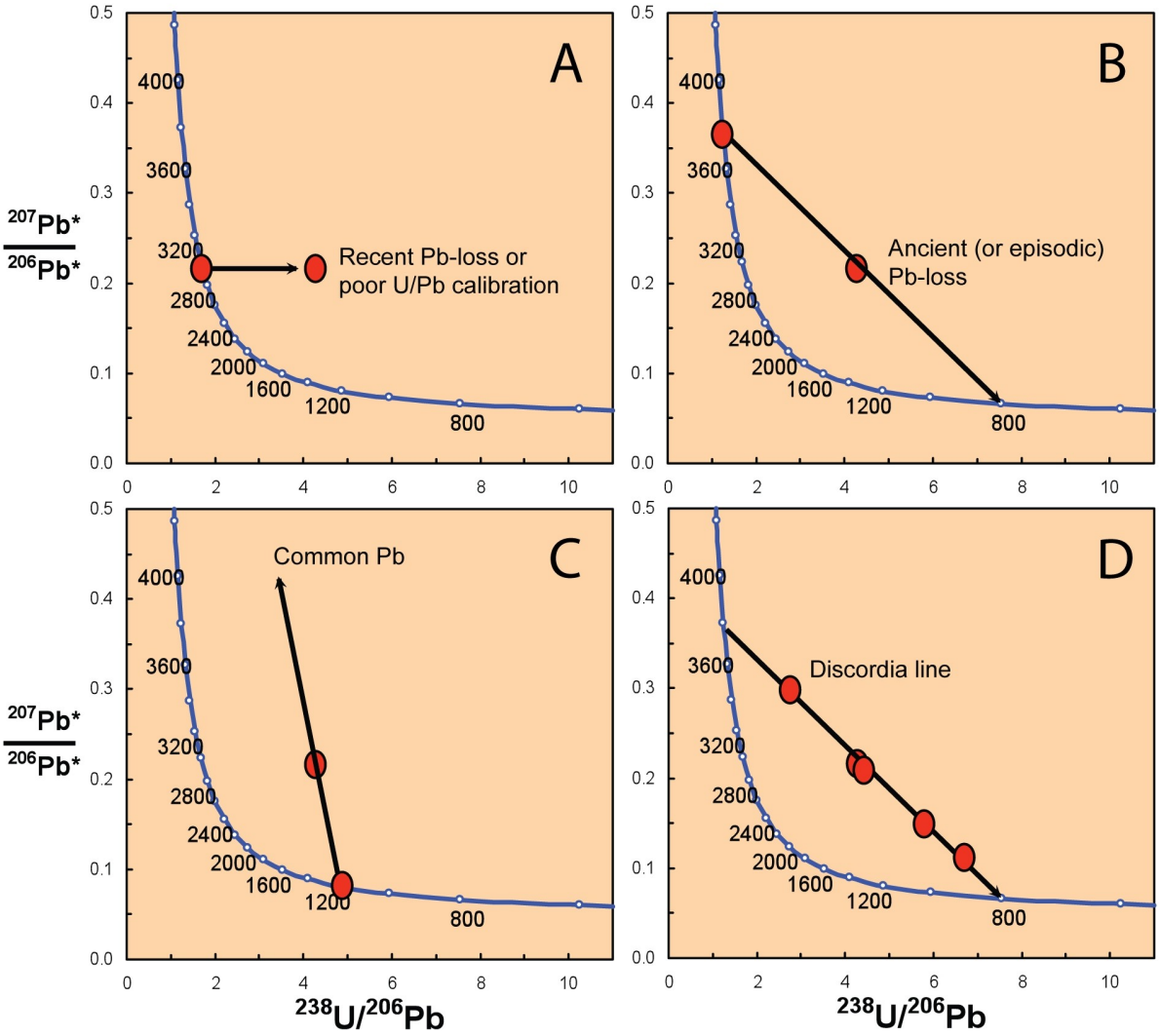

Fig. 4. Inverse (Tera-Wasserburg) U-Pb concordia diagrams illustrating the effects of (A) recent Pb-loss or U/Pb calibration error, (B) episodic Pb-loss, (C) common Pb contamination and (D) discordance due to either episodic Pb-loss or mixing of two age components. See text for discussion.

Tabel. 2.

Sample/[a] spot #	Structural class/[b] (from BSE)	Pb (ppm)	U (ppm)	Th/U calc.	$^{206}Pb/^{204}Pb$ meas.	$^{238}U/^{206}Pb$ corrected	±σ %	$^{207}Pb/^{206}Pb$ corrected	±σ %	Disc. %/[d] 2σ limit	$^{207}Pb/^{206}Pb$ age (Ma)	±σ	$\delta^{18}O$	±‰	mass bias and interference corrected 176Yb/177Hf	2SE	mass bias and interference corrected 176Lu/177Hf	2SE	mass bias and interference corrected 176Hf/177Hf	2SE
Logan n3420 ***(Acid volcanic)***																				
03a	zoned magm	42	141	0,193	17071	3,898	0,99	0,0922	0,77	0,11	1472	15	10,77	0,32	0,000120	0,000035	0,000002	0,000000	0,282132	0,000048
03b	zoned magm												9,87	0,34						
05a	zoned magm	48	163	0,159	99671	3,864	1,02	0,0919	0,72		1465	14	9,70	0,32	0,000046	0,000026	0,000001	0,000000	0,282088	0,000034
06a	zoned magm	55	185	0,191	85784	3,890	0,97	0,0918	0,67		1464	13	9,59	0,32						
07a	zoned magm	53	185	0,127	50270	3,972	0,94	0,0919	0,70		1466	13	8,05	0,33	0,000165	0,000049	0,000003	0,000000	0,282081	0,000058
08a	zoned magm	63	215	0,149	15462	3,867	1,02	0,0915	0,80		1458	15	8,83	0,35	0,000079	0,000029	0,000001	0,000000	0,282097	0,000044
09a	zoned magm	105	357	0,107	89221	3,827	0,95	0,0920	0,50		1468	10	8,18	0,32	0,000231	0,000080	0,000004	0,000001	0,282143	0,000046
10a	zoned magm	108	363	0,188	97618	3,860	0,94	0,0918	0,60		1463	11	11,82	1,17	0,000143	0,000033	0,000003	0,000001	0,282109	0,000057
11a	zoned magm	109	363	0,221	43359	3,858	0,98	0,0915	0,51		1458	10	8,28	0,37	0,000114	0,000063	0,000002	0,000001	0,282081	0,000055
12a	*zoned magm*												8,89	0,32						
															0,000089	0,000043	0,000001	0,000000	0,282101	0,000045
Lake n3421 ***(Dark fine-grained rock)***																				
06a	wz magm	47	180	0,413	1381	4,638	1,03	0,0802	1,45		1201	28	6,05	0,34	0,045955	0,004286	0,001309	0,000101	0,282198	0,000056
06b	wz magm	95	361	0,740	1796	4,851	1,00	0,0796	1,31		1188	26								
07a	wz magm	24	99	0,301	30790	4,942	1,05	0,0820	1,41		1246	27	6,59	0,32	0,103194	0,014051	0,002947	0,000383	0,282236	0,000060
08a	*wz magm*	*56*	*243*	*-0,708*	*176*	*4,769*	*0,97*	*0,0417*	*12,90*		*-244*	*298*	7,06	0,36	0,065663	0,009542	0,001838	0,000246	0,282298	0,000064
09a	wz magm	62	246	0,410	98194	4,729	1,29	0,0805	0,67		1209	13	6,94	0,34	0,074852	0,011209	0,002247	0,000327	0,282369	0,000079
10a	wz magm	114	433	0,614	10995	4,750	1,00	0,0823	0,56	-0,09	1252	11	6,91	0,31	0,117201	0,004714	0,003558	0,000139	0,282251	0,000064
11a	wz magm	109	419	0,586	1044	4,853	0,98	0,0815	1,07		1235	21	7,08	0,32	0,073582	0,004726	0,002190	0,000127	0,282278	0,000046
12a	wz magm	92	353	0,496	10431	4,694	0,92	0,0812	0,67		1226	13	6,76	0,34	0,105132	0,008893	0,003315	0,000256	0,282319	0,000079
13a	wz magm	100	379	0,465	116631	4,592	0,93	0,0812	0,56	0,14	1226	11	6,73	0,32	0,031193	0,003855	0,000959	0,000098	0,282259	0,000036
14a	wz magm	27	110	0,306	21381	4,741	1,01	0,0818	1,15		1240	22	6,54	0,34						
15a	wz magm	23	91	0,291	15573	4,726	0,94	0,0832	1,21		1273	23	6,60	0,35						
16a	wz magm	60	234	0,373	13873	4,669	0,93	0,0808	1,04		1216	20	6,10	0,34						
17a	wz magm	53	220	0,287	7860	4,879	0,93	0,0796	1,05		1188	21	7,49	0,33						
18a	wz magm												6,35	0,33						
19a	wz magm												6,74	0,30						
20a	wz magm												6,44	0,37						
21a	wz magm												6,48	0,34						
22a	wz magm												6,27	0,35						
Morrow n3422 ***(Post-kinematic granite)***																				
05a	wz B OD	183	626	0,269	127547	4,017	1,01	0,0910	0,41		1447	8	6,58	0,32	0,046009	0,001089	0,001671	0,000039	0,282149	0,000039
06a	*uz D OD*	*726*	*4357*	*0,220*	*1025*	6,922	1,93	*0,0736*	*2,34*	*-1,34*	*1030*	*47*	9,59	0,37	0,061405	0,000841	0,002369	0,000027	0,282228	0,000031
07a	wz D OD	95	308	0,341	77124	3,850	0,98	0,0923	0,57		1473	11	8,09	0,32	0,048300	0,000406	0,001743	0,000012	0,282133	0,000037
08a	zoned D OD	156	508	0,362	23421	3,900	1,03	0,0917	0,42		1461	8	6,87	0,30	0,053112	0,001539	0,001927	0,000046	0,282136	0,000047
08b	wz B YD	296	1555	0,031	106132	5,686	0,96	0,0737	0,37		1035	7	7,33	0,30	0,075072	0,002737	0,002583	0,000076	0,282102	0,000036
09a	*wz B YD edge*	*272*	*1405*	*0,070*	*8939*	5,632	0,94	*0,0719*	*0,47*	*4,13*	*982*	*9*			0,039323	0,000513	0,001642	0,000020	0,282270	0,000035
10a	*wz D OD crack*	*95*	*335*	*0,318*	*476*	4,184	0,92	*0,0891*	*1,43*		*1406*	*27*			0,046444	0,001130	0,001704	0,000037	0,282141	0,000035
11a	uz B YD	223	1141	0,147	130097	5,706	0,95	0,0733	0,38		1022	8	7,08	0,33						
11b	*wz D OD*	*142*	*474*	*0,339*	*5106*	3,976	0,92	*0,0925*	*0,56*		*1478*	*11*	6,53	0,33	0,049340	0,002439	0,001813	0,000084	0,282192	0,000053
12a	uz D OD	195	647	0,325	78904	3,976	0,92	0,0907	0,44		1440	8	6,62	0,30	0,052986	0,001633	0,001977	0,000055	0,282174	0,000033
12b	*Altered B*	*231*	*1019*	*0,198*	*264448*	5,019	2,01	*0,0796*	*1,24*		*1188*	*24*	6,53	0,34						
12c	uz D OD	240	813	0,333	222023	4,043	0,95	0,0913	0,34		1453	7	6,60	0,32	0,046882	0,001139	0,001742	0,000040	0,282176	0,000037
13a	*uz D OD edge*	*1073*	*6080*	*0,329*	*1771*	6,694	3,14	*0,0719*	*1,94*		*982*	*39*	8,35	0,32	0,072125	0,001321	0,002809	0,000038	0,282264	0,000027
13b															0,071957	0,001375	0,002770	0,000041	0,282273	0,000032
14a	wz B OD	254	844	0,371	19744	3,985	0,95	0,0899	0,36		1424	7	6,71	0,33	0,036867	0,000297	0,001337	0,000010	0,282140	0,000038
14b	wz B OD	247	818	0,377	719706	3,974	0,92	0,0901	0,50		1427	9	6,80	0,30						
15a	wz B OD	244	773	0,442	112447	3,861	0,94	0,0909	0,37	0,34	1445	7	7,07	0,33	0,078470	0,001508	0,002434	0,000042	0,282123	0,000045

[a] Italics denote discordant data not used for age calculation

[b] BSE: D dark, B bright; oscz oscillatory zoned, wz weakly zoned, uz unzoned, magm magmatic, crack spot intersects with crack,

[c] % of common ^{206}Pb in measured ^{206}Pb, estimated from ^{204}Pb assuming a present day Stacey and Kramers (1975) model for terrestrial Pb-isotope

[d] Age discordance at closest approach of error ellipse to concordia (2σ level).

Tabel. 2.continued

Sample/[a] spot #	Structural class/[b] (from BSE)	Pb (ppm)	U (ppm)	Th/U calc.	$^{206}Pb/^{204}Pb$ meas.	$^{238}U/^{206}Pb$ corrected	±σ %	$^{207}Pb/^{206}Pb$ corrected	±σ %	Disc. %/[d] 2σ limit	$^{207}Pb/^{206}Pb$ age (Ma)	±σ	$\delta^{18}O$	±‰	mass bias and interference corrected 176Yb/177Hf	2SE	mass bias and interference corrected 176Lu/177Hf	2SE	mass bias and interference corrected 176Hf/177Hf	2SE
Morrow n3422 *(Post-kinematic granite) continued*																				
15b	wz D OD	105	351	0,318	70383	3,960	0,93	0,0924	0,55		1476	10	7,65	0,31						
15c	wz D OD	80	272	0,276	47484	3,975	0,95	0,0925	0,62		1478	12	6,74	0,31						
16a	wz D OD	125	430	0,272	20827	4,026	0,92	0,0904	0,66		1435	13	6,69	0,33						
17a	wz B OD	437	1417	0,340	205972	3,863	0,93	0,0917	0,27		1462	5	6,56	0,31						
18a	wz B YD	297	1557	0,077	102598	5,753	0,92	0,0734	0,36		1025	7	7,39	0,37						
19a	wz B OD	236	780	0,324	39305	3,916	0,92	0,0905	0,42		1436	8	6,31	0,34						
20a	*Altered D*	*816*	*4765*	*0,366*	*917*	6,976	0,68	*0,0710*	*0,64*	*-5,92*	*957*	*13*			0,078168	0,000415	0,002819	0,000008	0,282270	0,000040
20b															0,068350	0,001021	0,002492	0,000041	0,282271	0,000039
21a	wz B YD	523	2598	0,193	55930	5,609	0,77	0,0732	0,28	1,54	1020	6			0,041285	0,001080	0,001719	0,000028	0,282249	0,000026
22a	*Altered & OD*	*410*	*2435*	*0,142*	*580*	6,627	0,87	*0,0706*	*2,04*		*947*	*41*								
23a	*Altered & OD*	*397*	*2001*	*0,231*	*4642*	5,753	0,74	*0,0728*	*0,41*		*1010*	*8*			0,043784	0,003869	0,001493	0,000124	0,282242	0,000048
24a	uz D OD	302	995	0,311	123572	3,884	0,77	0,0911	0,26	0,11	1448	5	6,87	0,33						
24b	*Altered & OD*	*430*	*2109*	*0,058*	*8566*	5,350	0,80	*0,0747*	*1,03*		*1062*	*21*	7,80	0,34						
25a	wz B YD												7,45	0,34						
26a	uz D OD												7,22	0,32						
27a	uz B OD												6,82	0,34						
Herman n3423 *(Meta-granite)*																				
01a	zoned B OD	124	615	0,154	68850	5,570	0,96	0,0745	0,53		1056	11	7,80	0,33	0,036580	0,000497	0,001426	0,000018	0,282191	0,000040
02a	zoned D OD	119	610	0,173	56399	5,749	0,94	0,0740	0,55		1041	11	7,76	0,33	0,067246	0,011929	0,002186	0,000342	0,282177	0,000057
03a	zoned D OD	129	714	0,159	26828	6,239	0,94	0,0749	0,53	-7,19	1067	11	8,16	0,35	0,066014	0,012626	0,002176	0,000373	0,282260	0,000049
04a	zoned B OD	103	512	0,161	56604	5,579	0,94	0,0745	0,59		1054	12	7,53	0,36	0,041504	0,000609	0,001525	0,000017	0,282173	0,000045
04b	zoned B OD	86	416	0,219	26617	5,477	0,94	0,0739	0,70		1038	14	7,75	0,33						
05a	zoned B YD	148	701	0,188	43259	5,356	0,72	0,0742	0,45	2,48	1048	9	8,47	0,34	0,365528	0,051446	0,010797	0,001490	0,282229	0,000062
06a	zoned B OD	307	1577	0,118	16201	5,702	0,86	0,0742	0,32		1047	6	7,73	0,37	0,113666	0,016409	0,003697	0,000467	0,282191	0,000034
07a	zoned B OD	134	654	0,120	76714	5,429	0,76	0,0745	0,42	0,44	1055	8			0,107066	0,010077	0,003395	0,000276	0,282177	0,000043
08a	zoned B YD	152	845	0,108	25196	6,149	0,70	0,0740	0,41	-4,20	1040	8	8,97	0,38	0,665313	0,037321	0,019575	0,001063	0,281991	0,000107
09a	zoned B OD	171	817	0,192	59073	5,400	0,78	0,0745	0,39	1,25	1054	8	9,42	0,31	0,091886	0,006143	0,002749	0,000156	0,282188	0,000060
9b	zoned B OD												7,44	0,39						
10a	zoned B OD												8,86	0,34						
11a	zoned B OD												8,22	0,38						
12a	zoned B OD												8,28	0,34						
13a	zoned B OD												8,32	0,43						
14a	zoned B OD												6,79	0,37						
15a	zoned B YD												9,12	0,32						
16a	zoned B YD												9,10	0,47						
Hopkins n3424 *(Meta-pegmatite)*																				
01a	uz D	29	76	0,634	12572	3,379	0,92	0,1031	1,02		1681	19	5,57	0,41	0,031702	0,000868	0,001018	0,000024	0,281842	0,000043
01b	uz D	29	78	0,622	26931	3,481	0,96	0,0992	1,55		1610	29	4,60	0,39						
02a	uz D crack	29	87	0,463	12780	3,695	1,02	0,1001	1,25		1626	23	5,77	0,36	0,013269	0,001830	0,000444	0,000058	0,282110	0,000080
03a	uz D	19	51	0,576	14411	3,399	1,06	0,1028	1,27		1676	23	5,96	0,47	0,018236	0,000109	0,000599	0,000012	0,281917	0,000063
03b	uz D	19	54	0,546	8355	3,609	0,97	0,0975	1,43		1577	27	5,23	0,37						
Scioto n3427, n3428 & n3429 (Orthogneiss to post-kiematic granite)																				
27-01a	*uz D OD*	*737*	*4885*	*0,024*	*8318*	7,164	0,69	*0,0717*	*0,23*	*-12,79*	*977*	*5*	8,17	0,34						
27-02a	*uz D OD*	*15*	*65*	*1,382*	*342*	6,326	0,68	*0,0701*	*5,17*		*930*	*103*	10,97	0,37						
27-03a	*uz D OD crack*	*217*	*5066*	*0,026*	*540*	24,778	0,68	*0,0512*	*1,57*		*252*	*36*	11,16	0,35						
27-04a	*uz D OD crack*	*490*	*3151*	*0,014*	*6336*	6,926	0,71	*0,0720*	*0,31*	*-10,20*	*986*	*6*								
27-05a	*uz D OD crack*	*356*	*3859*	*0,056*	*870*	11,810	0,83	*0,0648*	*1,48*	*-20,82*	*767*	*31*								
27-06a	*uz D OD crack*	*356*	*3364*	*0,028*	*1404*	10,179	0,71	*0,0663*	*0,78*	*-21,10*	*816*	*16*								

[a] Italics denote discordant data not used for age calculation

[b] BSE: D dark, B bright; oscz oscillatory zoned, wz weakly zoned, uz unzoned, magm magmatic, crack spot intersects with crack,

[c] % of common ^{206}Pb in measured ^{206}Pb, estimated from ^{204}Pb assuming a present day Stacey and Kramers (1975) model for terrestrial Pb-isotope

[d] Age discordance at closest approach of error ellipse to concordia (2σ level).

Tabel. 2.continued

Sample/[a] spot #	Structural class/[b] (from BSE)	Pb (ppm)	U (ppm)	Th/U calc.	$^{206}Pb/^{204}Pb$ meas.	$^{238}U/^{206}Pb$ corrected	±σ %	$^{207}Pb/^{206}Pb$ corrected	±σ %	Disc. %/[d] 2σ limit	$^{207}Pb/^{206}Pb$ age (Ma)	±σ	$\delta^{18}O$	±‰	mass bias and interference corrected 176Yb/177Hf	2SE	mass bias and interference corrected 176Lu/177Hf	2SE	mass bias and interference corrected 176Hf/177Hf	2SE
Scioto n3427, n3428 & n3429 (Orthogneiss to post-kiematic granite) continued																				
27-07a	*uz D OD crack*	*258*	*4170*	*0,028*	*798*	17,379	2,60	*0,0598*	*1,27*	*-27,14*	*595*	*27*	13,27	0,33						
27-07b	*uz B YD*												10,83	0,37						
27-08a	*uz D OD*	*368*	*4349*	*0,017*	*1406*	12,685	0,94	*0,0648*	*0,52*	*-33,28*	*769*	*11*								
27-09a	*uz D OD crack*	*262*	*2800*	*0,029*	*872*	11,512	3,12	*0,0648*	*1,23*	*-20,38*	*767*	*26*	14,77	0,40						
27-10a	*uz B YD*												10,50	0,32						
27-11a	*Altered B OD*												10,60	0,36						
27-12a	*uz B YD*												10,49	0,39						
27-13a	*uz D YD*												10,62	0,40						
28-01a	uz B YD	316	1663	0,108	>1e6	5,827	0,72	0,0735	0,26		1029	5	10,64	0,35	0,052331	0,007588	0,002049	0,000260	0,282256	0,000049
28-02a	uz B YD	320	1668	0,126	428470	5,786	0,68	0,0732	0,26		1019	5	10,61	0,32	0,034559	0,002858	0,001363	0,000095	0,282252	0,000038
28-02b	uz D YD	40	173	1,028	23750	5,663	0,69	0,0736	0,92		1031	19	11,87	0,34						
28-03a	uz D OD	14	17	0,001	9381	8,555	0,73	1,7897	2,09		1028	39	10,52	0,35	0,025231	0,001336	0,000966	0,000044	0,282276	0,000035
28-04a	*uz D OD crack*	*575*	*4588*	*0,007*	*3296*	4,082	0,68	*0,0701*	*0,30*	*-22,43*	*931*	*6*			0,148624	0,013225	0,004639	0,000377	0,282342	0,000035
28-05a	*uz D OD inclusion*	*147*	*499*	*0,380*	*2847*	10,413	0,91	*0,0890*	*0,89*		*1404*	*17*			0,092952	0,000634	0,002748	0,000023	0,282198	0,000063
28-06a	*uz D OD crack*	*277*	*2598*	*0,094*	*742*	13,468	3,60	*0,0676*	*0,81*	*-26,16*	*856*	*17*								
28-07a	*uz D OD*	*266*	*3369*	*0,005*	*725*	5,483	0,68	*0,0609*	*1,51*	*-13,58*	*637*	*32*								
28-08a	OD & YD inclusion	807	4110	0,007	34145	10,276	0,69	0,0740	0,18	2,33	1040	4	9,58	0,35						
28-09a	*uz D OD crack*	*388*	*3716*	*0,012*	*1752*	9,220	1,33	*0,0676*	*0,43*	*-28,03*	*855*	*9*								
28-10a	uz B YD	265	1366	0,127	199178	15,069	0,74	0,0726	0,31	0,90	1002	6	10,09	0,34	0,034559	0,002858	0,001363	0,000095	0,282252	0,000038
28-10b	*uz B YD*												10,29	0,33						
28-11a	uz B YD	423	2216	0,093	42971	12,136	0,92	0,0729	0,25		1010	5	12,15	0,37	0,031284	0,002173	0,001235	0,000066	0,282230	0,000044
28-12a	uz B YD	333	1707	0,120	156507	9,845	0,78	0,0734	0,27		1025	5	11,23	0,35	0,070937	0,006465	0,002416	0,000185	0,282224	0,000050
28-13a	uz B YD	364	1908	0,053	612483	9,362	0,68	0,0736	0,26		1031	5	11,03	0,35	0,027925	0,000504	0,001076	0,000010	0,282265	0,000037
28-14a	uz B YD	52	227	1,031	16769	10,567	1,61	0,0714	0,82		970	17	11,72	0,33	0,042892	0,002031	0,001472	0,000042	0,282271	0,000042
28-15a	uz B YD	266	1380	0,122	142951	11,334	0,85	0,0728	0,32		1008	6	10,36	0,36	0,054848	0,003862	0,001813	0,000117	0,282247	0,000041
28-16a	uz B YD	361	1851	0,064	240590	5,998	1,05	0,0733	0,26	1,16	1023	5	9,93	0,41						
28-17a	uz B YD	263	1356	0,104	564123	5,726	1,04	0,0734	0,32		1026	6	10,63	0,34						
28-18a	uz B YD												10,71	0,39						
28-19a	uz B YD												11,26	0,34						
28-20a	uz B YD												10,97	0,35						
28-21a	uz B YD												11,33	0,31						
29-01a	*uz D OD*	*312*	*2685*	*0,003*	*196*	5,760	1,05	*0,0708*	*11,24*		*953*	*214*	10,53	0,36						
29-02a	*uz D OD*	*312*	*4413*	*0,006*	*372*	5,691	1,05	*0,0637*	*2,33*	*-24,38*	*731*	*49*								
29-02b	*uz D OD crack*	*330*	*3738*	*0,004*	*471*	5,707	1,06	*0,0676*	*1,03*	*-33,99*	*857*	*21*								
29-03a	*uz D OD*	*275*	*2526*	*0,009*	*857*	5,942	1,05	*0,0672*	*0,74*	*-21,69*	*844*	*15*	13,71	0,37						
29-04a	*uz D OD*	*601*	*5234*	*0,006*	*1677*	5,753	1,05	*0,0716*	*0,44*	*-31,52*	*976*	*9*								
29-05a	*uz D OD crack*	*248*	*2449*	*0,016*	*261*	5,596	1,04	*0,0647*	*2,38*	*-5,72*	*765*	*49*								
29-06a	*uz D OD*	*266*	*2808*	*0,015*	*762*	5,697	1,05	*0,0655*	*1,11*	*-23,48*	*791*	*23*								
29-07a	*uz B YD*												10,34	0,38						
29-08a	*uz D YD*												11,50	0,44						
29-09a	*uz D YD*												11,18	0,34						
29-10a	*uz B YD*												11,66	0,34						
29-11a	*uz B YD*												10,85	0,41						
29-12a	*uz B YD*												11,51	0,42						
29-13a	*uz B YD*												11,67	0,38						
29-14a	*uz D OD*												11,99	0,40						

[a] Italics denote discordant data not used for age calculation

[b] BSE: D dark, B bright; oscz oscillatory zoned, wz weakly zoned, uz unzoned, magm magmatic, crack spot intersects with crack,

[c] % of common ^{206}Pb in measured ^{206}Pb, estimated from ^{204}Pb assuming a present day Stacey and Kramers (1975) model for terrestrial Pb-isotope

[d] Age discordance at closest approach of error ellipse to concordia (2σ level).

(non-crystalline) non-annealing crystal lattice at cool surface conditions (Fig. 4A, Faure & Mensing, 2005). In an inverse Tera-Wasserburg diagram, this is seen as horizontal displacement of the zircon to the right of the concordia curve (Fig. 4A). Alternatively, apparent recent Pb-loss or Pb-enrichment/U-loss might be caused by incorrect U/Pb calibration, which will result in horizontal data displacement towards the right and left respectively. Notably, for any recent Pb-loss, the $^{207}Pb/^{206}Pb$ date is unaffected, or will represent a minimum age. Episodic Pb-loss might occur due to e.g. ancient metamorphic events or other processes that cause partial Pb-loss. For incomplete processes, partial Pb-loss will be recorded as a point located in between the initial crystallization age and the Pb-loss event (Fig. 4B). Importantly, such data cannot be distinguished from recent Pb-loss in the case of a single data point c.f. Fig. 4A and B. This example highlights that discordant $^{207}Pb/^{206}Pb$ dates are minimum ages. Common Pb has high $^{207}Pb/^{206}Pb$ ~1, which will displace the data point along a steep path towards high $^{207}Pb/^{206}Pb$ dates (Fig. 4C). If different zircon fractions lose different amounts of Pb in a single episodic Pb-loss event, they will plot on a straight line with the upper intercept defining the time of crystallization and the lower intercept defining the time of the Pb-loss event. This line is called a discordia (Fig. 4D). For a discordia to be meaningful, the U/Pb ratios must be accurately measured and the effects of cPb and recent Pb-loss must be negligible.

3.5 Secondary Ion Mass Spectrometry (SIMS)

The Secondary Ion Mass Spectrometer (SIMS) is a powerful instrument for the *in situ* analysis of the chemical and isotopic compositions of small volumes of solid materials. A beam of high energy primary ions are focused onto the area of interest and eroding a crater in a shape of an ellipse, with a spatial precision of 10-25 µm across. The penetration at depth is less than <2 µm and the mass sputtered is in the range of 10^{-10} to 10^{-9} g (Stern 2009). The SIMS analysis can hence be regarded as a surface analytical technique. Atoms and molecules sputtered by the high energy primary ions are focused into a secondary ion beam, later captured by a detector after passing a mass analyser. The primary beam is produced through a cold-cathode duoplasma and the ion of choice, predominantly $^{16}O^-$ or O_2^-, is filtered out. The secondary ions are focused trough electrostatic lenses and deflectors into a curved electrostatic energy filter, which bend low energy ions more than high energy ones. (Ireland & Williams, 2003) The apparatus filter the energy spectrum of interest and those ions enter a magnetic sector, i.e. the mass analyser. This sector is also curved and separate ions by mass/z ratio, were z is the ionic valence. An ion multiplier captures the separated ions. The ions are measured sequentially through dynamic peak jumping where each mass is counted for a short time period before it switches to the next mass (Bennighoven et.al. 1987).

3.6 Secondary Ion Mass Spectrometry (SIMS) in U-Th-Pb on Zircon

For zircon U-Pb dating, U, Th, Pb, ^{204}Pb, ^{206}Pb, ^{207}Pb, ^{208}Pb, ThO, Zr_2O and either ^{235}U and ^{238}U or their oxides UO and/or UO_2 are measured (Bennighoven et.al., 1987). Zr_2O is measured as an internal standard for concentration calculations of the different elements. The Pb isotope ratios are measured for age calculations and common Pb corrections. U is measured for concentrations and U/Pb and ThO is used for Th/Pb. Resolving isobaric interferences between different ions or ion complexes is important, and high mass resolution is therefore required. For example, $HfO_2^-$and $HfSi^-$ have similar mass to the Pb ions as well as some of the REE hydroxides, Hg^+ and WO^+. For example, some of these interferences can produce apparent high cPb concentrations resulting in overcorrected isotopic Pb-ratios.

Standards are always used as reference material to normalize data and to calibrate element ratios. Zircon with uniform and known distribution of Pb, U and Th content and uniform and known ratios is used as standard material. These standards are continuously measured before, in between, and after analysis of natural samples to detect variations and fluctuations in the measurements. This procedure enables the correction of mass bias, mass fractionation and other fluctuations (Ireland and Williams, 2003).

In this study SIMS zircon analysis was made at the NORDSIM facility, at the Swedish Museum of Natural History, using a Cameca IMS 1280. Analytical procedures followed Whitehouse et al. (1999) and Whitehouse & Kamber (2005). The primary beam was focused to a ~15µm large ellipse and set at ~5nV. Calculations and diagrams were produced using Isoplot 3.70 (Ludwig 2008).

3.7 O- analysis on zircon

O is the most abundant element on Earth with three naturally occurring isotopes, ^{16}O, ^{17}O and ^{18}O. Their abundances are ^{16}O: 99.763%, ^{17}O: 0.0375% and ^{18}O: 0.1995%. Since they are all stable and non-radiogenic, mass-dependent fractionation is the foremost process that varies their ratios, although other physio-chemical processes such as kinetic effects are also important due to their differences in properties (Hoefs 1997).

Water evaporation enriches the lighter ^{16}O isotope in the vapour phase because of its lower mass. This leads to a difference in isotopic composition between the vapour and residual liquid phase. The isotopic difference is reported as the relative deviation from Standard Mean Ocean Water (SMOW) in parts per mil; a standard defined by Craig (1961) and is calculated according to equation 3 (Faure & Mensig, 2005).

$$\delta^{18}O = [(^{18}O/^{16}O)_{spl}/(^{18}O/^{16}O)_{SMOW}-1] \times 10^3 \qquad [eq. 3]$$

Different geological reservoirs range over different spans of $\delta^{18}O$ values as outlined by Hoefs (1997) who lists the most important geological reservoirs and their respective spans of $\delta^{18}O$ values, viz. meteoric water ~-45‰ to 10‰, ocean water ~0‰, sedimentary rocks ~5‰ to 40‰, metamorphic rocks ~0‰ to 25‰, granitic rocks ~-5‰ to 15‰ and basaltic rocks ~5‰ to 10‰. Chondritic meteorites, bulk Earth and MORB all have values around 5.7‰ $\delta^{18}O$ (Rollinson 1993; Fig. 5).

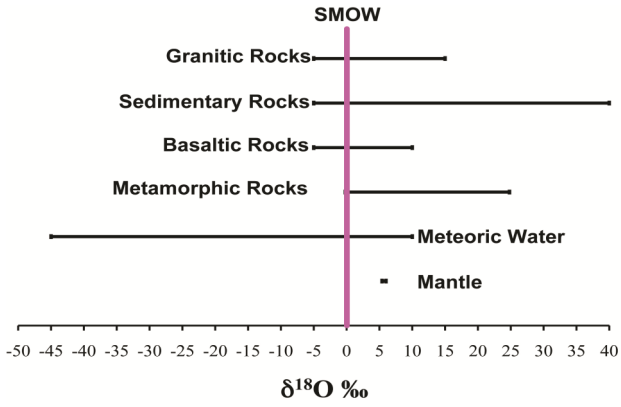

Fig. 5. 'Caltech' diagram (i.e. something plotted against nothing) for different geological reservoirs showing their respective $\delta^{18}O$ span. Data from Rollinson (1993).

As noted above, continental crust displays greater variation in $\delta^{18}O$ relative to the Earth's Mantle (Fig. 5). This, and the fact that non-metamict zircon generally preserve their $\delta^{18}O$ values of crystallization (Valley et al. 2005), makes it possible to recognize crustal recycling and to get an indication of the composition of the host rock. However, zircon O- isotope ratios are only applicable with textural control (Valley 2003). Overgrowths, mixed inherited and new age domains or radiation damaged areas can all cause misleading results.

3.8 Laser Ablation Inductively Coupled Plasma Mass Spectrometry (LA-ICP-MS)

LA-ICP-MS is used to determine isotopic ratios of various solid materials. Detailed description of the methodology is found in Košler & Sylvester (2003) and in Frei & Gerdes (2009).

In (Multi Collector) LA-(MC)-ICP-MS a pulsed laser beam, of high intensity photons with uniform wavelength, is used to create aerosols through vaporization and ablation. These aerosols are transported through plastic tubing into the inductively coupled argon plasma. The plasma is a hot, radiant, and partially ionized and produces temperatures in the region of 8.000-10.000 K. The plasma generates ions that are led into the mass analyser (predominantly singly charged cations). A magnetic field separates the ions according to their mass to charge ratios (as explained above). LA-ICP-MS also allows *in situ* measurements and small amounts of sample even though the craters are about 20-40 μm^3 larger than for conventional SIMS analyses.

3.9 Hf analysis on Zircon

^{176}Lu decays via β^- to ^{176}Hf with a mean $\lambda^{176}Lu$ of $1.867 \pm 0.008 \times 10^{-11}$ $year^{-1}$ (Söderlund et al. 2004). ^{177}Hf is used as the reference isotope because of its constant natural abundance. During partial melting, Lu/Hf fractionation is driven by the higher incompatibility of Hf over Lu. This has led to a depleted mantle with suprachondritic $^{176}Hf/^{177}Hf$ and a crust with subchondritic $^{176}Hf/^{177}Hf$. At the time of Earth formation, the Hf isotope composition was chondritic and has since fractionated into its present reservoirs. The divergence of the Hf isotopic composition is measured as parts per ten thousand deviations from a Chondritic Uniform Reservoir (CHUR):

$$\varepsilon_{Hf}=[(^{176}Hf/^{177}Hf)_t/(^{176}Hf/^{177}Hf)_{Chondrites}-1] \times 10^4 \quad [eq4]$$

Positive ε_{Hf} values indicate that the sample has higher $^{176}Hf/^{177}Hf$ value than the chondritic reference at the time t, hence derived from a depleted source. Negative values indicate derivation from an enriched source, either through remelting of depleted mantle derived crust with extended residence time or through mixing between depleted juvenile components and ancient enriched crust (Kinny & Maas 2003).

Mixing of juvenile magma and reworked crustal components adds complexity to the system and is not uncommon. Also, sectored crystal grains such as complex zircon with core-rim relations can indicate mixing or give misleading, geologically insignificant results if one does not have full textural control. *In situ* analyses guided by BSE/CL imaging is therefore required (Kinny and Maas, 2003).

In a zircon the $^{176}Lu/^{177}Hf$ is normally very low (in situ Greenland zircon yield $^{176}Lu/^{177}Hf = 0.0008 \pm 0.0005$, 1σ, n=244; A. Scherstén *pers. comm.*). This means that the effect of radiogenic Hf on the $^{176}Hf/^{177}Hf$ is almost negligible and the zircon preserves the initial crystallization $^{176}Hf/^{177}Hf$. This ratio can be used to calculate model Hf-ages, as part of a Lu/Hf isochron and to determine initial ε_{Hf} values. To accomplish the latter, a crystallization age of the sample must be known, eg. by U-Pb dating (Kinny & Maas 2003).

3.10 Analytical method of Hf analysis on Zircon

All Hf-analysis was made *in situ* at the Memorial University, St Johns, New Foundland, Canada, using a Finnigan Neptune Multicollector ICP-MS connected to a GeoLas Laser ablation system. The Multi Collector LA-ICP-MS was equipped with nine Faraday detectors and ^{171}Yb, ^{173}Yb, $^{174}Hf+Yb$, ^{175}Lu, $^{176}Hf+Yb+Lu$, ^{177}Hf, ^{178}Hf and ^{179}Hf data was collected during 600 pulses, ~60 seconds. Laser repetition rate of 10 Hz was applied and laser flux was maintained at 5 J/cm^2. Abla-

tion was conducted with He carrier gas in the ablation cell and with Ar makeup carrier gas added afterwards via T-piece just before the torch. The gas background was measured for 30 s in the beginning of each run and used for blank corrections. Blank corrected signal intensities were corrected for isobaric interferences of Yb and Lu on ^{176}Hf. ^{179}Hf/^{177}Hf = 0.7325 (Patchett & Tatsumoto 1980) and the exponential law, was used for mass bias correction of Hf. ^{173}Yb/^{171}Yb = 1.1301 and ^{176}Yb/^{171}Yb = 0.7938 (Segal et al. 2003), with the exponential law, was used for mass bias correction of Yb. No invariant ratio for Lu is available as Lu only has two naturally occurring isotopes (^{175}Lu and ^{176}Lu). Therefore it was assumed that the mass bias constant for Lu is the same as for Yb, which β-value was used to correct for Lu with ^{176}Lu/^{175}Lu = 0.2656 (Chu et al. 2002).

In this study, zircon phases dated by U-Pb analyses were also used for Hf-analysis. Some extra spots, in other grains, were added to obtain statistically satisfying data. A spot size between 49 and 69 µm was used as close to U-Pb craters as possible. Cracks, inclusions and texturally complex domains were avoided. Data quality was controlled using standards Plesovice (Sláma et al 2008), R-33 (Black et al 2004), FC-1 and Temora (Woodhead & Hergt 2005).

Depleted Mantle values (^{176}Hf/^{177}Hf = 0.283250 & ^{176}Lu/^{177}Hf = 0.0384) from Nowell et al. (1998) were used in calculations.

3.11 Zircon O-Hf isotopes

Combined zircon O-Hf data allows the discrimination between new and recycled crust (Hawkesworth & Kemp 2006). Furthermore, because zircon is chemically highly robust, the Hf and O isotope ratios can/may remain undisturbed even through high-grade metamorphism (Gerdes & Zeh 2009).

Kemp et al. (2006) demonstrate the strength of the zircon approach with recent data from southeast Australia where detrital and inherited zircon were analysed for U-Pb ages, Hf and O isotope compositions. Their zircon yield an age distributions range from ~3.2 to 0.5 Ga with crystallization peaks at 1.1 and 0.5 Ga. This suggests crust formation peaks at these ages. Nevertheless, when zircon U-Pb age data is combined with Hf and O-isotopes, low δ^{18}O zircon plot along two well-defined arrays in time-ε_{Hf} space (Fig. 6 and Fig. 7). These two arrays point to crustal formation events that are not recorded in the zircon age data. Each array likely represents extended crustal residence times of juvenile components, which were derived from a depleted mantle source at around 3.3 and 1.9 Ga respectively. Zircon with heavy δ^{18}O (>6.5 ‰) scatter between the two arrays implies mixed sources between at least two contrasting reservoirs, which should be enveloped by the arrays if no other primary source components are involved (Kemp et al. 2006).

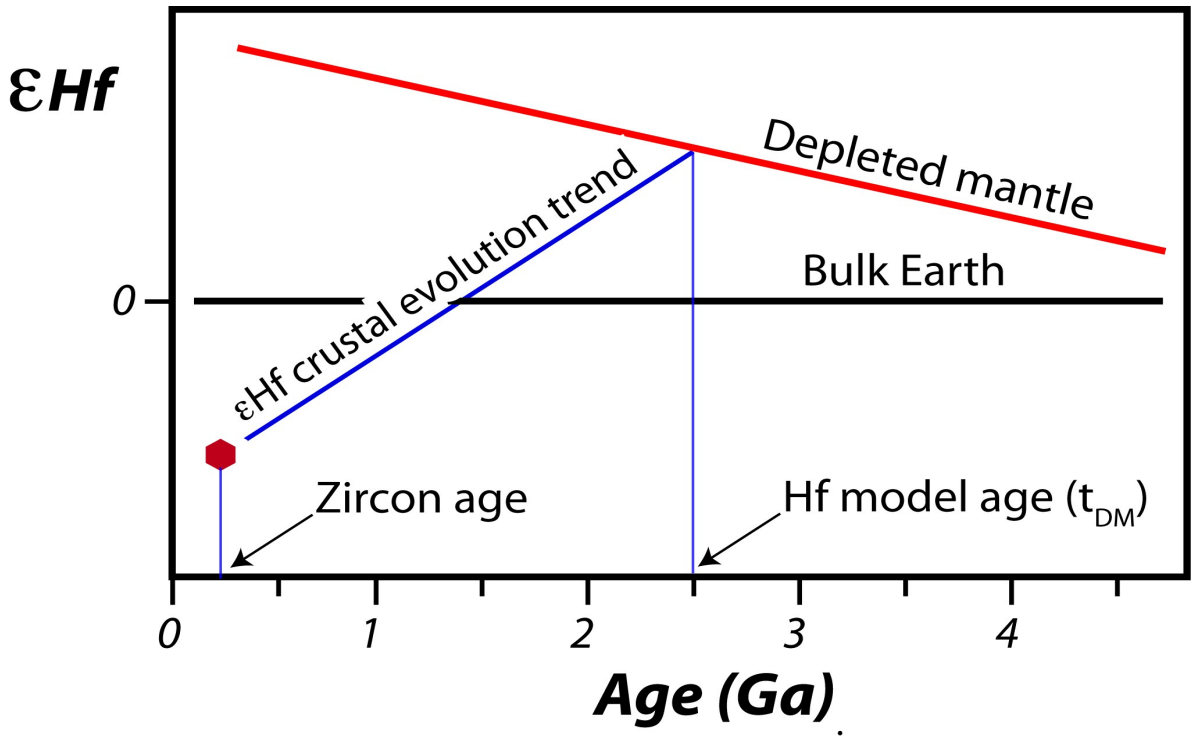

Fig. 6. A schematic age - εHf diagram where ε_{Hf} is the deviation from chondritic uniform reservoir (CHUR $\varepsilon_{Hf} \equiv 0$ = Bulk Earth) in parts per ten thousand. Depleted mantle has suprachondritic Lu/Hf, which leads to positive εHf with time (red curve), while basaltic and granitic crust has sub-chondritic Lu/Hf, which leads to negative εHf with time (blue curve). Zircon has exceptionally low Lu/Hf, and the Hf isotope composition remains nearly constant for eons. U-Pb dating combined with in-situ Hf isotope analyses allows precise plotting of the zircon in the diagram, and a Hf model (t_{DM}) age can be calculated (here 2.5 Ga), i.e. the zircon is derived from crustal precursor material that was extracted from the mantle at t_{DM}.

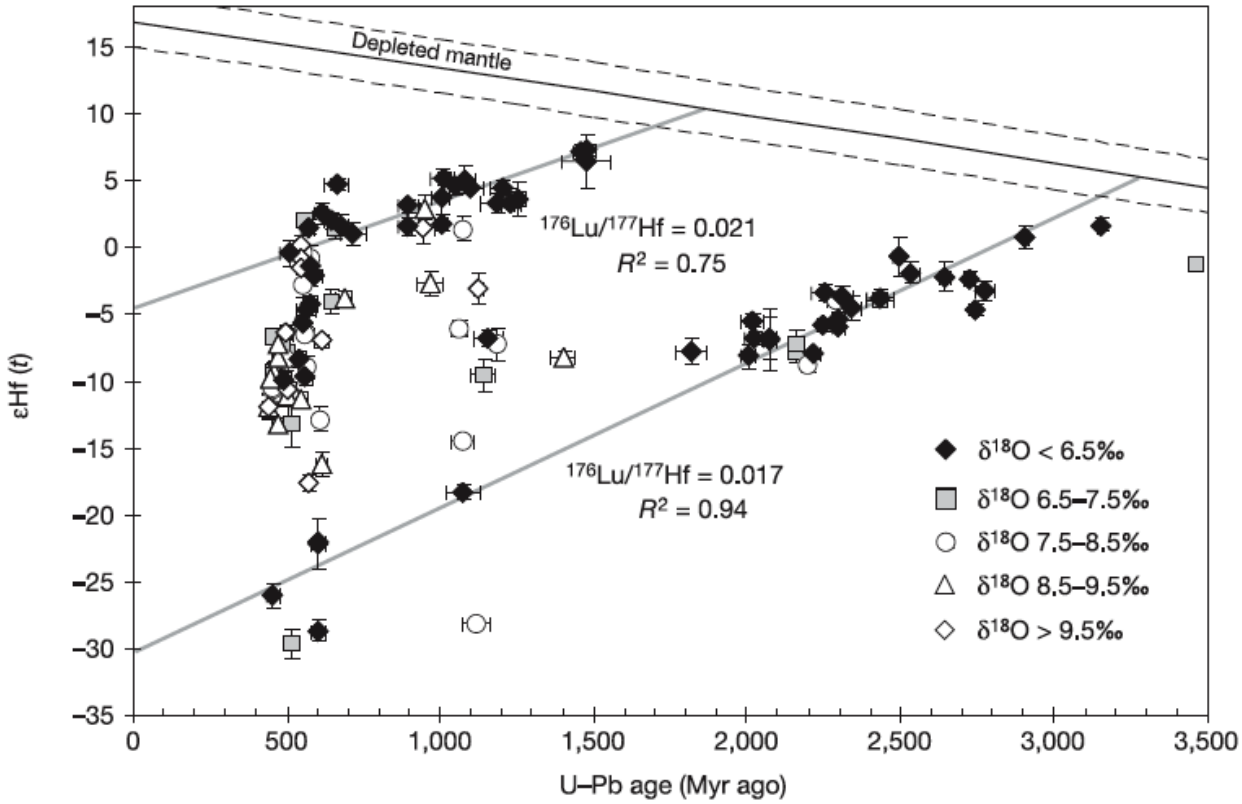

Fig. 7. Plot from Kemp et al. (2006) showing ε_{Hf} versus crystallization age for inherited and detrital zircon, contoured for O-isotope composition. The depleted mantle evolution curve (solid line) was extrapolated from modern-day values. Dashed lines on either side of this curve encompass most of the range shown by modern mid-ocean ridge basalt. Regression lines (grey, with R^2 values indicated) through the two arrays defined by low $\delta^{18}O$ zircon correspond to the Hf isotope evolution of protoliths extracted from the mantle at either 1.87 +0.19/-0.12 Ga or 3.28 ±0.10 Ga, with $^{176}Lu/^{177}Hf = 0.021$ or 0.017, respectively. These $^{176}Lu/^{177}Hf$ ratios fall within the range of values shown by juvenile igneous rocks of all ages. The zircon that plot between the linear arrays presumably reflect melting of mixed-age igneous or metasedimentary precursors during crustal reworking.

4 Samples

Nine samples were taken from six different drill cores penetrating the Precambrian basement of Ohio. One (*Logan*) was taken from the alleged unmetamorphosed foreland, west of the Grenville Front, and eight from the Grenville Province east thereof. The nine samples were collected from drill core as shown in Fig 3, and are listed in Table 3 below.

There is always some uncertainty concerning how representative the samples are of the locality when working with drill core samples. The small amount of sample retrieved from drill cores and the minimal knowledge of the surroundings makes this uncertainty even greater. The petrography and zircon population of the drill core samples are described below. Optical microscopy was used for petrography and additional SEM analysis on textures and mineral inclusions in zircon.

Table. 3. Drill-Core samples

Sample	Core no.	X-coord 83 (UTM zone 17)	Y-coord 83 (UTM zone 17)	Sample depth interval (meter)	Rock description	Operator
Logan	645	1614624,94	290219,16	1005-1006	Acid volcanic	*Ohio Oil co.*
Hopkins Amf	750	1709645,48	546845,74	1144-1435	Mafic Amphibolite	*Kewanee oil co.*
Hopkins Meta peg	750	1709645,48	546845,74	1435-1435.5	Meta-pegmatite	*Kewanee oil co.*
Scioto 6A	2958	1876804,97	215544,3	1710.5-1711	Orthogneiss	*USS Chemicals*
Scioto 6B	2958	1876804,97	215544,3	1711-1711.5	Boundary between 6A & 6C	*USS Chemicals*
Scioto 6C	2958	1876804,97	215544,3	1711.5-1712	Post-kinematic granite	*USS Chemicals*
Morrow	2925	1854064,88	329468,44	1247-1250	Post-kinematic granite	*Empire Reeves*
Herman	2864	2009312,1	599301,02	1357-1357.5	Meta-granite	*Sun Oil co.*
Lake	2904	2335029,49	762090,37	1849.5-1852	Dark fine-grained rock	*Chalio Chemicals inc.*

4.1 Logan (Acid volcanic)

4.1.1 Sample description

The rock analysed from the *Logan* drill core is a deep red aphanitic rock with some lighter areas mainly surrounding phenocrysts (Appendix. 1). Based on the grain size, colour and flow patterns in the rock it is interpreted to be of volcanic origin, possibly lava. The apparent lack of macroscopic metamorphic characteristics and the geographical location of the drill core suggest this sample to be a part of the Eastern Granite Rhyolite Province.

Most of this volcanic rock is aphanitic, and individual minerals are too small to identify. Throughout the sample, phenocrysts of quartz are abundant. Some phenocrysts of chlorite, biotite and feldspar, all altered, are also present but not at all to the same extent. These iron rich fluids have oxidized the rock and opaque phases are abundant both in the aphanitic matrix and as inclusions in chlorite, biotite and feldspars. Thin bands of mica with kinematic indicators such as δ and σ structures around altered phenocrysts are found throughout the thin section. Together with the mica, small amounts of quartz are found. Some cracks in the rock are also filled with mica and quartz.

Except for the thin bands of mica, no metamorphic indicators are found in this rock, suggesting a low grade of metamorphism.

4.1.2 Zircon

Zircon appear as phenocrysts, and are simple euhedral crystals, randomly distributed in the thin section. Zircon grains are 30-100 µm along the C-axis and 20-50 µm along the A/B-axis in this sample (Fig. 8). They are, transparent with no morphological signs of secondary alteration.

In BSE-images oscillatory growth zoning is visible in all grains. Cracks are present but not abundant. Inclusions of apatite, feldspars and/or pyrite are found in most grains. The zircon grains do not show any signs of alteration after igneous crystallization.

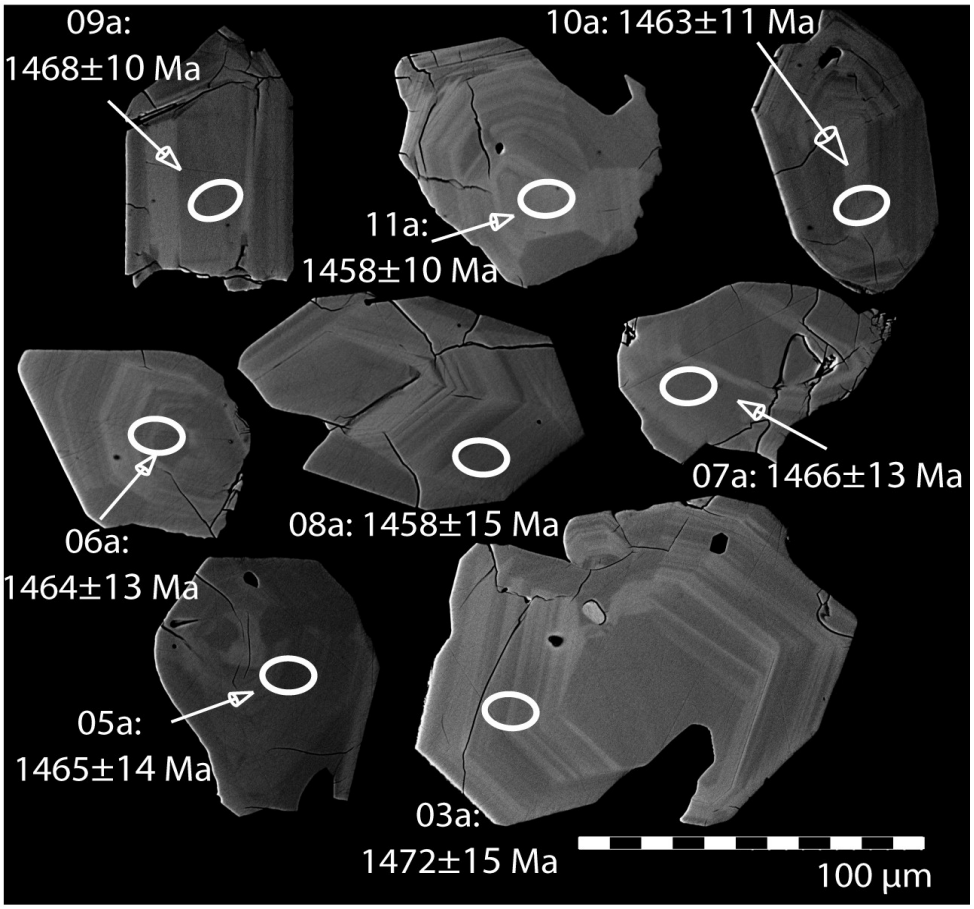

Fig. 8. Back Scattered Electron (BSE) images for selected zircon grains from the *Logan* drill-core sample. Analysis sites for ion microprobe age determinations are marked with white ellipses. Spot numbers with corresponding $^{207}Pb/^{206}Pb$ ages (Ma) are given for each spot. In most instances, these analysis sites are identical to those for the O- and Hf- isotope analyses. Note however, that the Hf analysis spot radius is about two to three times the size of the U-Pb spots while the O spot size and location is identical to those for U-Pb.

4.2 Hopkins

4.2.1 Sample description

The Hopkins core is composed of interlayered metasupracrustal and metaigneous rocks. Two samples were selected, amphibolite and deformed metapegmatite.

4.2.1.1 Hopkins 2A (Amphibolite)

This is a fine to medium grained dark grey rock with a slight greenish tone. A slight lineation is visible in hand sample because of the orientation of the mafic minerals (Appendix. 2).

The rock is classified as an amphibolite and has generally sub- to anhedral grains. It consists of hornblende (~40%), plagioclase (~25%), biotite (~10%), opaque phases (~10%), quartz (~5%) and apatite (~5%). The only identified accessory mineral is zircon (only found in thin section, not through separation). The hornblende and biotite show a slight preferred orientation. The hornblende has a dark green colour and the biotite is reddish brown. The quartz and plagioclase show no signs of alteration, and quartz grains show no signs of sub grains, but many grains of plagioclase and quartz respectively, have inclusions of predominantly biotite. As inclusions, the biotite shows no sign of preferred orientation. Occasional 120° triple junctions are present and only the biotite shows inequant behaviour. The most common inclusions in hornblende are opaque phases, apatite and quartz, which all are abundant.

4.2.1.2 Hopkins 2B (Metapegmatite)

Macroscopically the rock is pinkish with large muscovite grains in aggregates and bands (Appendix. 3). It is made up of feldspars (~40 %, both K-feldspar and plagioclase are present, but plagioclase is more abundant), quartz (~40%), muscovite (~10%), garnet (~5%), apatite (~3%) and calcite (~2%). It is coarse grained and the micas are well developed and follow a clear orientation. The micas grow in aggregates and are often surrounded by quartz. The larger quartz domains are divided into sub grains.

Both kinds of feldspars are slightly altered, at grain boundaries and in tiny cleavages. Most of the garnets are euhedral, some with tiny inclusions of muscovite. Accessory minerals are rutile occurring as needles in quartz grains and zircon.

4.2.2 Zircon (Metapegmatite)

Only three grains were retrieved from this sample there is an uncertainty concerning how representative these grains are for the rock. The grains are ~50-100 µm along the C-axis and 30-50 µm along the A/B-axis (Fig. 9). Texturally they are all simple with slight or no signs of secondary alteration. They are almost free from cracks and no visible inclusions were found on the obtained grains.

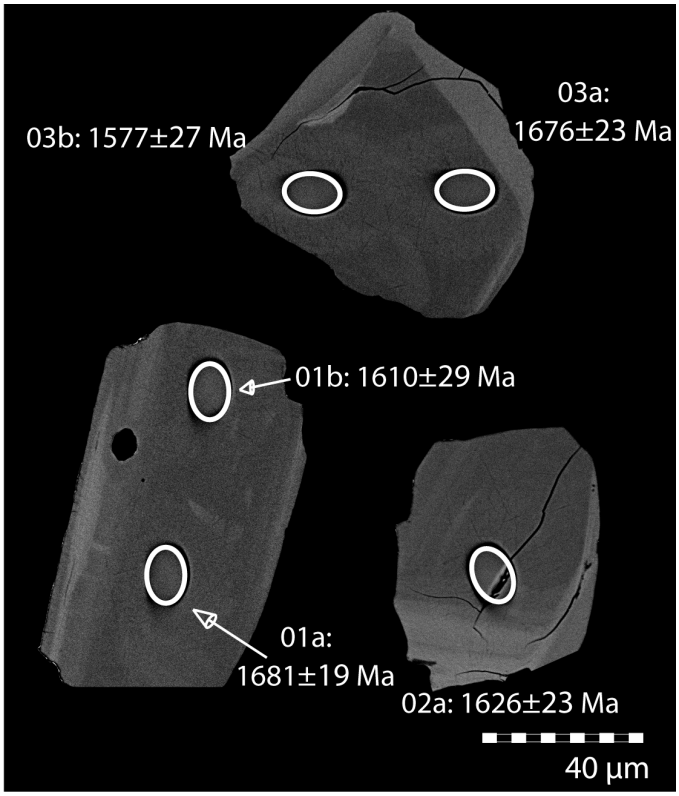

Fig. 9. Back Scattered Electron (BSE) images for selected zircon grains from the *Hopkins* drill-core sample. Analysis sites for ion microprobe age determinations are marked with white ellipses. Spot numbers with corresponding $^{207}Pb/^{206}Pb$ ages (Ma) are given for each spot. In most instances, these analysis sites are identical to those for the O- and Hf- isotope analyses. Note however, that the Hf analysis spot radius is about two to three times the size of the U-Pb spots while the O spot size and location is identical to those for U-Pb.

4.3 Scioto

The Scioto core penetrates down to 1407 meters. It predominantly consists of a red to dark grey, medium to coarse-grained banded orthogneiss. At the sample depth of 1710.5-1712 m (A-C) there is a transition between a banded orthogneiss gneiss, which is dominating the upper part of the core and a sub-isotropic, red coarse-grained seemingly non-metamorphosed granite over a range of less than three metres. Across the contact zone, veins or bands of the red granite occur within the banded gneiss.

4.3.1 Sample description

Three samples were examined from this core; lithologically banded orthogneiss representing the top most section (sample 6A), banded orthogneiss with unstrained cm-wide bands of red granite (sample 6B) occurring in a transition zone to undeformed post-kinematic coarse-grained red granite representing the lowermost part of the core (sample 6C).

4.3.1.1 Scioto 6A (Orthogneiss)

This compositionally banded orthogneiss vary in grain size, from medium- to coarse grained. Macroscopically the rock has a brownish, red tone with a conspicuous gneiss banding defined by alternating more mafic and more felsic layers (Appendix. 4).

The mineral composition is mainly feldspar (~35%), quartz (~25%), hornblende (~10%), biotite (~10%), opaque phases (~10%), apatite (~3%), and chlorite (~2%). Accessory minerals are mainly sphene, zircon, epidote, muscovite and various iron oxides. Biotite and hornblende is slightly orientated which is easily seen in macroscopic view. The hornblende has olive green colour and the biotite is reddish brown. They both appear to have grown in an originally polygonal structure, but have been consumed in a later stage into its present interlobate shape.

Most of the feldspars are perthite with lamella of albite in orthoclase. Ten percent of the feldspars are sericitisized or saussuritisized, most likely during retrograde metamorphism. Myrmekite intergrowth is also present in a few grains of K-feldspar. The whole rock, but mainly amphibole and biotite, appear with granoblastic 120° triple junctions at grain boundaries. The biotite has later been partially chloritizised. Quartz grains are mostly anhedral, many with inclusions of hornblende, apatite, zircon, and biotite.

4.3.1.2 Scioto 6B (Boundary between Orthogneiss and undeformed post-kinematic granite)

This rock is sampled within the boundary between a hornblende-biotite orthogneiss and a post kinematic granite that is unevenly medium- to coarse grained (Appendix. 5). Macroscopically the rock has a deeper red tone than 6A and larger feldspar grains. It consists essentially of ~45% feldspars, ~35% hornblende, ~10% biotite, ~4% opaque phases, ~3% quartz and ~2% apatite.

The accessory minerals are mainly zircon, sphene, muscovite, epidote and various iron oxides. ~60% of the feldspar is perthite and sericitisation and saussuritisation is widespread and covers ~5% of all feldspar grains. Myrmekite intergrowth in K-feldspar is also present in some of the grains. The hornblende and biotite show more signs of polygonal structure, than in 6A, but are consumed both at grain boundaries and trough inclusions. Hornblende, biotite and feldspar seem to be primary magmatic, but the biotite has later been partly chloritizised and the hornblende consumed by various minerals.

The most common inclusion in the hornblende is feldspar, but quartz and biotite is not uncommon. The most common inclusion in the quartz grains is muscovite and feldspar and larger quartz grains are divided into sub grains only detectable in crossed polars. The iron oxides appear mostly along brain boundaries and in cleavages inside grains.

4.3.1.3 Scioto 6C (Post-kinematic granite)

This is an unequigranular, medium- to coarse grained undeformed and unmetamorphosed post-kinematic granite with a macroscopically red appearance (Appendix. 6).

Its main minerals are feldspar (~50%), quartz (~30%), hornblende (~7%), biotite (~5%), opaque phases (~2%) and apatite (~2%). Accessory minerals are zircon, sphene, muscovite, chlorite, epidote and iron oxides.

Feldspar and quartz often grow in 120° triple junctions at grain boundaries. Hornblende and biotite are not as abundant as in 6A and 6B but are shaped similar, with a relict polygonal structure now consumed by other minerals, mainly chlorite and feldspar. The colour of the hornblende is darker green than in 6A and the biotite is darker brown. Macroscopically a slight preferred orientation of mafic minerals and phyllosilicates is visible. Almost all feldspar in the rock is perthitic orthoclase (Mensig & Faure, 1983) with the exception of a few plagioclase grains. Sericite and saussurite is not as abundant as in 6A and 6B but is found along grain boundaries and in cleavages. Also in this rock myrmekite intergrowth in K-feldspar is present. Some quartz grains are divided into sub grains detectable only in XPL, and the most common inclusions are feldspars and zircon.

4.3.2 Zircon

The zircon populations in the three different samples from the Scioto core (samples 6A, 6B and 6C) are remarkably similar in external morphology and internal texture. The zircon characteristics of these samples are therefore described together.

The characteristic zircon is 150-1000 µm along its C-axis and 50-100µm along its A/B-axis (Fig. 11). They are euhedral to subhedral texturally complex grains with core-rim relations. All zircon are more or less transparent with a slight to distinct red/orange colour, mostly on the surface and around cracks. The

red colour is probably due to iron oxide staining, as seen in thin section. The majority of the grains are cracked, but inclusions appear uncommon.

In BSE these zircon have three distinct characteristic textural domains. A dark, texturally old inner core, sometimes showing an oscillatory zoning characteristic for igneous zircon. The igneous cores are observed to be partially to totally replaced by BSE-bright domains hosting a weak oscillatory ghost zoning reported as characteristic for zircon formed from *solid-state* recrystallization (Hoskin & Black 2000). Recrystallization has in some cases totally consumed the relict core showing a BSE bright inner structure of the zircon with euhedral oscillatory ghost zoned pattern.

The third phase is the texturally youngest and occurs as a BSE-dark euhedral rim occurring on most grains. These younger domains are at most ≤ 20µm thick at the pyramid terminations. Cracks are common in these domains and they all show a weak, broad-banded zoning. This type of zircon is interpreted to represent completely recrystallised/newly grown zircon form from dissolution-reprecipitaion of protolith zircon (Roberts & Finger 1997; Rubatto 2008). The BSE-bright, ghost-zoned recrystallized zircon phase is by far the dominating feature in the sample. The texturally youngest domains only constitute a small fraction and were too small to analyse.

Inclusions of quartz, pyrite, apatite, biotite and feldspars are present in most of the BSE bright domains.

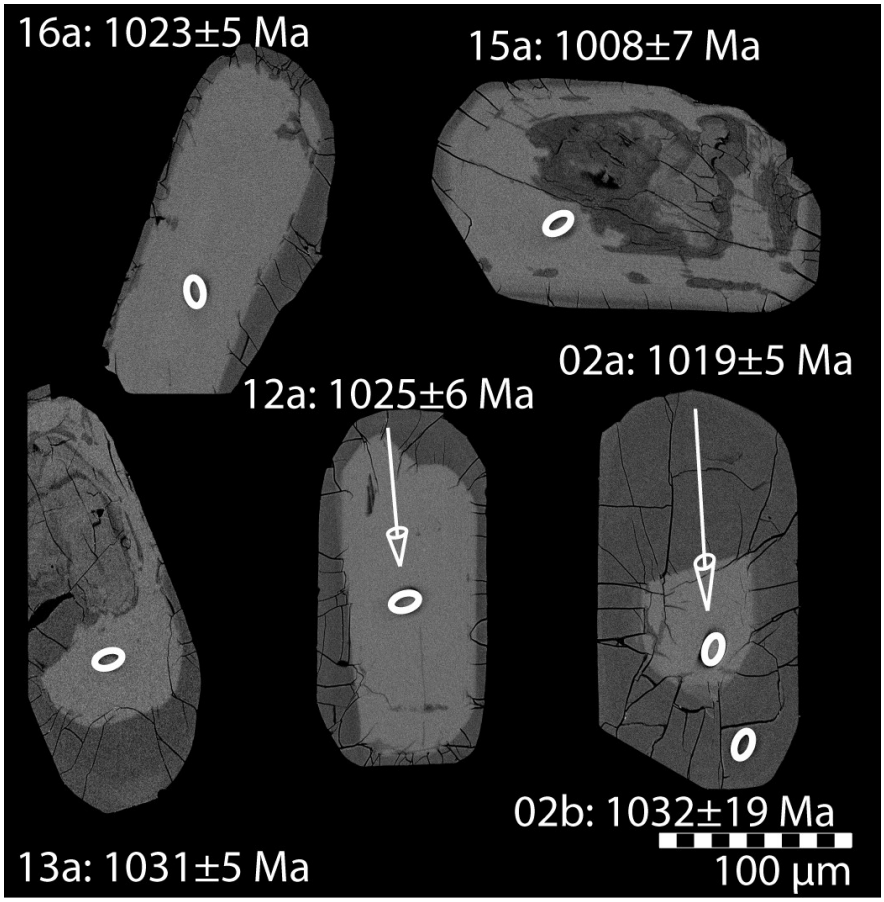

Fig. 10. Back Scattered Electron (BSE) images for selected zircon grains from the *Scioto* drill-core sample. Analysis sites for ion microprobe age determinations are marked with white ellipses. Spot numbers with corresponding $^{207}Pb/^{206}Pb$ ages (Ma) are given for each spot. In most instances, these analysis sites are identical to those for the O- and Hf- isotope analyses. Note however, that the Hf analysis spot radius is about two to three times the size of the U-Pb spots while the O spot size and location is identical to those for U-Pb.

4.4 Morrow (Post-kinematic granite)

4.4.1 Sample description

This sub-isotropic rock is a feldspar rich coarse-grained post kinematic granite with a red colour. The rock is similar to the undeformed red granite examined in the lowermost part of the *Scioto* core (Sample 6C, Appendix. 7). According to Lidiak et al., (1966) it contains assimilated amphibolite xenoliths and is located in the Grenville Province.

This post-kinematic granite contains of feldspar (~40%), quartz (~35%), opaque phases (~10%), biotite (~3%), hornblende (~3%), muscovite (~3%) and apatite (~3%). Accessory minerals found in this thin section are zircon, chlorite, calcite, epidote and also various iron oxides.

Macroscopically it is a dark red granitic rock apparently undeformed and unmetamorphosed.
The rock is coarse grained with fine grained minerals along grain boundaries and along cleavages. This suggests that the rock was affected by some deformation. The feldspars vary from plagioclase to K-feldspar with plagioclase being the slightly more common mineral, and are more or less altered, especially the larger grains. In contrast to similar samples like Scioto 6C, perthite was not found in this sample. All biotite is light brown with a slight red tone and show signs of alteration. Both the biotite and the olive green hornblende are sub- to anhedral.

Iron oxides are present in many cracks and around most of the zircon. Apatites appear mostly as inclusions in feldspars. Other inclusions in feldspar are zircon, quartz, and opaque phases. Inclusions in quartz are predominantly zircon and iron oxides, but some larger inclusions of feldspar can be found in some quartz grains. Most of the grain boundaries between larger grains are triple junctions with c. 120° angles.

4.4.2 Zircon

The zircon in this sample are euhedral and similar to the zircon populations found in the samples from the *Scioto* cores, both in size, appearance and internal textural characteristics (Fig. 11). Zircon is mostly found within feldspars but also in quartz and at grain boundaries between the two. The texturally oldest domains are dark and show an igneous oscillatory zoning. Cracks are more abundant in these domains than in corresponding domains in zircon from *Scioto*. As in *Scioto,* these domains are succeeded and consumed by a BSE bright domain of *solid-state* recrystallized ghost zoned zircon. However, texturally older domains are in some grains better preserved in this sample than in corresponding domains from *Scioto*, and have been successfully analysed. The texturally youngest domains are interpreted as *dissolution-reprecipitation* recrystallized rims and are BSE bright. These domains are unfortunately too small to analyze (<10µm). Inclusions are found in almost all grains, mostly in texturally older domains. Apatite is the most common inclusion, but quartz, biotite, various feldspars and pyrite has also been identified.

Fig. 11. Back Scattered Electron (BSE) images for selected zircon grains from the *Morrow* drill-core sample. Analysis sites for ion microprobe age determinations are marked with white ellipses. Spot numbers with corresponding $^{207}Pb/^{206}Pb$ ages (Ma) are given for each spot. In most instances, these analysis sites are identical to those for the O- and Hf- isotope analyses. Note however, that the Hf analysis spot radius is about two to three times the size of the U-Pb spots while the O spot size and location is identical to those for U-Pb.

4.5 Herman (Meta-granite)

4.5.1 Sample description

The sample consists of gneissic granite with quartz and feldspar grains clustered into bands in an aphanitic orange fabric. The rock is heavily altered with areas of pink and grey. The pink areas are the altered feldspar and the grey consists of mainly quartz (Appendix. 8).

The matrix consists of fine grained altered feldspar, (~40%). Fine grains of K-feldspar is scattered in the matrix and increase in abundance at grain boundaries to the larger quartz and feldspar grains. Some fine grains of muscovite are also present.

Except for the ~40% altered material, possibly sericite or saussurite , the rock consists of quartz (~30%), opaque phases (~10%), chlorite (~7%), feldspar (~5%) and muscovite (~3%). Accessory minerals are zircon, apatite, epidote and zoisite.

The chlorite appears as chloritisized biotite and is found as flakes agglomerated into bands with weak wavy characteristics together with small amounts of muscovite.

Some veins are filled with quartz, otherwise thin layers of aphanitic material are found throughout almost all grain boundaries and veins. The quartz grains are almost inclusion free, except for a few opaque inclusions. It is possible that this rock is a lithified regolith weathered when the Precambrian basement was at the surface and later experienced a retrograde greenschist metamorphism where the biotite chloritisized.

4.5.2 Zircon

In this sample the zircon is slightly smaller than in e.g. *Scioto* and *Morrow*, 100-400 µm along their C-axis and 50-100 µm along the A/B-axis (Fig. 12). Most of the grains are subhedral, but both euhedral and anhedral grains are present. They are greyish in colour, transparent and often have turbid inner domains of texturally older zircon. The grains are severely cracked.

In BSE images remnants of a relict, dark, texturally older domain is visible in some grains. In most grains however, this domain is totally recrystallized appearing as sector zoned domains alternating between bright and dark bands. The zoning in these domains are broader than corresponding domains in *Scioto* and *Morrow* and interpreted to be syn-magmatic *solid-state* recrystallized zircon or *solid-state* recrystallized xenocrystic zircon.

The texturally youngest domain exists only marginally in these zircon grains and when present show a sector zoned pattern. Unfortunately these domains have been too small to analyse (<10 µm wide). Black inclusions, to small to identify mineralogically, are found almost exclusively within and around the cores.

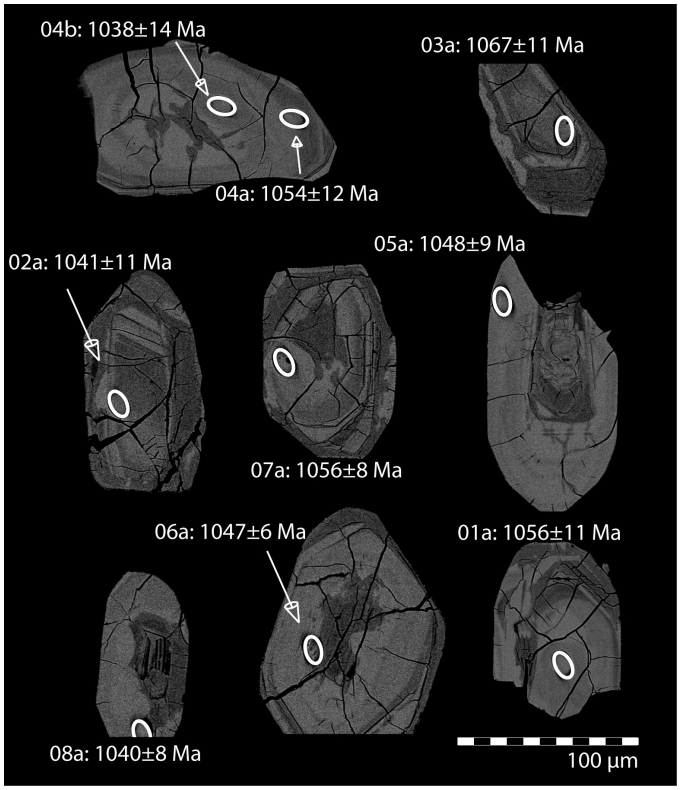

Fig.12. Back Scattered Electron (BSE) images for selected zircon grains from the *Herman* drill-core sample. Analysis sites for ion microprobe age determinations are marked with white ellipses. Spot numbers with corresponding $^{207}Pb/^{206}Pb$ ages (Ma) are given for each spot. In most instances, these analysis sites are identical to those for the O- and Hf- isotope analyses. Note however, that the Hf analysis spot radius is about two to three times the size of the U-Pb spots while the O spot size and location is identical to those for U-Pb.

4.6 Lake (Dark fine-grained rock)

4.6.1 Sample description

The lithology of the core alternates between chlorite-sericite-biotite schist with grains of secondary K-feldspar and it has been assumed that this rock was originally a gabbro or diorite (Vargo 1972), but I adapt the more cautious term dark fine-grained rock. The sample was taken at the base of the core from a chloritized meta-diorite. In discrete brittle-ductile deformation zones, the core shows steep ~80° lineation defined by biotite and chlorite (Vargo 1972).

This altered, dark-grey, rock is fine grained with almost exclusively anhedral grains (Appendix. 9). It consists of feldspar (~40%), chlorite (~20%), actinolite (~15%), biotite (~10%), opaque phases and (~10%). Calcite (~3%) is present in a thin secondary vein. Plagioclase is by far the most common feldspar, but some K-feldspar is also present. The actinolite has a deep pale green colour and the biotite is light brown. Accessory minerals found are zircon, muscovite and epidote.

Most of the feldspar is altered trough saussuritization, some totally altered into clusters of aphanitic epidote rich zones. The mafic minerals and opaque phases cluster in this rock.

An approximately one mm thick vein of post-metamorphic zoned calcite, with some chlorite and biotite, cuts through the sample.

The general petrogenesis and the fact that the rock is silica undersaturated with no appearance of quartz indicate an intermediate to mafic protolith that later experienced amphibolite facies metamorphism. The presence of chlorite indicates a later retrograde greenschist metamorphism.

4.6.2 Zircon

Zircon grains in this rock are 50-200 µm along the C-axis and 30-70 µm along the A/B-axis (Fig. 13). Most are subhedral, both simple and some with thin rims (too thin to analyse) of texturally younger zircon occure. Zircon is predominantly found in close proximity to biotite and with dark brown to black pleochroic haloes, caused by radiation damage from the zircon.

The texturally older domains are irregularly zoned (Fig. 13). An increased BSE brightness is associated with some cracks. Trains of black inclusions are found in several grains and consist of impure biotite. Scattered inclusions of feldspars and quartz are also present.

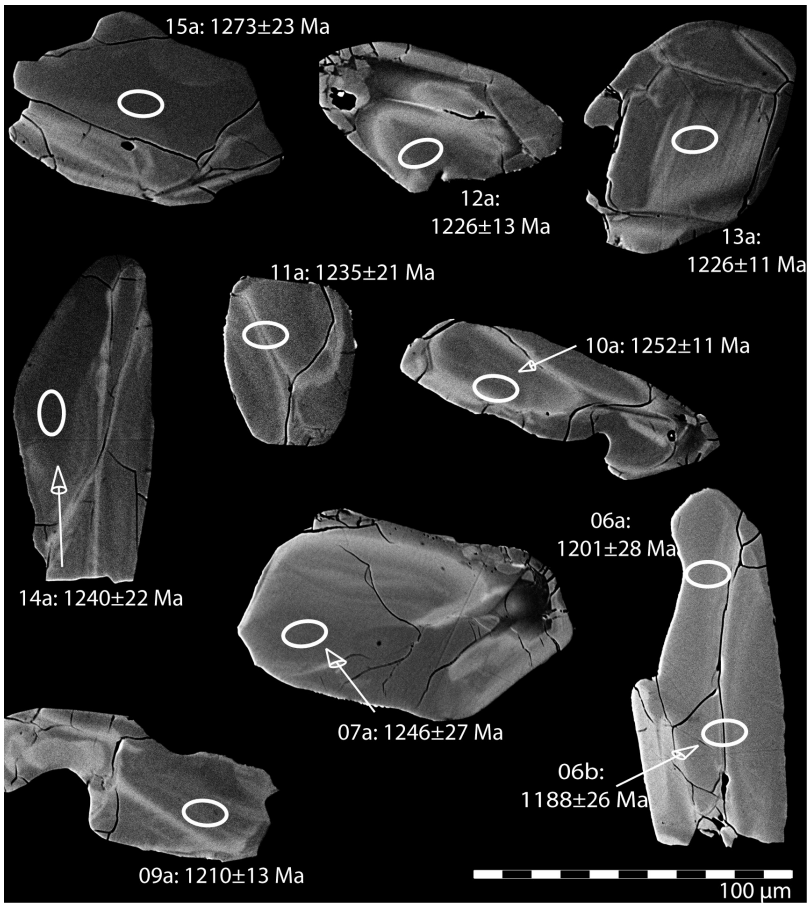

Fig. 13. Back Scattered Electron (BSE) images for selected zircon grains from the *Lake* drill-core sample. Analysis sites for ion microprobe age determinations are marked with white ellipses. Spot numbers with corresponding $^{207}Pb/^{206}Pb$ ages (Ma) are given for each spot. In most instances, these analysis sites are identical to those for the O- and Hf- isotope analyses. Note however, that the Hf analysis spot radius is about two to three times the size of the U-Pb spots while the O spot size and location is identical to those for U-Pb.

5 Analytical results and interpretation of isotopic data

5.1 U-Th-Pb, O and Hf

The U-Th-Pb, O and Hf data are listed in Table 2 and the *in situ* sample sites are shown in Fig 9-14. $^{207}Pb/^{206}Pb$ weighted average ages are used in all age determinations and for the calculations of initial ε_{Hf} values. All age errors are presented at the 2σ-level, but decay constant errors are ignored. All Tera-Wasserburg diagrams are found in Appendix 10.

5.1.1 Logan

Eight concordant analyses in oscillatory zoned texturally homogeneous zircon defines a Tera-Wasserburg concordia age of 1471 ±3 Ma (MSWD=1.1) and a weighted average $^{207}Pb/^{206}Pb$ age of 1464 ±8 Ma (MSWD=0.2). No indication of common Pb or correctional problems was noted in any of the spot data. The 1471 ±3 Ma concordia age is interpreted to date igneous crystallization of the *Logan* volcanic rock. $\delta^{18}O$ from ten analyses range from 8.05‰ to 11.82‰ with a weighted average from all spots of 9.2 ±0.7‰ (2σ MSWD=7.1) indicating the presence of a crustal component at crystallization.

Initial ε_{Hf} values (n=8) form a tight cluster that range between 8.2 to 10.4 for seven spots, one spot was rejected on statistical grounds, yielding a weighted average of 9.0 ±0.6 (2σ MSWD=0.95) (Fig. 14). This data gives this rock an almost juvenile signature plotting close to the depleted mantle.

5.1.2 Hopkins

Six grains were recovered in earlier analytical work on this sample, but only three zircon grains were retrieved for analysis in this study. All grains are homogenous in BSE. Five spots analysed in the three grains yielded a $^{207}Pb/^{206}Pb$ weighted average age of 1643 ±54 Ma (MSWD=3.5). All spots were placed in homogenous BSE un-zoned domains except of -02a, which hit a crack. The data scatter slightly producing the large margin of error, and the possibility of lab-introduced contamination can not be excluded. Another possibility is a xenocrystic inheritance of the zircon to the pegmatite.

Compositions from five $\delta^{18}O$ analyses range from 4.60‰ to 5.96‰ with a weighted average of 5.4 ±0.7‰ (2σ MSWD=1.7). This is a juvenile signature that is within error identical to mantle and MORB values.

Three ε_{Hf} analyses scatter a great deal with values of 2.5, 5.7 and 12.7 respectively. Errors, especially on the spot yielding the value of 12.7, are large at ±2.8 (2σ). The weighted mean of this sample yields 5 ±11 (2σ MSWD=20).

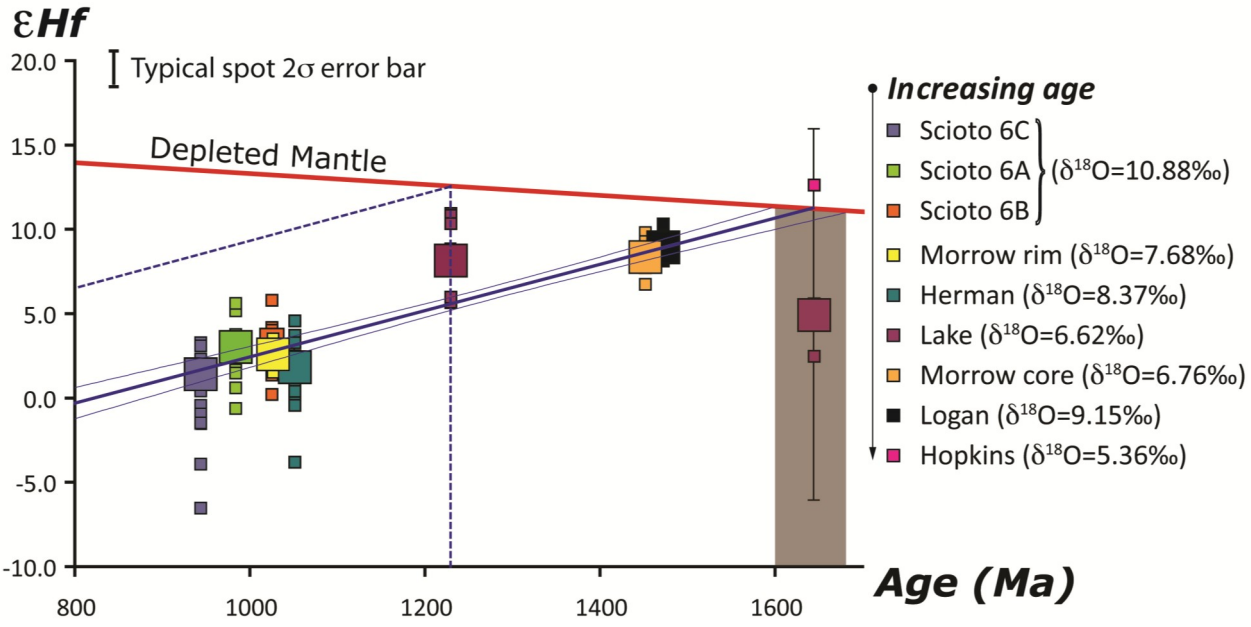

Fig. 14. ε_{Hf} vs $^{207}Pb/^{206}Pb$ ages for all samples in this study. Ages represent interpreted igneous or metamorphic crystallization ages for individual populations. Individual zircon spot ε_{Hf} values are indicated by the small squares, while the weighted average for each population is given by the large squares. For clarity, error bars are left out for individual spots (except *Hopkins*) and the error bars for the weighted averages are smaller than their symbol sizes. Depleted Mantle evolution data are from Nowell et al. (1998) and is indicated by the red line. The solid heavy blue line represents a regression (R^2=0.95) for the average data of *Scioto, Morrow, Herman* and *Logan*, which corresponds to a single crustal reservoir with $^{176}Lu/^{177}Hf = 0.014$ and t_{DM} = 1640 ±40 Ma. Thin blue curves represent the error envelope of the regression and the model age envelope is given by the grey field. Two crustal evolution models with corresponding t_{DM}-ages are given by the hatched blue lines. O isotope data is given in the legend.

5.1.3 Scioto

In these samples thirty-two grains were analysed with thirty-four spots placed in different domains. All grains come from the same drill-core but from three different depths, n3427-29 (6A-6C). Only thirteen spots, all from grains from n3428 (6B), were used for age calculation. Remaining spots were discarded due to high common Pb (low $^{206}Pb/^{204}Pb$) or uncertainties surrounding large corrections (see Table 2.). All used spots except for n3428-03a were, previous of analysis, interpreted as recrystallized ghost zoned domains. n3428 -03a were interpreted to be a texturally older (not recrystallized) domain. All spots in texturally older domains of this sample yielded discordant data, and the attempt to date pre-metamorphic ages failed. The remaining thirteen spots yielded a $^{207}Pb/^{206}Pb$ weighted average age of 1024 ±8 Ma (MSWD=4.6). Common Pb corrected and uncorrected Tera-Wasserburg data generated ages of 1003 ±39 Ma (MSWD=2.2) and 1020 ±30 Ma (MSWD=2.1) respectively.

Grains from sample 6A and 6C were analysed prior to this thesis work, and dated to 982 ±21Ma (MSWD=1.9) and 942 ±24 Ma (MSWD=1.6) respectively (Andersson & Baranoski 2001). These ages were obtained from the texturally youngest domains (BSE-dark, unzoned, euhedral distinct rims), which were not analysed in this study.

Thirty-eight $\delta^{18}O$ analyses of this sample yield a range from 8.17‰ to 14.77‰ with a weighted average from thirty-four spots of 10.9 ±0.2‰ (2σ MSWD=2.7). These O-data are high and indicate a substantial component of evolved crust in the magma from which the zircon crystallized. Initial ε_{Hf} (*n*=11) range from 1.4 to 4.1 with a weighted average of 3.5 ±0.9 (2σ MSWD=3.3). ε_{Hf} values are in agreement with the O-data insofar both indicating a non-juvenile source.

5.1.4 Morrow

A total of 33 analyses were obtained from texturally different phases of zircon. Analyses 6a, 9a, 10a, 11b, 13a, 20a, 22a, 23a and 24b were discarded due to large analytical corrections and high cPb values. 12b was discarded due to probable Pb-loss. Analyses n3422-8b, 11a, 18a and 21a were aimed at the texturally younger BSE-bright ghost zoned domains. Analyses n3422-5a, 7a, 8a, 12a, 12c, 14a, 14b, 15a, 15b, 15c, 16a, 17a, 19a and 24a were used for dating texturally older domains. The four spots used to date the texturally younger BSE-bright, weakly zoned domains yielded a $^{207}Pb/^{206}Pb$ weighted average age of 1025 ±7 Ma (MSWD=0.8), interpreted to date the time of a *solid-state* recrystallization event. Texturally older domains analysed were both BSE dark and bright and were weakly oscillatory zoned. These yielded a Tera-Wasserburg concordia age of 1454 ±18 Ma (MSWD=2.8) and a $^{207}Pb/^{206}Pb$ weighted average age of 1449 ±9 Ma (MSWD = 4.0) and are interpreted as an igneous protolith age.

Twenty-five $\delta^{18}O$ analyses range from 6.31‰ to 9.59‰ with a mean from twenty-three spots of 7.0 ±0.2‰ (2σ MSWD=1.9). Divided between core and rim, the weighted means yield 6.8 ±0.2‰ (2σ MSWD=0.97) and 7.7 ±0.9‰ (2σ MSWD=7.9) respectively. The high MSWD for the rims reflect excess scatter due to either disturbed zones as indicated by discordant U-Pb data in three spots, or incomplete metamorphic recrystallization homogenisation. Removing these three data reduces MSWD to 3.0 while the mean and uncertainty remains effectively the same. The high $\delta^{18}O$ ~8‰ reflects a slightly higher influence of evolved crust at the time of the latest crystallization compared to crystallization of the older domains.

Hf data from grain cores (*n*=9) yield a weighted average of 8.5 ±0.6 (2σ MSWD=1.4) and from rims (*n*=6) 2.6 ±0.5 (2σ MSWD=1.2). Both groups fall onto the same crustal evolution line (Fig. 14). In accordance with O-data these analysis reflect crustal influence increasing from texturally older to younger domains.

5.1.5 Herman

Ten spots were distributed on nine texturally different zircon domains (Fig. 12). These domains include both BSE-bright texturally young (-05a) and BSE-dark texturally old (-03a) domains. In addition, one analysis hit a euhedral tip (-04a). Together, these data yield an upper intercept Tera-Wasserburg age of 1050 ±6 Ma (MSWD=0.8). Discordance is in accordance with either recent Pb-loss or slight U/Pb calibration errors as highlighted in Fig 4A. The $^{207}Pb/^{206}Pb$ age is insensitive to any of these effects and the $^{207}Pb/^{206}Pb$ weighted average yield an age of 1050 ±6 Ma (MSWD=0.7). The calculated ages are interpreted to date igneous crystallization or possibly *solid-state* recrystallization of xenocrystic zircon.

Twenty $\delta^{18}O$ analyses range from 6.79‰ to 9.42‰ with a weighted average from nineteen spots of 8.4 ±0.3‰ (2σ MSWD=3.3) reflecting a substantial crustal component at crystallization.

The initial ε_{Hf} (*n*=13) range from -3.7 to 4.7 with twelve spots generating a weighted average of 1.9 ±1.2 (2σ MSWD=6.6). All thirteen spots generate a t_{DM} weighted mean of 1490 ±47 Ma (MSWD=1.6). Except of a slight outlier, these data cluster fairly well, indicating a non-juvenile component for this sample.

5.1.6 Lake

Thirteen spots in weakly irregularly zoned BSE-bright domains in thirteen different grains were analysed. One, n3421-08a, was discarded from the age calculation due to high cPb. The remaining twelve spots yielded a Tera-Wasserburg age of 1231 ±21 Ma (MSWD=1.9) and a $^{207}Pb/^{206}Pb$ weighted average age of 1228 ±10 Ma (MSWD=1.7), which is interpreted to date crystallization of the igneous protolith.

The $\delta^{18}O$ values of seventeen analyses from this sample range from 6.05‰ to 7.49‰ with a weighted average from all spots of 6.6 ±0.2‰ (2σ MSWD=1.2). Fourteen analyses of ε_{Hf} range from 5.7 to 11.0 and thirteen spots, one reject, yield a weighted average of 8.2 ±1.0 (2σ MSWD=3.1). This sample yields a t_{DM} (*n*=14) of 1401 ±41Ma (MSWD=0.8).

5.1.7 Summary of geochronological results

Scioto-, *Morrow*-rims and *Herman* yield the youngest ages at 1024 Ma, 1025 Ma and 1050 Ma respectively. These samples fall within the Ottawan orogenic phase. *Herman* reflects an igneous protolith age or, as for *Scioto* and *Morrow*-rims, an age associated with high-grade metamorphism. Lake gives an igneous crystallization age of 1228 Ma which puts it into the Elzevirian phase of the tectonic evolution. The cores from *Morrow* and the igneous zoned domains from *Logan*, on either side of the Grenville Front yield ages of 1449 Ma and 1464 Ma respectively, which represent late Elsonian ages. The oldest zircon dated in this thesis is *Hopkins*, which gives an age of 1643 Ma and puts it in the Labradorian period.

There is no clear correlation between ages and $\delta^{18}O$ values or between $\delta^{18}O$ values and geographical location. However, there is a moderate negative correlation between Th/U and $\delta^{18}O$ (Fig. 15). *Hopkins* clearly has the most juvenile O values at a mean of 5.3‰ followed by *Lake*, *Morrow* and *Herman* at 6.6‰, 7.0‰ and 8.3‰ respectively. *Logan* and *Scioto* has the highest $\delta^{18}O$ values with 9.2‰ and 10.9‰ respectively. The overall moderate negative correlation for Th/U and $\delta^{18}O$ (Fig. 15) is probably best explained by increasing influence of heavy $\delta^{18}O$ metamorphic fluids during zircon re-crystallisation or metamorphic growth. Given the slow diffusion of O in zircon, O-isotope exchange might only be anticipated to any significant degree in dissolution-reprecipitation processes, while solid-state recrystallization processes might be less affected, if at all.

Lake, *Logan* and *Morrow* cores have the most juvenile ε_{Hf} signature of these samples, with *Logan* plotting close to the Depleted Mantle (DM) curve. The younger samples, *Morrow rims, Herman* and *Scioto* all indicate influence of recycled continental crust, plotting way below the DM curve. *Hopkins* data scatter allot, but indicate a probable juvenile signature.

6 Discussion

6.1 Zircon U-Pb, Hf and O-isotopes in an geological context

6.1.1 Logan

The igneous textures and 1471 ±3 Ma age for *Logan* manifest a magmatic episode that predates the Grenvillian orogeny. This age correspond to the Pinwarian stage of crustal development in NE America. The Pinwarian orogenic stage is according to Rivers (1997) related to continental arc-building. It remains, however, unknown if this stage of the crustal development represents new growth or reworking of existing continental crust. It is therefore striking that all zircon from *Logan* are characterised by heavy zircon $\delta^{18}O$ from 8.05‰ to 11.82‰ and with a weighted average of 9.2 ±0.7‰ (2σ MSWD=7.1). These high values are unusually high and barely within the range of modern arc lavas, and provide a indication for a significant recycled component. A juvenile component would have considerably lower $\delta^{18}O$ around 5.7-6.5‰, which is

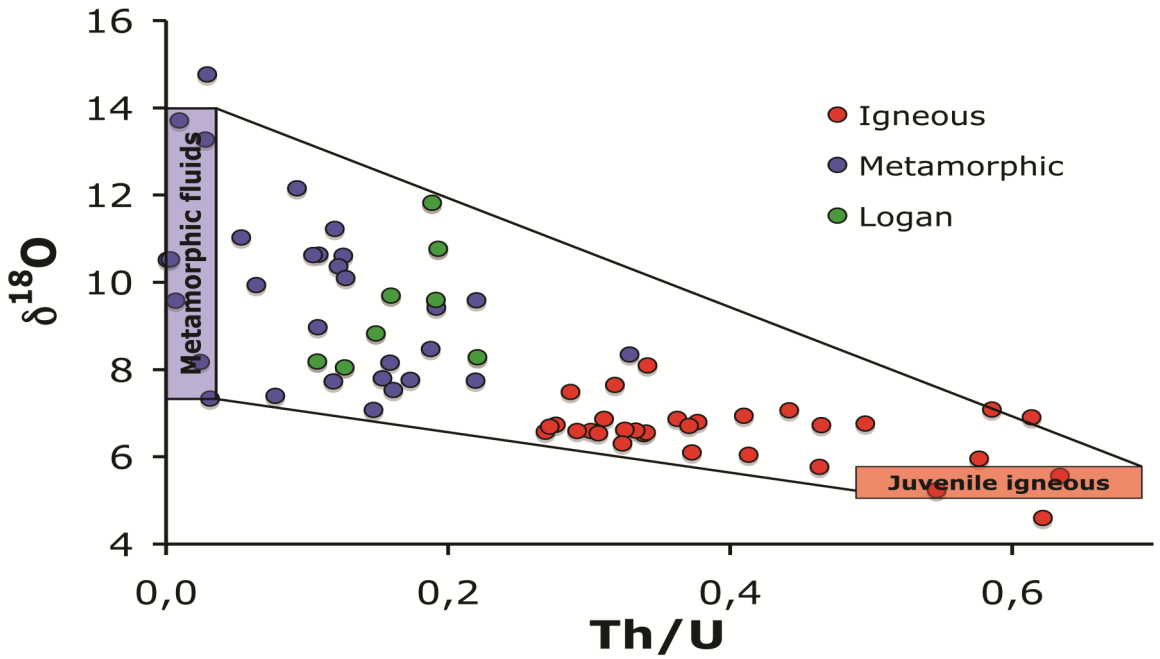

Fig. 15. Negative correlation between $\delta^{18}O$ and Th/U. The relationship (Linear regression: R^2 ~0.6) demonstrating the effect of heavy $\delta^{18}O$ metamorphic fluids on zircon during metamorphism. A decrease in Th/U value indicates an increased metamorphism due to the larger difference in ionic radii between Th^{4+} and Si^{4+} than U^{4+} and Si^{4+}. *Logan* deviates from the general trend and has probably been effected by meteoric fluids since its host rock is of volcanic origin.

also within the main range of arc values (Valley et al. 2005; Hawkesworth & Kemp 2006; Kemp et al. 2006). Contrasting evidence is obtained from Hf-isotopes with a weighted mean ε_{Hf} value of 9.0 ±0.6 (2σ MSWD=0.95) indicating a juvenile source, plotting close to the Depleted Mantle curve (Fig 14).
A possible explanation for this apparently contradictory result is juvenile magmatism related to subduction, with some contribution from the uppermost part of the slab. As noted by Kolondy & Epstein (1976), the slab might be overlain by pelagic clays, marine carbonates or siliceous oozes which normally have $\delta^{18}O$ values of ~15–25‰, ~25–32‰ and ~35–42‰ respectively. Input from such components should significantly increase the $\delta^{18}O$ value of the melt (Bindeman et al. 2005). Assuming a 1:1 concentration ratio for O between the juvenile magma and the contaminant constrains the amount of heavy O-material to between 10-45 wt% depending on its composition. That is, influx of siliceous ooze only require smaller degrees of contamination, while pelagic clays would imply mixing towards the upper bound of my estimate of 45 wt%. An alternative assumption with little to no influx of pelagic sediments is still viable due to the fact that $\delta^{18}O$ values of the upper part of a subducting slab, as known from ophiolite complexes, can be as high as 14‰ (Rollinson,1993). Given such a model, the ε_{Hf} value could stay virtually unaffected due to small contrast in Hf-isotopic ratios between the subducting oceanic crust and the mantle (Rollinson 1993). Yet again, the observed ε_{Hf} is compatible with a sedimentary component if the integrated crustal residence time is short, in this case <200 Myr for an average crustal $^{176}Lu/^{177}Hf$ ~0.014.

These results imply that the host rock of originated from an environment related to subduction and juvenile magmatism with an upper bound of 45 wt% influence of reworked continental components.

6.1.2 Hopkins

These zircon grains seem to have preserved their primary igneous texture from crystallization, once again proving the robustness of zircon. The $^{207}Pb/^{206}Pb$ weighted average crystallization age of 1643 ±54 Ma (MSWD=3.5) corresponds to the Labradorian stage of geological evolution. The Labradorian stage is associated with the growth of an outboard arc and accompanying accretion (Rivers 1997). Although poorly constrained, this age provide an important revision of the age structure of the eastern North American continent as it supersedes the Nd T_{DM}-line by Van Schmus et al. (1996) and Fisher et al. (2010). Despite the limited data set, this is probably a significant finding as the overall data set imply crustal residence times that imply formation ≥1550 Ma as a conservative estimate (Fig. 14).

The combined $\delta^{18}O$ and ε_{Hf} data from this sample indicate a juvenile source. The $\delta^{18}O$ weighted average of 5.4 ±0.7‰ (2σ MSWD=1.7) is within margin of error of the mantle value as well as for most oceanic and continental arc lavas (Bindeman et al. 2005). The ε_{Hf}-values scatter, with values of 2.5, 5.7 and 12.7 respectively. Primary mixing in the island arc environment cannot explain the observed variation, as Hf-isotopes display a limited range of compositions in modern arc systems (König et al. 2008). However, metamorphic effects or analytical errors could explain this scatter. At any rate, the poorly constrained average of 5 ±11 (2σ MSWD=20) demands a juvenile source at ≥1600 Ma.

6.1.3 Scioto

These zircon grains seem to have undergone *solid-state* recrystallization and partially or totally lost its igneous textures. At a later stage the zircon was probably affected by an aggressive melt during metamorphism and recrystallized the texturally youngest domains trough *dissolution-reprecipitation*. The $^{207}Pb/^{206}Pb$ weighted average age of 1025 ±8 Ma (MSWD=4.6) reflects the *solid-state* recrystallization during a metamorphic event. This age corresponds to the late-Ottawan orogenic phase (Rivers 1997; 2008) which is part of the continent-continent collision. $\delta^{18}O$ in these samples are exceptionally high with a weighted average of 10.9 ±0.2‰ (2σ MSWD=2.7). This clearly indicates the influence of reworked continental crust or substantial reaction with metamorphic fluids (Valley et al. 2005) and is corresponding to the ε_{Hf} mean value of 3.5 ±0.9 (2σ MSWD=3.3). The different samples from this core (6A-C) are homogenous with respect to O and Hf data. This again proves the robustness of zircon considering the different metamorphic textures shown in the microscopic lithology, and indicates a mutual host rock to 6A-C.

6.1.4 Morrow

As in the grain cores from *Scioto*, cores in this sample have been affected by *solid-state* recrystallization, but not to the same extent. In a few well preserved grains, the igneous zoning texture is preserved and yield a late -Pinwarian $^{207}Pb/^{206}Pb$ weighted average age of 1449 ±9 Ma (MSWD = 4.0). The Pinwarian is related to the formation of a continental margin arc (Rivers 1997), which is a possible crystallization environment for these zircon. The texturally younger *solid state* recrystallized domains show slight signs of zoning and yield a $^{207}Pb/^{206}Pb$ weighted average age of 1025 ±7 Ma (MSWD=0.8) corresponding to the late Ottawan orogenic phase.

O-isotope data indicate a non-juvenile source. The higher $\delta^{18}O$ value of the rims (7.7 ±0.9‰) than the cores (6.8 ±0.2‰) suggests a heavy O composition of the melt related to the late Ottawan metamorphism, and probably substantial involvement of metamorphic heavy $\delta^{18}O$ fluids (c.f. Fig. 15).

The ε_{Hf} values of 8.5 ±0.6 (2σ MSWD=1.4) and 2.6 ±0.5 (2σ MSWD=1.2) for cores and rims respectively both indicate the presence of a non-juvenile source.

6.1.5 Herman

The $^{207}Pb/^{206}Pb$ weighted average age of 1050 ±6 Ma (MSWD=0.7) is difficult to interpret. This age can reflect a syn-magmatic *solid-state* recrystallization and more or less give an igneous protolith age. Another possibility is a *solid-state* recrystallization of xenocrystic zircon reflecting a metamorphic age. The petrographic character of the rock and the lack of local geological information due to the nature of drill-core investigations make it difficult to distinguish between the two scenarios.

The heavy $\delta^{18}O$ mean values of 8.4 ±0.3‰ (2σ MSWD=3.3) seem to bee indicative of the area and indicate the involvement of continental components to the magma. Hf data from this sample give the same indication with a ε_{Hf} average of 1.9 ±1.2 (2σ MSWD=6.6).

6.1.6 Lake

Irregular textural appearance in these zircon grains is interpreted to reflect crystallization in an intermediate to mafic magma, possibly with the presence of fluids. The U-Pb analysis is concordant and the $^{207}Pb/^{206}Pb$ weighted average age of 1230 ±10 Ma (MSWD=1.7) correspond to the Elzevirian orogeny (Windley 1986; McLelland et al. 1988; Gower et al. 1990; McEachern & van Breemen 1993; Corriveau et al. 1994; Rivers 1997). According to Corrigan & Hanmer (1995) back arc magmatism during this period ended at 1230 Ma. This puts this sample in the latest subduction related magmatism of the Elzevirian.

Apart from *Hopkins*, *Lake* zircon presents the lightest $\delta^{18}O$ signature of the region with a weighted average of 6.6 ±0.2‰ (2σ MSWD=1.2). The ε_{Hf} values are also a bit divergent from the rest of the samples indicating a slightly more juvenile source than the rest with a weighted average of 8.2 ±1.0 (2σ MSWD=3.1). Combined O-Hf data suggests a different host rock, with a more juvenile composition, than the other samples in this thesis.

6.2 Towards a general model for the evolution of the continental basement under Ohio

There is no doubt that these subsurface basement rocks are related to the Grenville orogen, yielding ages spanning from ~1650 Ma to ~940 Ma. The older ages of *Hopkins, Logan, Lake* and the cores of *Morrow* reflect igneous protolith crystallization ages related to arc building in early- to mid- stages of the orogen (Rivers, 2008). The younger ages of *Scioto,* and the rims of *Morrow* reflect metamorphic ages during continent-continent collision at later stages of the orogen. The age of *Herman* can be either the age of an igneous protolith or date a metamorphic event. The 1650 Ma age of the Hopkins zircon is unexpectedly old and in conflict with previously published data of the area (Van Schmus et al. 1996; Fisher et al. 2010).

It is noticeable that $\delta^{18}O$ signatures of subsurface Ohio are slowly increasing towards heavy values with time, indicating involvement of reworked continental components that were affected by metamorphic fluids. Furthermore, it is apparent from the Hf data for samples *Scioto, Herman, Lake* and for the rims of *Morrow* that these rocks were derived from a crustal source with an extended crustal residence time that saw little or no juvenile additions during magma generation or metamorphic recrystallization. In the case of *Logan* and the cores of *Morrow* the continental signatures in the Hf data is not as obvious since these rocks have fairly depleted signatures (Fig. 14). The $\delta^{18}O$ of *Hopkins* suggest a truly juvenile source, which the Hf data could be in agreement with. However, scatter in that data makes it difficult to draw any definite conclusions. Nevertheless, all samples except for *Logan* fall on the same crustal evolution array, in time- ε_{Hf} space, with a $^{176}Lu/^{177}Hf$ value that corresponds to 0.014. This array represents a possible protolith whole rock with a t_{DM} at 1640 ±40 Ma. Notably, the model age is within error of the *Hopkins* igneous crystallization age, and we call this model "Grenvillian array". The simplest explanation for this observation is a crustal formation event at ~1640 Ma, with a residence time of ~0 Myr of the protocrust for *Hopkins* (Fig. 14). *Logan* and *Morrow* cores cluster on the Grenvillian array at around 1460 Ma and both these rocks could therefore be completely drawn from this reservoir without the addition of new continental crust. It follows that the continent did not grow during this period, but was rather reworked through igneous processes. Further reworking of this crustal mass at ~1000 Ma, form a cluster of rocks on the Grenvillian array, *Scioto, Herman* and *Morrow* rims.

Lake is the only sample that deviates significantly from the Grenvillian array as it plots between the array and the depleted mantle curve. This indicates a more depleted source, which can be explained by the following model. A new crust forming event generated depleted melts with $\varepsilon_{Hf} \leq 12.5$ at ~1230 Ma, which mixed with an enriched existing crustal component $\varepsilon_{Hf} \leq 5$. A potential candidate for the enriched component could be the existing crust as defined by the Grenvillian array (Fig. 14). Given such a model and assuming a Hf-concentration ratio of 1:1, the juvenile crustal component in *Lake* range between 0-33%.

7 Acknowledgements

This project was enabled through the financial support from the Swedish Science Council through grant VR#2008-3447 to Anders Scherstén, the Swedish Geological Survey through Jenny Andersson, the Memorial University, Newfoundland through John M. Hanchar and the Earth and Ecosystem Science department, Lund University. I would like to thank my supervisors Anders Scherstén and Jenny Andersson for their invaluable support and insights throughout the work of this thesis. Thanks to Martin. J, Whitehouse and the Nordsim laboratory for all their help and for giving me the opportunity to use their lab. My co-

supervisor Mark. T, Baranoski and the Ohio Division of Geological Survey provided me with the samples that made this thesis possible. I am grateful for the help and hospitality provided by my co-supervisor John M. Hanchar and Christopher M. Fisher during my visit at Memorial University, Newfoundland. Thank you! I would also like to thank Mimmi Nilsson, my loyal studying-partner and friend for making the years leading up to this project a lot more fun. Last but not least I would like to thank my family for all the love and support throughout the years.

8 References

Andersson, J., Baranoski, M., 2001. U-Pb zircon geochrolnology of the subsurface Grenville Province in the Eastern Midcontinent, USA: implications for the Grenvillian-Sveco-norwegian linc. Unpublished manuscript. Geological Survey of Sweden, Uppsala, Sweden.

Baranoski, M.T., Brown, V.M., and Watts, D., 2007. Deep gas well encounters ultramafic kimberlite –like material in the Sauk Sequence of southeastern Ohio, USA. Geosphere. June 2007, vol. 3, no. 3, 177–183. doi: 10.1130/ GES00063.1; 6 figures.

Baranoski, M.T., Dean, S.L., Wicks, J.L., and Brown, V.M., 2009, Unconformity–bounded seismic refl ection sequences defi ne Grenville–age rift system and foreland basins beneath the Phanerozoic in Ohio. Geosphere. April 2009, vol. 5, no. 2, 140–151. doi: 10.1130/ GES00202.1; 5 fi gures; 3 tables.

Benninghoven, A., Rüdenauer, F.G., Werner, H.W., 1987. Secondary Ion Mass Spectrometry: Basic Concepts, Instrumental Aspects, Applications, and Trends, p. 1264. John Wiley & Sons, New York.

Bindeman, I.N., Eiler, J.M., Yogodzinski, G.M., Tatsumi, Y., Stern, C.R., Grove, T.L., Portnyagin, M., Hoernle, K., Danyushevsky, L.V., 2005. Oxygen isotope evidence for slab melting in modem and ancient subduction zones. Earth and Planetary Science Letters. 235 (3–4), 480–496.

Black, L.P., Kamoc, S.L., Allen, C.M., Davis, D.W., Alienkoff, J.N., Valley, J.W., Mundil, R., Campbell, I.H., Korch, R.J., Williams, I.S., Foudoulis, C., 2004. Improved 206Pb/238U microprobe geochronology by the monitoring of a trace-element-related matrix effect; SHRIMP, ID–TIMS, ELA–ICP–MS and oxygen isotope documentation for a series of zircon standards, Chemical Geology, 205, 115–140.

van Breemen, O., Corriveau, L., 1995. Evolution of the Central Metasedimentary Belt in Quebec, Grenville orogen: U-Pb geochronology. *In* Precambrian '95, International Conference on Tectonics and Metallogeny of Early/Mid Precambrian orogenic Belts, Program and Abstracts, Montreal, p. 137.

Cherniak, D.J., Watson, E.B., 2003. Diffusion in zircon. *In* Hanchar, J.M., Hoskin., P.W. O. (ed.): Reviews in Mineralogy and Geochemistry, 53, 113–143. Zircon., 2003.

Cherniak, D.J., Hanchar, J.M., Watson, E.B., 1997. Rare-earth diffusion in zircon. Chemical Geology, 134, 289–301.

Chu, N.C., Taylor, R.N., Chavagnac, V., Nesbitt, R.W., Boella, R.M. Milton, J.A., German, C.R., Bayon, G., Burton, K., 2002. Hf isotope ratio analysis using multi-collector inductively coupled plasma mass spectrometry: an evaluation of isobaric interference corrections. Journal of Analytical Atomic Spectrometry, 17 (12), 1567–1574.

Corfu, F., Hanchar, J.M., Hoskin, P.W.O., Kinny, P.D., 2003. Atlas of zircon texture. *In* Hanchar, J.M., Hoskin., P.W. O. (ed.): Reviews in Mineralogy and Geochemistry, 53, 469–500. Zircon., 2003.

Corrigan, D., Hanmer, S., 1995. Arc accretion, thickening, postcollisional extension and plutonism in the Grenville orogen; constraints from the Mauricie region, south-central Quebec. *In* Precambrian '95, International Conference on Tectonicsand Metallogeny of Early/Mid Precambrian orogenic Belts, Program and Abstracts, Montreal, p. 106.

Corriveau, L., Morin, D., van Breemen, O., Amelin, Y., Rivard, B., 1994. The CMB of Quebec: its evolution and its third dimension. *In* LITHOPROBE ECSOOT and Abitibi Grenville Workshop, An Overview of the Grenville Province from the Great Lakes to the Labrador Sea, Abstract. LITHOPROBE, unpublished.

Craig, H., 1961. Isotopic variations in meteoric waters. Science, 133, 1702–1703.

Davis, D.W., Paces, J.B., 1990. Time resolution of geologic events on the Keweenaw Peninsula and implications for the development of the Midcontinent rift system: Earth and Planetary Science Letters, v. 97, 54–64, doi:10.1016/0012 –821X(90)90098–I.

Dodson, M.H., 1973. Closure temperature in cooling geochronological and petrological systems. Contribution to Mineralogy and Petrology, 40, 259–274.

Drahovzal, J.A., Harris, D.C., Wickstrom, L.H., Walker, D., Baranoski, M.T., Keith, B., Furer, L.C., 1992. The East Continent Rift Basin: A new discovery: Ohio. Division of Geological Survey Information Circular, 57, p. 25.

Egerton, R. F., 2005. Physical principles of electron microscopy: An introduction to TEM, SEM, and AEM. Springer, p. 202.

Faure, G., Mensing, T.M., 2005: Principles of isotope geology third edition. John Wiley & Sons, p. 589.

Faure, G., Barbis, F.C., 1983. Detection of neoformed adularia by Rb-Sr age determinations of granitic rocks in Ohio. *In* Augustithis, S.S. (ed.): Leaching and diffusion in rocks and their weathering products, 307–320. Theophrastus, Athens, Greece.

Ficher, C.M., Loewy, S.L., Miller, C.F., Berquist, P., Randall, W., Van Schmus, R.D., Hatcher, J. Wooden, J.L. Fullagar, P.D., 2010. Whole-rock Pb and Sm-Nd isotopic constraints on the growth of southeastern Laurentia during Grenvillian orogenesis. (Unpublished)

Finch, R.J., Hanchar, J.M., 2003. Structure and Chemistry of Zircon and Zircon–Group Minerals. *In* Hanchar, J.M., Hoskin., P.W. O. (ed.): Reviews in Mineralogy and Geochemistry, 53, 1–21. Zircon, 2003.

Fraser, G., Ellis, D., Eggins, S., 1997. Zirconium abundance in granulite-facies minerals, with implications for zircon geochronology in high-grade rocks. Geology, 25, 607-610.

Frei, D., Gerdes, A., 2009. Precise and accurate in situ U–Pb dating of zircon with high sample throughput by automated LA-SF-ICP-MS. Chemical Geology, 261, 261–270.

Geissler, T., Schaltelegger, U., Tomaschek, F., 2007. Re-equilibrium of zircon in aqueous fluids and melts. Elements, 3, 43–50.

Gerdes, A., Zeh, A., 2009. Zircon formation versus zircon alteration — New insights from combined U–Pb and Lu–Hf in-situ LA-ICP-MS analyses, and consequences for the interpretation of Archean zircon from the Central Zone of the Limpopo Belt. Chemical Geology, 261, 230–243. doi:10.1016/ j.chemgeo.2008.03.005

Goodge, J.W., Vervoort, J.D., 2006. Origin of Mesoproterozoic A-type granites in Laurentia: Hf isotope evidence. Earth and Planetary Science Letters. 243, 711–731. doi:10.1016/ j.epsl.2006.01.040

Gower.C.F., Krogh.T.E., 2002. A U-Pb geochronological review of the Proterozoic history of the eastern Grenville Province. Canadian Journal of Earth Science, 39, 795–829.

Gower, C.F., Ryan, A.B., Rivers, T., 1990. Mid-Proterozoic Laurenti~Baltica: an overview of its geological evolution and a summary of the contributions made by this volume. *In* Gower, C.F., Rivers, T., Ryan, A.B. (ed.): Mid–Proterozoic Laurentia–Baltica, GAC Special Paper, 38, 1–20. St. John's, NF, Canada.

Harley, S.L., Kelly, N.M., Möller, A., 2007. Zircon Behavour and the Thermal Histories of Mountain Chains: Elements, 3, 25–30.

Harley, S.L., Kelly, N.M., 2007. Zircon, Tiny but timely: Elements, 3, 13–18.

Hawkesworth, C.J., Kemp, A.I.S., 2006. Using hafnium and oxygen isotopes in zircons to unravel the record of crustal evolution. Chemical Geology, 226, 144–162.

Hoefs, J., 1997. Stable isotope geochemistry, 4th edition, p. 201. Springer–Verlag, Heidelberg and New York.

Hofmann, C. M., Faure, G., Janssens, A., 1972. Age determination of a granite gneiss from the Precambrian basement of Scioto County, Ohio: The Ohio Journal of Science, 72, 49–53.

Hoskins, P.W.O., Black, P.L., 2000. Metamorphic zircon formation by solid–state recrystallization of protolith igneous zircon. Journal of Metamorphic Geology, 18, 4, 423–439.

Hoskin, P.W.O., Schaltegger, U., 2003. The Composition of Zircon and Igneous and Metamorphic Petrogenesis. *In* Hanchar, J.M., Hoskin., P.W. O. (ed.): Reviews in Mineralogy and Geochemistry, 53, 27–55. Zircon., 2003.

Ireland, T. R., Williams, I.S., 2003. Considerations in zircon geochronology by SIMS. *In* Hanchar, J.M., Hoskin., P.W. O. (ed.): Reviews in Mineralogy and Geochemistry, 53, 215–241. Zircon., 2003.

Jaffey, A.H., Flynn, K. F., Glendenin, L. F., Bentley, W. C., Fssling, A. M., 1971 Precision measurements of half-lives and specific activities of ^{235}U and ^{238}U, Physical Review C, 4 ,1889-1906.

Karlström, K.E., Åhäll, K., Harlan, S.S., Williams, M.L., McLelland, J., Geissman, J.W., 2001. Long–lived (1.8–1.0 Ga) convergent orogen in southern Laurentia, its extensions to Australia and Baltica, and implications for refining Rodinia. Precambrian Research, 111, 5–30.

Kemp, A.I.S., Hawkesworth, C.J., Paterson, B.A., Kinny, P.D., 2006. Episodic growth of the Gondwana supercontinent from hafnium and oxygen isotopes in zircon. Nature, 439, 580–583 10.1038/nature04505.

Kinny, P.D., Maas, R., 2003. Lu–Hf and Sm–Nd isotope systems in zircon. *In* Hanchar, J.M., Hoskin., P.W. O. (ed.): Reviews in Mineralogy and Geochemistry, 53, 327–341. Zircon., 2003.

Kolodny, Y., Epstein, S., 1976. Stable isotope geochemistry of deep sea cherts. Geochimica et Cosmochimica Acta, 40, 1195–1209.

Košler, J., Sylvester, P.J., 2003. Present Trends and the Future of Zircon in Geochronology: Laser Ablation ICPMS. *In* Hanchar, J.M., Hoskin., P.W. O. (ed.): Reviews in Mineralogy and Geochemistry, 53, 243–271. Zircon., 2003.

König, S., Münker, C., Schuth, S., Garbe–Schönberg, D., 2008. Mobility of tungsten in subduction zones. Earth and Planetary Science Letters, 274, 82–92.

Lee, J.K.W., Williams, I.S., Ellis, D.J., 1997. Pb, U and Th diffusion in natural zircon. Nature, 390, 159–163.

Le Roux, J.L., Glendenin, L.E., 1963. Half-hfe of ^{232}Th, Proceedings of the National Meeting on Nuclear Energy, Pretoria, South Africa, April, 83-94.

Lidiak, E.G., Marion, R.F., Thomas, H.H., Bass, M.N., 1966. Geochronology of the midcontinent region, United States; [Part] 4, Eastern area. Journal of Geophysical Research, 71, 22, 5427–5438.

Luciuc, J.E., von Frese. R.R.B., 1988. Aeromagnetic and gravity anomaly constrains on the crustal geology of Ohio. Geological Society of America Bulletin, 100, 104–116, doi: 10.1130/0016–7606(1988) 100<0104:AAGACO>2.3CO;2.

Ludwig, K. R., 2008. Isoplot 3.70. A geochronological toolkit for Microsoft Excel. Berkeley Geochronology Center Special Publication, 4.

McEachern, S.J., van Breemen, O., 1993. Age of deformation within the Central Metasedimentary Belt boundary thrust zone, southwest Grenville Orogen: constraints on the collision of the Mid-Proterozoic Elzevir terrane. Canadian Journal of Earth Sciences, 30, 1155–1165.

McLelland, J.M., Lochhead, A., Vyhnal, C., 1988. Evidence for multiple metamorphic events in the Adirondack Mountains, New York. Journal of Geology, 96, 279–298.

Mensing, T.M., Faure, G., 1983. Identification and age of neoformed Paleozoic feldspar (adularia) in a Precambrian basement core from Scioto County, Ohio, USA. Contrib. Mineral. Petrol. 82, 327–333.

Mosher, S., 1998. Tectonic evolution of the southern Laurentian Grenville orogenic belt. Geological Society of America Bulletin, 110, 1357–1375.

Nowell, G.M., Kempton, P.D., Noble, S.R., Fitton, J.G., Saunders, A.D., Mahoney, J.J., Taylor, R.N., 1998. High precision Hf isotope measurements of MORB and OIB by thermal ionisation mass spectrometry: insights into depleted mantle. Chemical Geology, 149, 211–233.

Ohio Division of Geological Survey., 2010. Compilation of data, analyses, and references for Proterozoic drill core stored at the Ohio Division of Geological Survey, H.R. Collins Core Repository, Delaware, Ohio, 43015-7635: Ohio Division of Geological Survey. Unpublished data format.

Ohio History Central., 2006. *Bedrock, 2010-09-06* http://www.ohiohistorycentral.org/entry.php?rec=2776

Patchett, P.J., Tatsumoto, M. , 1980. A routine high–precision method for Lu–Hf isotope geochemistry and chronology. Contributions to Mineralogy and Petrology, 75, 3, 263–267.

Roberts. M.P., Finger. F., 1997. Do U-Pb zircon ages from granulites reflect peak metamorphic conditions? Geology, 25, 319-322.

Rivers, T., 1997. Lithotectonic elements of the Grenville Province: review and tectonic implications. Precambrian research, 86, 117–154.

Rivers, T., 2008. Assembly and preservation of lower, mid, and upper orogenic crust in the Grenville Province–Implications for the evolution of large hot long-duration orogens. Precambrian research, 167, 237–259.

Rollinson, H. R., 1993. Using geochemical data; evaluation, presentation, interpretation, p. 352. Longman Scientific & Technical.

Rubatto, D., Hermann, J., 2007. Zircon behaviour in deeply subducted rocks. Elements, 3, 31–35.

Rubatto, D., Műntener, O., Barnhoorn, A., Gregory, C., 2008. Dissolution–reprecipitation of zircon at low-temperature, highpressure conditions (Lanzo Masif, Italy). American Mineralogist, 93, 1519–1529.

Santos, J.O.S., Hartmann. L.A., McNaughton. N.J., Easton. R.M., Rea. R.G., Potter. P.E., 2002. Sensitive high resolution ion microprobe (SHRIMP) detrital zircon geochronology provides new evidence for a hidden Neoproterozoic foreland basin to the Grenville Orogen in the eastern Midwest, U.S.A. Canadian Journal of Earth Science, 39, 1505-1515.

Scherer, E.E., Whitehouse, M.J., and Munker, C., 2007: Zircon as a monitor of crustal growth. Elements, 3, 19–24.

Segal, I., Halicz, L., Platzner, I.T., 2003. Accurate isotope ratio measurements of ytterbium by multiple collection inductively coupled plasma mass spectrometry applying erbium and hafnium in an improved double external normalization procedure. Journal of Analytical Atomic Spectrometry, 18, 1217–1223.

Shannon, R.D., 1976. Central Research and Development Department, Experimental Station, E. I. Du Pont de Nemours and Company, Wilmington, Delaware 19898, U.S.A. Published in Acta Crystallographica. (1976). A32, Pages 751–767.

Sláma, J., Kosler, J., Condon, D.J., Crowley, J.L., Gerdes, A., Hanchar, J.M., Horstwood, M.S.A., Morris, G.A., Nasdala, L., Norberg, N., Schaltegger, U., Schoene, B., Tubrett, M.N., Whitehouse, M.J., 2008. Plesovice zircon - A new natural reference material or U-Pb and Hf isotopic microanalysis. Chemical Geology, 249, 1-35.

Sommerauer, J., 1974. Trace element distribution patterns and combined electron microprobe techniques. Electron Microscopy Society of South Africa Prossedings, 4, 71–72.

Stacey, J.S., Kramers, D.J., 1975. Approximation of Terrestrial Lead Isotope Evolution by a Two–Stage Model. Earth and Planetary Science Letters, 26, 207–221.

Stern, R.A., 2009. Intropduction to SIMS in geology. *In* Fayek, F., (ed.): Secondary Ion Mass Spectrometry in the Earth Sciences, Gleaning the big picture from a small spot. Mineralogical Association of Canada, Short course Series, 41, p. 146

Söderlund, U., Johansson, L., 2002. A simple way to extract baddeleyite (ZrO2).Geochem. Geophys. Geosyst. 3, 2, 1–7. doi:10.1029/2001GC000212.

Söderlund, U., Patchett, P.J., Vervoort, J.D., Isachsen, C.E., 2004. The ^{176}Lu decay constant determined by Lu–Hf and U–Pb isotope systematics of Precambrian mafic intrusions, Earth and Planetary Science Letters, 219, 311–324.

Van Schmus, W.R. Bickford, M.E., Turek, A., 1996. Prtoerozoic geology of the east-central Midcontinent basement. Geological Society of America Special Paper 308, 7-32.

Van Wetrenen, W., Blundy. J., Wood. B., 1999. Cruystal–chemical controls on trace element portioning between garnet and anhydrous silicate melt. American Mineralogist, 84, 838–847.

Valley, J.W., Lackey, J.S., Cavosie, A.J., Clechenko, C.C., Spicuzza, M.J., Basei, M.A.S., Bindeman, I.N., Ferreira, V.P., Sial, A.N., King, E.M., Peck, W.H., Sinha, A.K., Wei, C.S., 2005. 4.4 billion years of crustal maturation: oxygen isotope ratios of magmatic zircon. Contribution to Mineral Petrology, 150, 561–580.

Valley, J.W., 2003. Oxygen Isotopes in Zircon. *In* Hanchar, J. M., Hoskin, P. W. O. (ed.): Reviews in Mineralogy and Geochemistry, 53, 343–380. Zircon., 2003.

Vargo, R. T., 1972. Sr-Rb age determination of a Precambrian rock from Lake County, Ohio: B. S. thesis, (unpub.), Ohio State University, p. 18.

Watson, E. B. & Liang, Y., 1995. A simple model for sector Precambrian zoning in slowly grown crystals: implications for growth rate and lattice diffusion, with emphasis on accessory minerals in crustal rocks. American Mineralogist, 80, 1179–1187.

Wiedenbeck, M., Hanchar, J.M., Peck, W.H., Sylvester, P., Valley, J., Whitehouse, M., Kronz, A., Morishita, Y., Nasdala, L., Fiebig, J., Franchi, I., Girard, J.–P., Greenwood, R.C., Hinton, R., Kita, N., Mason, P.R.D., Norman, M., Ogasawara, M., Piccoli, P.M., Rhede, D., Satoh, H., Schulz–Dobrick, B., Skar, O., Spicuzza, M.J., Terada, K., Tindle, A., Togashi, S., Vennemann, T., Xie, Q., Zheng, Y.–F., 2004. Further characterization of the 91500 zircon crystal. Geostandards and Geoanalytical Research, 28, 9–39.

Windley, B.F., 1986. Comparative tectonics of the western Grenville and the western Himalaya. *In* Moore, J.M.,

Vargo, R. T., 1972. Sr-Rb age determination of a Precambrian rock from Lake County, Ohio: B. S. thesis, (unpub.), Ohio State University, p. 18.

Whitehouse, M. J., Kamber, B. S., 2005. Assigning dates to thin gneissic veins in high–grade metamorphic terranes: a cautionary tale from Akilia, Southwest Greenland. Journal of Petrology, 46, 291–318.

Whitehouse, M. J., Kamber, B. S., Moorbath, S., 1999. Age significance of U–Th–Pb zircon data from early Archean rocks of west Greenland – a reassessment based on combined ion microprobe and imaging studies. Chemical Geology, 160, 210–224.

Woodhead, J., Hergt, J., 2005. A preliminary appraisal of seven natural zircon reference materials for in situ Hf isotope determination, Geostandards and Geoanalytical Research, 29, 183–195.

Appendix. I. Logan (Acid Volcanic)

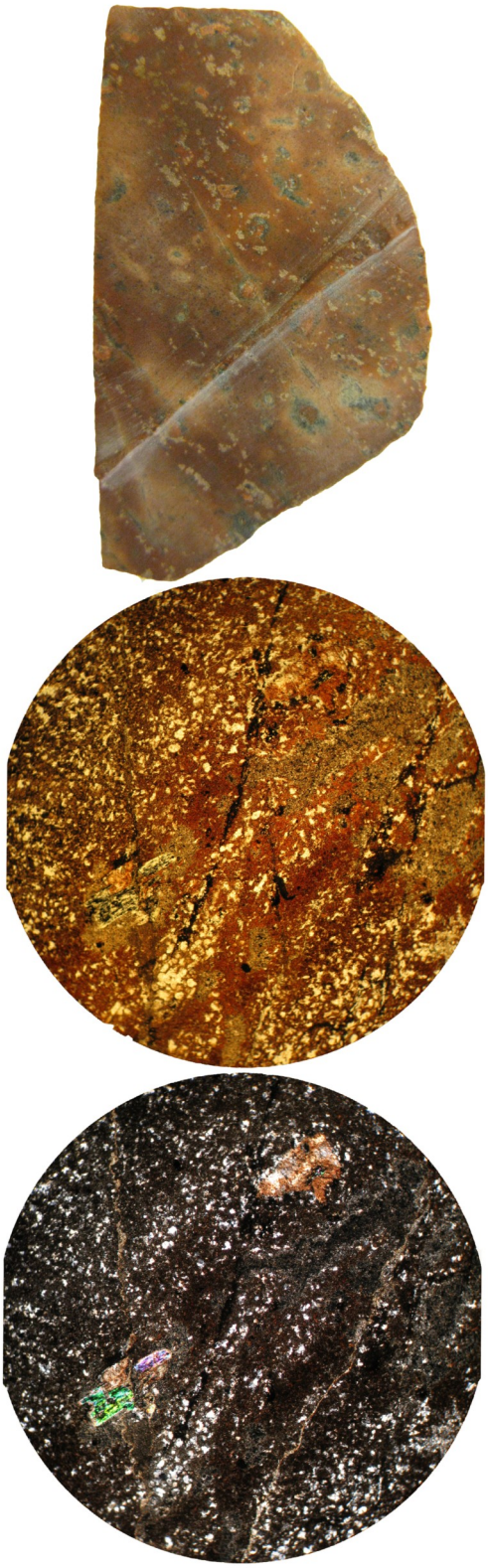

Small drill-core sample aliquot (top) showing macroscopic features. Plane polarised thin section view of a representative area (middle). Cross polarised thin section view of the same area as for the plane polarised view (bottom).

Appendix. II. Hpokins (Amfibolite)

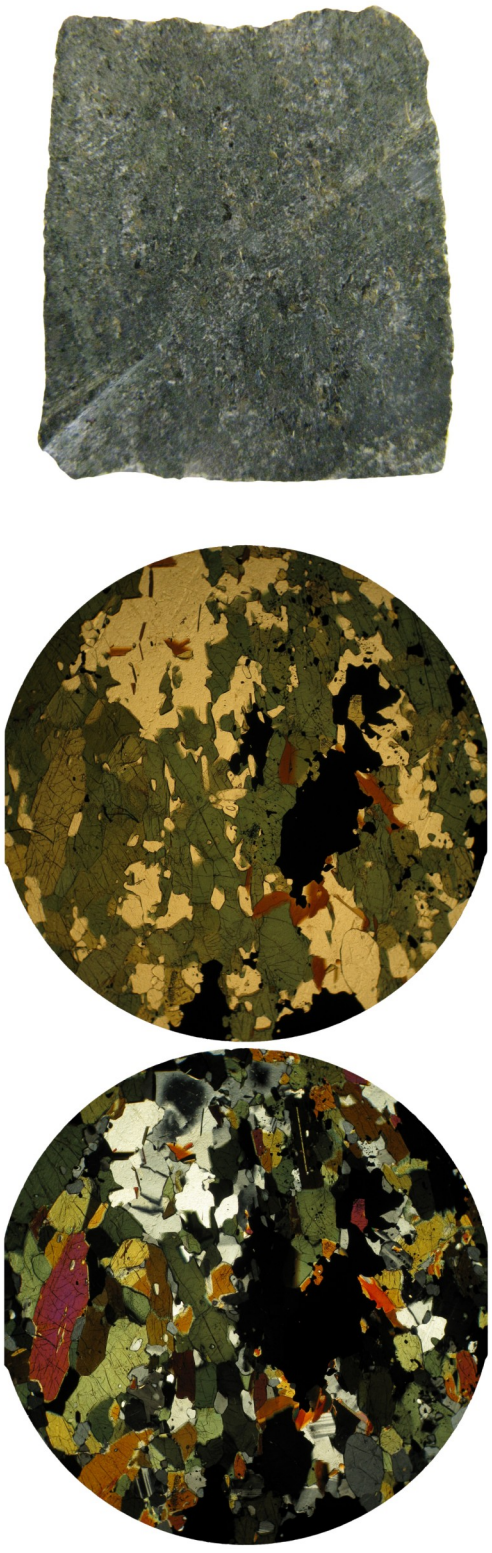

Small drill-core sample aliquot (top) showing macroscopic features. Plane polarised thin section view of a representative area (middle). Cross polarised thin section view of the same area as for the plane polarised view (bottom).

Appendix. III. Hopkins (Meta-pegmaitie)

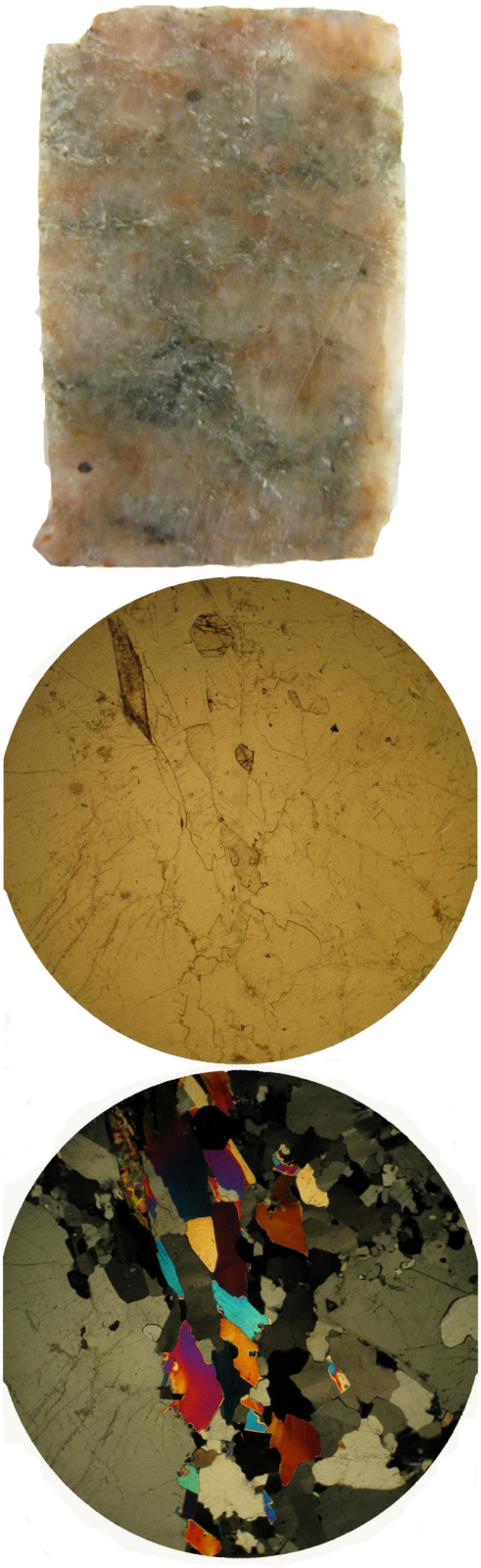

Small drill-core sample aliquot (top) showing macroscopic features. Plane polarised thin section view of a representative area (middle). Cross polarised thin section view of the same area as for the plane polarised view (bottom).

Appendix. IV. Scioto 6A (Orthogneiss)

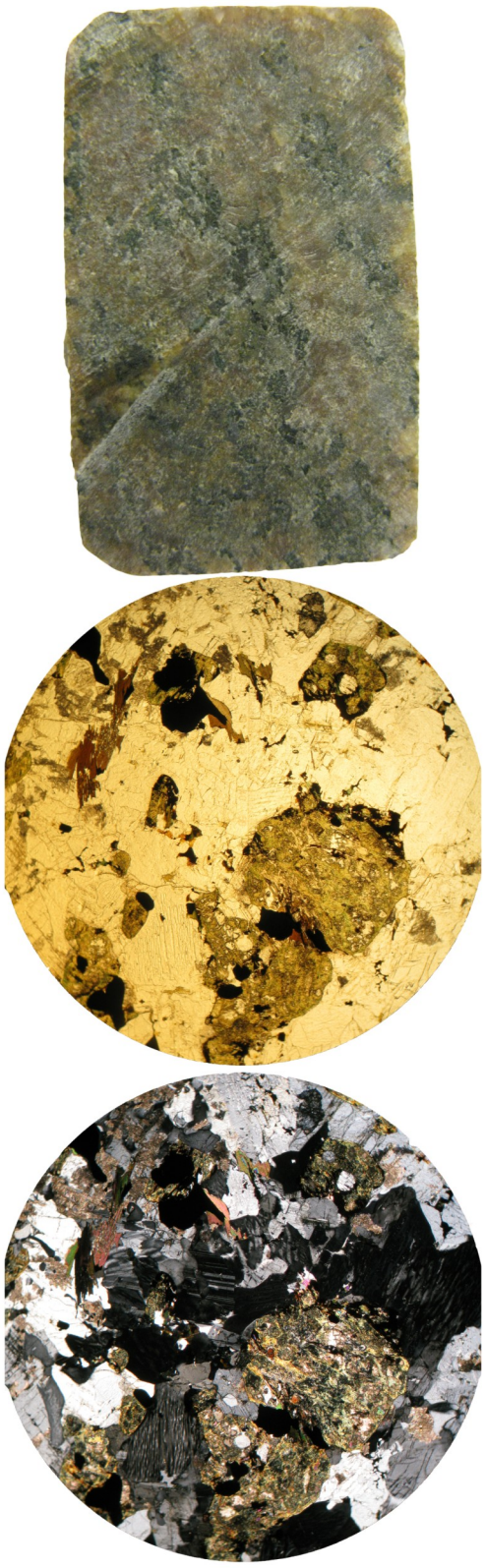

Small drill-core sample aliquot (top) showing macroscopic features. Plane polarised thin section view of a representative area (middle). Cross polarised thin section view of the same area as for the plane polarised view (bottom).

Appendix. V. Scioto 6B (Boundary between 6A & 6C)

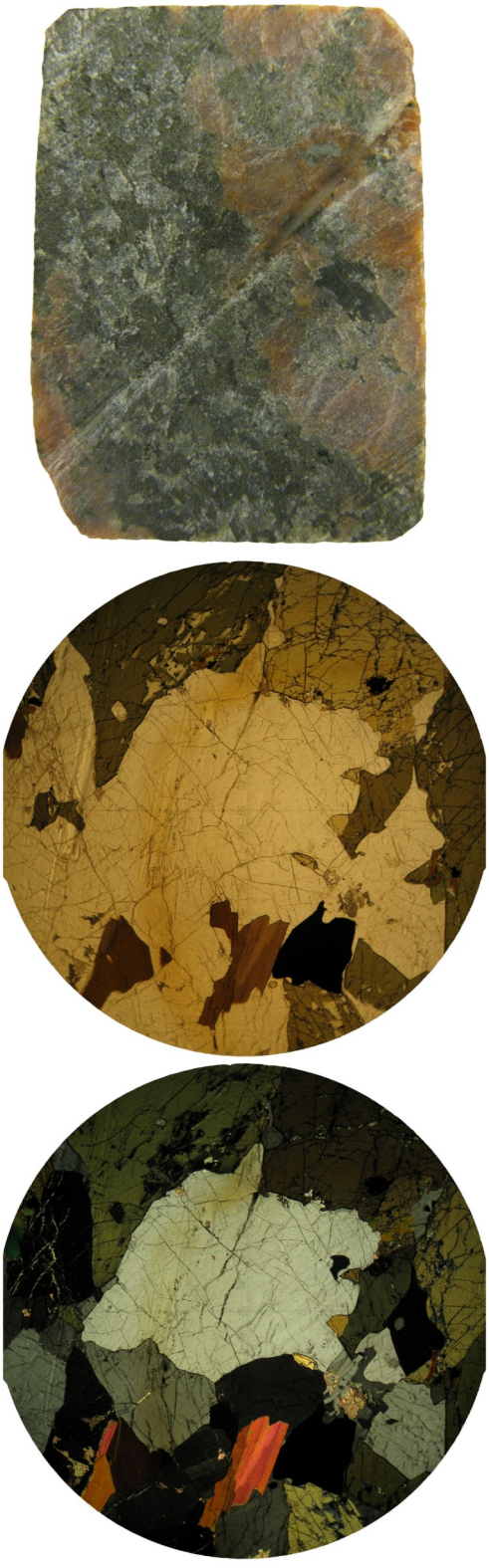

Small drill-core sample aliquot (top) showing macroscopic features. Plane polarised thin section view of a representative area (middle). Cross polarised thin section view of the same area as for the plane polarised view (bottom).

Appendix. VI. Scioto 6C (Post-kinematic granite)

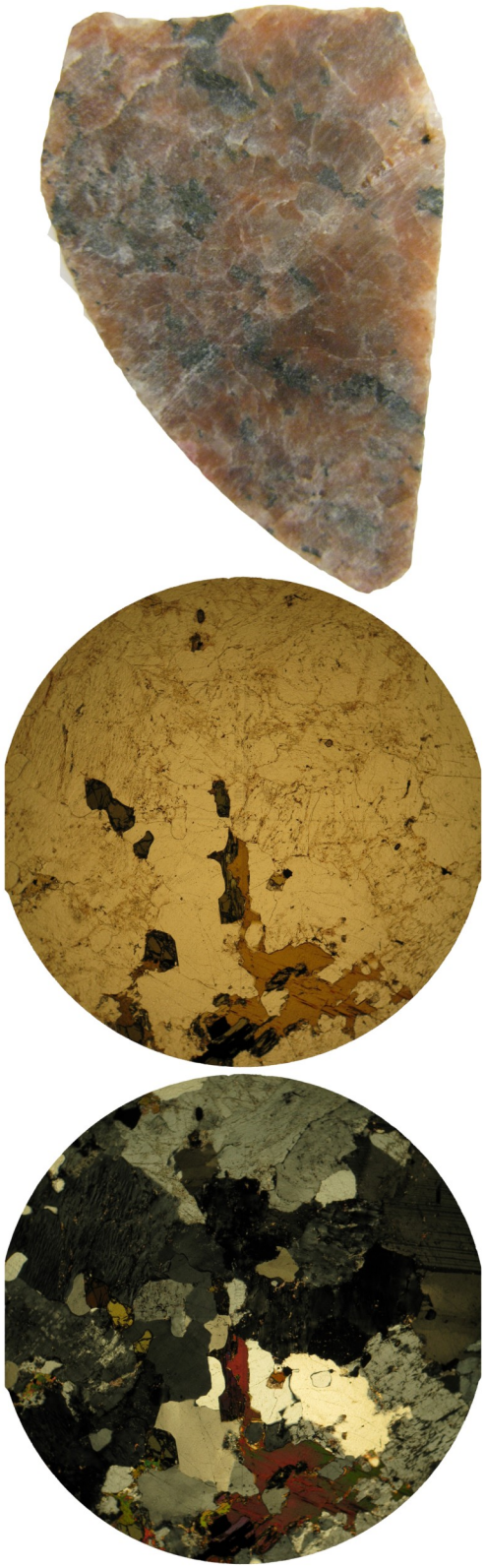

Small drill-core sample aliquot (top) showing macroscopic features. Plane polarised thin section view of a representative area (middle). Cross polarised thin section view of the same area as for the plane polarised view (bottom).

Appendix. VII. Morrow (Post-kinematic granite)

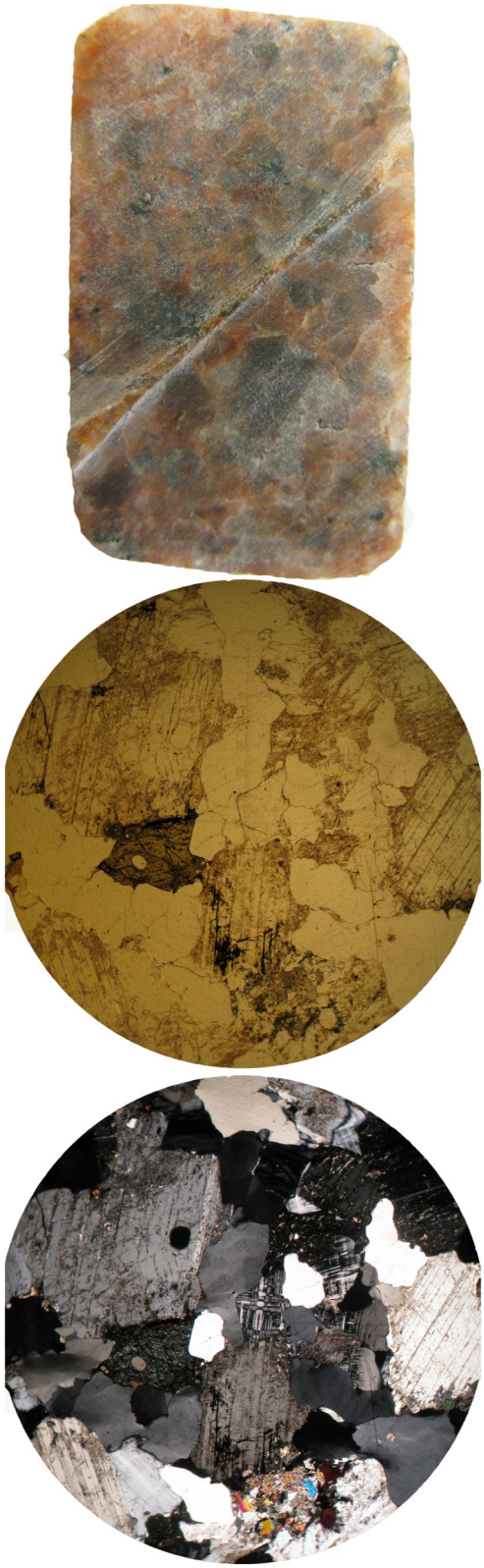

Small drill-core sample aliquot (top) showing macroscopic features. Plane polarised thin section view of a representative area (middle). Cross polarised thin section view of the same area as for the plane polarised view (bottom).

Appendix. VIII. Herman (Meta-granite)

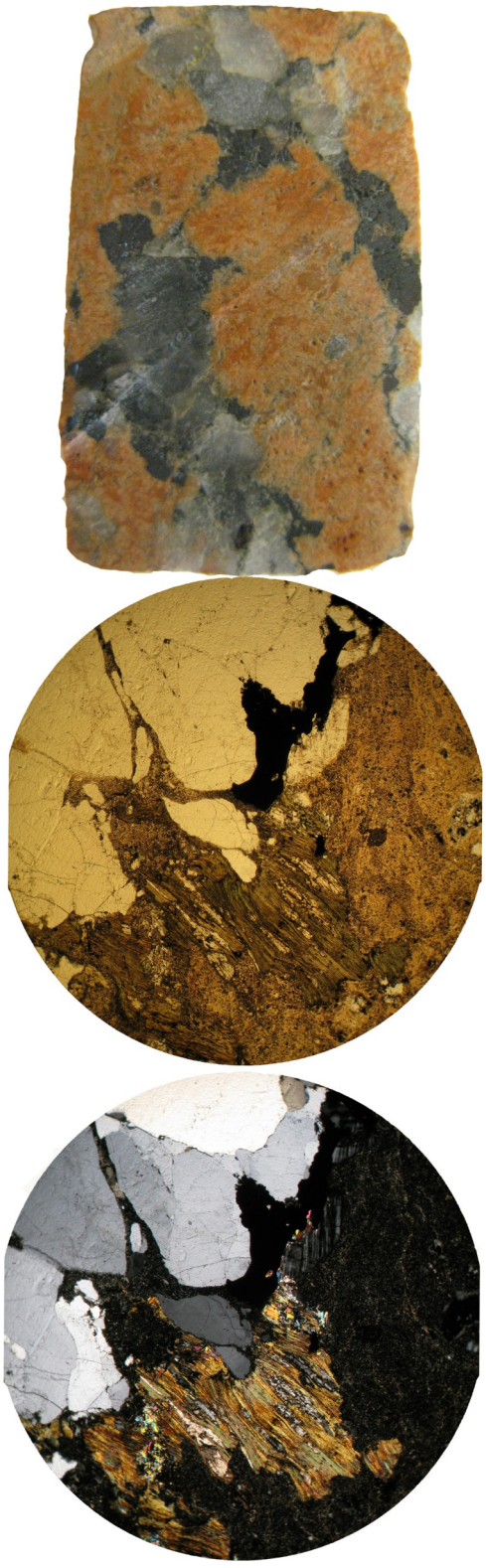

Small drill-core sample aliquot (top) showing macroscopic features. Plane polarised thin section view of a representative area (middle). Cross polarised thin section view of the same area as for the plane polarised view (bottom).

Appendix. IX. Lake (Dark fine-grained rock)

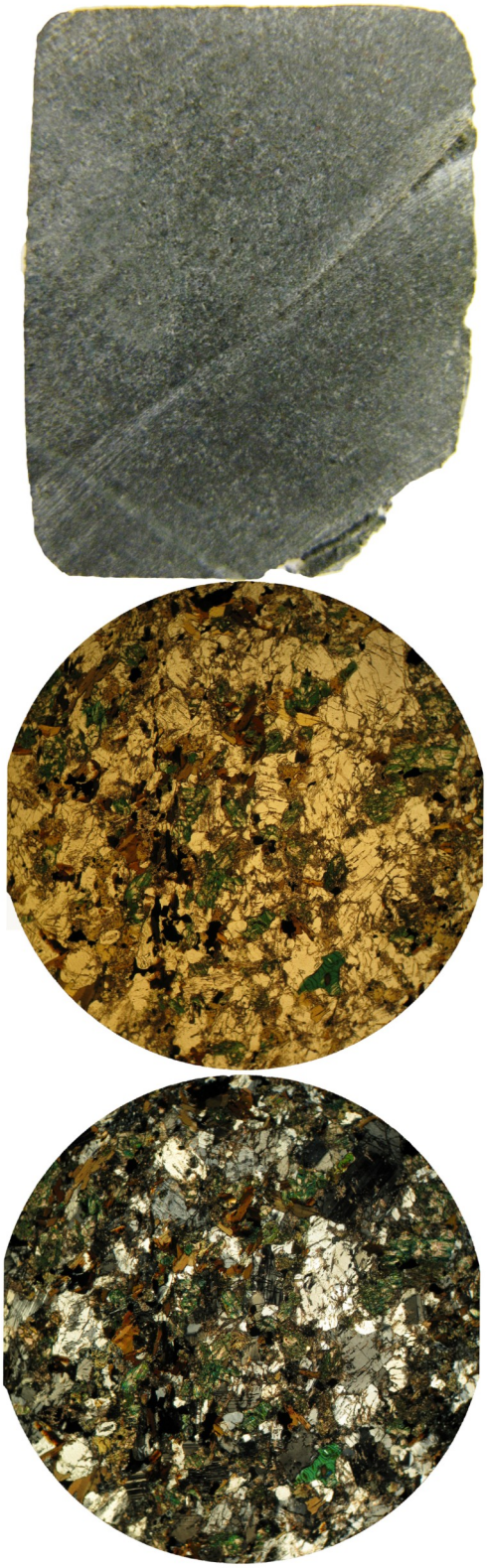

Small drill-core sample aliquot (top) showing macroscopic features. Plane polarised thin section view of a representative area (middle). Cross polarised thin section view of the same area as for the plane polarised view (bottom).

Appendix. X.

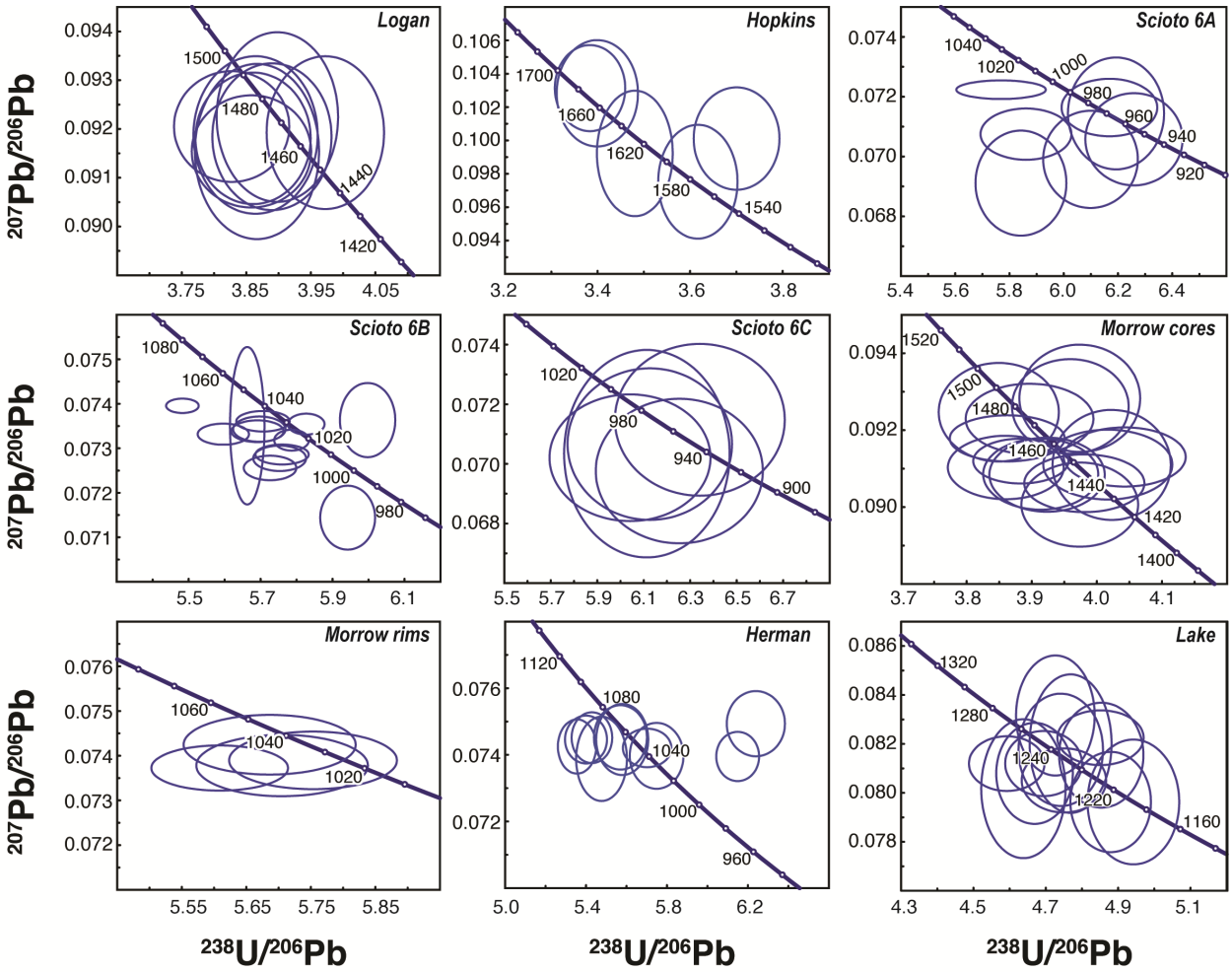

Tera-Wasserburg U-Pb diagrams for the analysed zircon spots from Ohio subsurface basement rocks. See Fig. 3 for drill-core locations. Concordant zircon from *Logan* yield both a concordia age (1471 ±3 Ma, MSWD = 1.1) and a $^{207}Pb/^{206}Pb$ age (1464 ±8 Ma, MSWD = 0.2). *Hopkins* yield a $^{207}Pb/^{206}Pb$ age of 1643 ±54 Ma (MSWD = 3.5). *Scioto 6A* yield a $^{207}Pb/^{206}Pb$ age of 982 ±21 Ma (MSWD = 1.9). *Scioto 6B* yield a $^{207}Pb/^{206}Pb$ age of 1025 ±8 Ma (MSWD = 4.6). *Scioto 6c* yield a $^{207}Pb/^{206}Pb$ age of 942 ±24 Ma (MSWD = 1.6). Concordant zircon from *Morrow* core zircon spots yield both a concordia age (1454 ±18 Ma, MSWD = 2.8) and a $^{207}Pb/^{206}Pb$ age (1449 ±9 Ma, MSWD = 4.0). Morrow rim zircon spots yield a $^{207}Pb/^{206}Pb$ age of 1025 ±7 Ma (MSWD = 0.8). *Herman* yield a $^{207}Pb/^{206}Pb$ age of 1050 ±6 Ma (MSWD = 0.7). *Lake* yield a $^{207}Pb/^{206}Pb$ age of 1228 ±10 Ma (MSWD = 1.7). Data for *Sioto 6A and 6C* are unpublished data from Jenny Andersson, Swedish Geological Survey, Uppsala.
See text (Section 5) for detailed discussion.

Tidigare skrifter i serien ”Examensarbeten i Geologi vid Lunds Universitet”:

215. Mikkelsen, Angelica, 2007: Relationer mellan grundvattenmagasin och geologiska strukturer i samband med tunnelborrning genom Hallandsås, Skåne.
216. Trondman, Anna-Kari, 2007: Stratigraphic studies of a Holocene sequence from Taniente Palet bog, Isla de los Estados, South America.
217. Månsson, Carl-Henrik & Siikanen, Jonas, 2007: Measuring techniques of Induced Polarization regarding data quality with an application on a test-site in Aarhus, Denmark and the tunnel construction at the Hallandsås Horst, Sweden.
218. Ohlsson, Erika, 2007: Classification of stony meteorites from north-west Africa and the Dhofar desert region in Oman.
219. Åkesson, Maria, 2008: Mud volcanoes - a review. (15 hskp)
220. Randsalu, Linda, 2008: Holocene relative sea-level changes in the Tasiusaq area, southern Greenland, with focus on the Ta1 and Ta3 basins. (30 hskp)
221. Fredh, Daniel, 2008: Holocene relative sea-level changes in the Tasiusaq area, southern Greenland, with focus on the Ta4 basin. (30 hskp)
222. Anjar, Johanna, 2008: A sedimentological and stratigraphical study of Weichselian sediments in the Tvärkroken gravel pit, Idre, west-central Sweden. (30 hskp)
223. Stefanowicz, Sissa, 2008: Palyno-stratigraphy and palaeoclimatic analysis of the Lower - Middle Jurassic (Pliens-bachian - Bathonian) of the Inner Hebrides, NW Scotland. (15 hskp)
224. Holm, Sanna, 2008: Variations in impactor flux to the Moon and Earth after 3.85 Ga. (15 hskp)
225. Bjärnborg, Karolina, 2008: Internal structures in detrital zircons from Hamrånge: a study of cathodolumine-scence and back-scattered electron images. (15 hskp)
226. Noresten, Barbro, 2008: A reconstruction of subglacial processes based on a classification of erosional forms at Ramsvikslandet, SW Sweden. (30 hskp)
227. Mehlqvist, Kristina, 2008: En mellanjuras-sisk flora från Bagå-formationen, Bornholm. (15 hskp)
228. Lindvall, Hanna, 2008: Kortvariga effekter av tefranedfall i lakustrin och terrestrisk miljö. (15 hskp)
229. Löfroth, Elin, 2008: Are solar activity and cosmic rays important factors behind climate change? (15 hskp)
230. Damberg, Lisa, 2008: Pyrit som källa för spårämnen – kalkstenar från övre och mellersta Danien, Skåne. (15 hskp)
331. Cegrell, Miriam & Mårtensson, Jimmy, 2008: Resistivity and IP measurements at the Bolmen Tunnel and Ådalsbanan, Sweden. (30 hskp)
232. Vang, Ina, 2008: Skarn minerals and geological structures at Kalkheia, Kristiansand, southern Norway. (15 hskp)
233. Arvidsson, Kristina, 2008: Vegetationen i Skandinavien under Eem och Weichsel samt fallstudie i submoräna organiska avlagringar från Nybygget, Småland. (15 hskp)
234. Persson, Jonas, 2008: An environmental magnetic study of a marine sediment core from Disko Bugt, West Greenland: implications for ocean current variability. (30 hskp)
235. Holm, Sanna, 2008: Titanium- and chromium-rich opaque minerals in condensed sediments: chondritic, lunar and terrestrial origins. (30 hskp)
236. Bohlin, Erik & Landen, Ludvig, 2008: Geofysiska mätmetoder för prospektering till ballastmaterial. (30 hskp)
237. Brodén, Olof, 2008: Primär och sekundär migration av hydrokarboner. (15 hskp)
238. Bergman, Bo, 2009: Geofysiska analyser (stångslingram, CVES och IP) av lagerföljd och lakvattenrörelser vid Albäcksdeponin, Trelleborg. (30 hskp)
239. Mehlqvist, Kristina, 2009: The spore record of early land plants from upper Silurian strata in Klinta 1 well, Skåne, Sweden. (45 hskp)
239. Mehlqvist, Kristina, 2009: The spore record of early land plants from upper Silurian strata in Klinta 1 well, Skåne, Sweden. (45 hskp)
240. Bjärnborg, Karolina, 2009: The copper sulphide mineralization of the Zinkgruvan deposit, Bergslagen, Sweden. (45 hskp)
241. Stenberg, Li, 2009: Historiska kartor som

hjälp vid jordartsgeologisk kartering – en pilotstudie från Vångs by i Blekinge. (15 hskp)

242. Nilsson, Mimmi, 2009: Robust U-Pb baddeleyite ages of mafic dykes and intrusions in southern West Greenland: constraints on the coherency of crustal blocks of the North Atlantic Craton. (30 hskp)
243. Hult, Elin, 2009: Oligocene to middle Miocene sediments from ODP leg 159, site 959 offshore Ivory Coast, equatorial West Africa. (15 hskp)
244. Olsson, Håkan, 2009: Climate archives and the Late Ordovician Boda Event. (15 hskp)
245. Wollein Waldetoft, Kristofer, 2009: Svekofennisk granit från olika metamorfa miljöer. (15 hskp)
246. Månsby, Urban, 2009: Late Cretaceous coprolites from the Kristianstad Basin, southern Sweden. (15 hskp)
247. MacGimpsey, I., 2008: Petroleum Geology of the Barents Sea. (15 hskp)
248. Jäckel, O., 2009: Comparison between two sediment X-ray Fluorescence records of the Late Holocene from Disko Bugt, West Greenland; Paleoclimatic and methodological implications. (45 hskp)
249. Andersen, Christine, 2009: The mineral composition of the Burkland Cu-sulphide deposit at Zinkgruvan, Sweden – a supplementary study. (15 hskp)
250. Riebe, My, 2009: Spinel group minerals in carbonaceous and ordinary chondrites. (15 hskp)
251. Nilsson, Filip, 2009: Föroreningsspridning och geologi vid Filborna i Helsingborg. (30 hskp)
252. Peetz, Romina, 2009: A geochemical characterization of the lower part of the Miocene shield-building lavas on Gran Canaria. (45 hskp)
253. Åkesson, Maria, 2010: Mass movements as contamination carriers in surface water systems – Swedish experiences and risks.
254. Löfroth, Elin, 2010: A Greenland ice core perspective on the dating of the Late Bronze Age Santorini eruption. (45 hskp)
255. Ellingsgaard, Óluva, 2009: Formation Evaluation of Interlava Volcaniclastic Rocks from the Faroe Islands and the Faroe-Shetland Basin. (45 hskp)
256. Arvidsson, Kristina, 2010: Geophysical and hydrogeological survey in a part of the Nhandugue River valley, Gorongosa National Park, Mozambique. (45 hskp)
257. Gren, Johan, 2010: Osteo-histology of Mesozoic marine tetrapods – implications for longevity, growth strategies and growth rates. (15 hskp)
258. Syversen, Fredrikke, 2010: Late Jurassic deposits in the Troll field. (15 hskp)
259. Andersson, Pontus, 2010: Hydrogeological investigation for the PEGASUS project, southern Skåne, Sweden. (30 hskp)
260. Noor, Amir, 2010: Upper Ordovician through lowermost Silurian stratigraphy and facies of the Borenshult-1 core, Östergötland, Sweden. (45 hskp)
261. Lewerentz, Alexander, 2010: On the occurrence of baddeleyite in zircon in silica-saturated rocks. (15 hskp)
262. Eriksson, Magnus, 2010: The Ordovician Orthoceratite Limestone and the Blommiga Bladet hardground complex at Horns Udde, Öland. (15 hskp)
263. Lindskog, Anders, 2010: From red to grey and back again: A detailed study of the lower Kundan (Middle Ordovician) 'Täljsten' interval and its enclosing strata in Västergötland, Sweden. (15 hskp)
264. Rääf, Rebecka, 2010: Changes in beyrichiid ostracode faunas during the Late Silurian Lau Event on Gotland, Sweden. (30 hskp)
265. Petersson, Andreas, 2010: Zircon U-Pb, Hf and O isotope constraints on the growth versus recycling of continental crust in the Grenville orogen, Ohio, USA. (45 hskp)

LUNDS UNIVERSITET

Geologiska enheten
Institutionen för geo- och ekosystemvetenskaper
Sölvegatan 12, 223 62 Lund